ESTIMATING THE MASS BALANCE OF GLACIERS IN THE GLACIER BAY AREA OF ALASKA, USA AND BRITISH COLUMBIA, CANADA

By

Austin Judson Johnson

RECOMMENDED: _____

_____

_____

_____
Advisory Committee Chair

_____
Chair, Department of Geology and Geophysics

APPROVED: _____
Dean, College of Natural Science and Mathematics

_____
Dean of the Graduate School

_____
Date

ESTIMATING THE MASS BALANCE OF GLACIERS IN THE GLACIER BAY AREA OF ALASKA, USA AND BRITISH COLUMBIA, CANADA

A

THESIS

Presented to the Faculty

of the University of Alaska Fairbanks

in Partial Fulfillment of the Requirements

for the Degree of

MASTER OF SCIENCE

By

Austin Judson Johnson, B.S.

Fairbanks, AK

May 2012

ABSTRACT

The mass balance rate for sixteen glaciers in the Glacier Bay area of Alaska and B.C. has been estimated with airborne laser altimetry, in which centerline surface elevations acquired during repeat altimetry flights between 1995 and 2011 are differenced. The individual glacier mass balances are extrapolated to the entire glaciated area of Glacier Bay using a normalized elevation method and an area-weighted average mass balance method. Mass balances are presented over four periods: 1) 1995 – 2000; 2) 2000 – 2005; 3) 2005 – 2009; 4) 2009 – 2011. The Glacier Bay mass balance record generally shows more negative mass balances during periods 2 and 4 (mass loss rates exceeded 5.0 Gt yr^{-1}) as compared to periods 1 and 3 (mass loss rates were less than 3.0 Gt yr^{-1}). The rate of mass loss between 1995 and 2011 compares closely to GRACE gravity signal changes and DEM differencing. The altimetry method has been validated against DEM differencing for glaciers located in Glacier Bay through the extrapolation of glacier centerline thinning rates from a difference DEM (simu-laser method). Simu-laser results show good agreement with sequential DEM differencing; we find the simu-laser method underestimates ice loss in Glacier Bay by 6% when compared to DEM differencing.

TABLE OF CONTENTS

LIST OF FIGURES

LIST OF TABLES

Page

LIST OF APPENDICES

Page

ACKNOWLEDGEMENTS

The late Keith Echelmeyer collected the 1995 and 2000 data and was the PI of the laser altimetry program from 1991 through 2005. Craig Lingle was the PI between 2006 and 2007. Paul Claus of Ultima Thule Outfitters took over pilot duties in 2002 and has been instrumental in the success of the project. The accommodations provided by the Claus family at their Ultima Thule Lodge are especially appreciated. Lee Zirnheld collected the 2005 and 2009 data and took the lead on GPS data processing. By Valentine also worked on data processing. Dave Burns reprocessed all the Glacier Bay GPS data and processed LiDAR data from 2011. Nate Murphy developed the laser altimetry mass balance GUI. Dave Hill provided the climate dataset. Justin Rich contributed updated glacier outlines and sampled the climate data to the Glacier Bay area. Thanks to Seth Campbell for the opportunity to spend three weeks on Kahiltna Glacier collecting ice core reconnaissance data. Thanks to Shad O'Neel for the opportunity to participate in the USGS Wolverine Glacier monitoring program. Thanks to my committee members (Anthony Arendt, Regine Hock, and Martin Truffer) for their time, suggestions, and helpful edits. Anthony also provided the updated GRACE mascon solutions. Special thanks to my advisor, Chris Larsen, for his patience, thoughtful reviews, and the opportunity to do fieldwork in some of the most spectacular areas of Alaska. Chris also wrote most of the scripts and code used in the analysis of laser altimetry data. Thanks to Dan Phillips for all the adventures in Maine. Finally, thanks to my family for their undying support and love. I truly hope that they will get to experience some of what I have seen in Alaska.

1. INTRODUCTION

The majority of glaciers in Alaska and northwestern Canada (referred hereafter as "Alaska" for brevity) have been experiencing overall retreat, surface lowering, and mass loss (Arendt et al., 2002; Berthier et al., 2010). The contribution to sea level rise (SLR) from the overall melt of Alaskan glaciers has been shown to be of the same approximate magnitude as that of the Greenland Ice Sheet or the Antarctic Ice Sheet (Meier et al., 2007; Wu et al., 2010; Jacob et al., 2012). The glaciers in the Glacier Bay region of Alaska are generally retreating (Larsen et al., 2007; Luthcke et al., 2008), with only a small number of glaciers advancing. There are a number of tidewater glaciers located in the Glacier Bay region; however, at the present none of the tidewater glaciers are experiencing rapid retreats like other glaciers in Alaska, e.g. Columbia Glacier (Walter et al., 2010) and South Sawyer Glacier (C. Larsen 2011, pers. comm.).

Monitoring the mass balance of glaciers via the conventional, or glaciological, method of observing stakes placed on a glacier's surface is time consuming and limited in scope and area (Dyurgerov, 2002). A strength of conventional mass balance studies is that they provide a high-resolution record of winter, summer, and annual mass balances along with snow density measurements (Dyurgerov, 2002). An alternative method for monitoring mass balance is to use airborne laser altimetry, which is a geodetic, or indirect, mass balance method. This method enables mass balance measurements on a more extensive regional scale as numerous glaciers can be profiled each year. Laser altimetry has been used to study ice sheet and alpine glacier mass balance in Greenland (Krabill et al., 2002), Antarctica (Pritchard et al., 2009), Svalbard (Nuth et al., 2010), Europe (Geist et al., 2005), the Canadian Arctic (Abdalati et al., 2004), and Alaska (Echelmeyer et al., 1996; Sapiano et al., 1998; Arendt et al., 2002; Foy et al., 2011).

In Alaska there are only a handful of glaciers that have had conventional mass balance records (Pelto and Miller, 1990; Heinrichs et al., 1996; Hodge et al., 1998; Miller and Pelto, 1999; Nolan et al., 2005; Van Beusekom et al., 2010). The laser altimetry program at the University of Alaska Fairbanks (UAF) has been able to profile over two hundred glaciers since 1993. More than one hundred thirty glaciers have been profiled at least twice and over ninety of those have been profiled three times or more, which gives mass balance for multiple time periods. This dataset of repeated profiles includes the Glacier Bay region, where eleven glaciers have been profiled at least three times since 1995.

Glacier surface elevation profiles that are acquired with laser altimetry are compared with earlier altimetry elevation profiles or with digital elevation models. If subsequent profiles are repeated at the same time of year then the surface elevation change can be used to estimate the mass balance rate ($\dot{B}$) for each glacier (Arendt et al., 2008). This is done by extrapolating the measured surface elevation changes along each of the flightlines to the entire surface area of the glacier. Converting to water equivalent (w.e.) then gives $\dot{B}$ in km^3 w.e. yr^{-1} (equivalent to Gt yr^{-1}) or in specific mass balance units m w.e.yr^{-1} if divided by the glacier area and density of water.

In this study, laser altimetry profiles of glacier surfaces are used to: 1) estimate the change in ice mass of glaciers in the Glacier Bay area that have been profiled with laser altimetry over four periods between 1995 and 2011; 2) extrapolate the ice mass change of the profiled glaciers to the entire Glacier Bay region to obtain mass change estimates for the whole region; 3) examine the variations in mass change since 1995; 4) check the validity of assumptions that include constant ice density, using glacier outlines from a single date, and that centerline thinning is representative across the width of a glacier; and 5) examine whether mass change can be correlated to climate or other variables such as glacier size, type, or location.

The profiled glaciers (those that have been surveyed by laser altimetry) are used herein to determine the mass balance and contribution to SLR of the entire Glacier Bay region since 1995 through two different regionalization methods. The first regional extrapolation method calculates a change in surface elevation vs. the average normalized glacier surface elevation curve for all the glaciers profiled during a particular time period, and applies that curve to the unprofiled glaciers to estimate the mass balance of those glaciers. The second regional extrapolation method applies the average area-weighted specific mass balance of the profiled glaciers during a particular period to the area of the unprofiled glaciers.

During the two earlier altimetry mass balance periods only four or five glaciers were profiled, while around a dozen glaciers were profiled during later periods. The greater sample sizes of the later periods are also used to examine how removing glaciers from the average normalized curve affects the estimated mass balance of the entire region.

The first section of this paper introduces the Glacier Bay area and its recent glacial history. The second section discusses the data that are acquired during laser altimetry flights. Section three goes over the methods that are used to estimate the mass balance rates for each of the profiled glaciers. The methods used to extrapolate the measured mass balances to the entire

glaciated area of Glacier Bay in order to estimate the regional mass loss a are discussed in more detail. The errors and uncertainties in estimating mass balance are also discussed.

Section four presents mass balance results for the profiled glaciers and the change in the mass balance rate over time is examined. The mass change of all glaciers in the Glacier Bay area is estimated, and the effect of removing individual glaciers from the extrapolation is examined. The validity of glacier-wide extrapolation from altimetry centerline profiles is examined by comparing simulated centerline mass balance estimates with sequential DEM differencing. The relationship between mass balance and the climate in the Glacier Bay area is examined through the use of a gridded climate data set.

Finally in section four, the mass balances are compared to mass change results from previous studies and to data from the Gravity Recovery and Climate Experiment (GRACE) mission, which is another geodetic method that uses satellite data to estimate mass distribution over broad regions. The pair of satellites records changes in gravity that are associated with changes in the distribution of mass on and within the Earth and can be used to estimate how much ice is being lost in an area. GRACE is currently able to detect surface mass changes at a 1 by 1 degree resolution (Luthcke et al., 2008; Arendt et al., 2009). The surface mass change can be converted to change in ice mass as long as variables that can affect mass distribution, like tectonic uplift and glacial isostatic adjustment, can be estimated and accounted for. The GRACE derived mass changes are used to examine regional ice loss and can be validated by the mass changes estimated with laser altimetry, e.g. Arendt et al. (2008).

Section five presents overall conclusions from this study. A case study on the tidewater retreat of Muir Glacier is presented in Appendix A.

1.1. Study Area

Glacier Bay is located directly adjacent to the Gulf of Alaska (Fig. 1). The vast mountains of the Fairweather Range (which contain some of the highest coastal mountains in the world), the Alsek Range, and the Chilkat Range are the result of the collision of the North American tectonic plate with ancient oceanic plates. Current tectonic activity in the area is dominated by the Queen Charlotte-Fairweather fault, which is a strike-slip fault located between the North American and Pacific plates. Mount Fairweather, which is only 25 km from the Pacific Ocean, is the highpoint of the Fairweather Range at 4,671 m and is the source of the Margerie, Grand Plateau, and

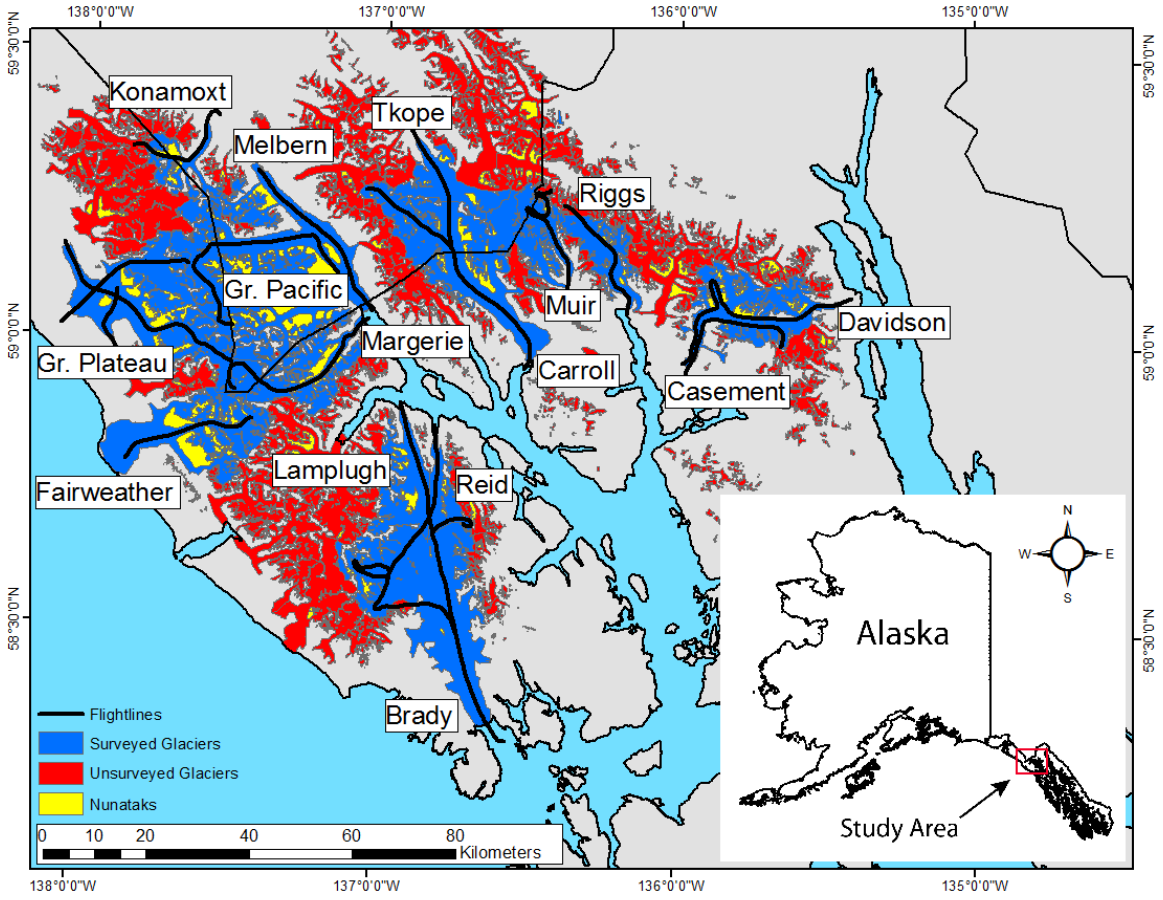

Fig. 1: Map of the Glacier Bay region showing which glaciers have been profiled with laser altimetry. Profiled glaciers are in blue, unprofiled glaciers are in red, and laser altimetry flightlines are in black.

Fairweather Glaciers. The maritime climate setting created by the Pacific Ocean, combined with the large vertical relief of the mountains, results in copious amounts of precipitation that feed the accumulation areas of Glacier Bay. The Fairweather Range is much higher, closer to the moisture source of the Pacific Ocean, and has steeper vertical relief than the more inland Alsek and Chilkat Ranges, resulting in the majority of the largest glaciers being located in the coastal Fairweather Range.

The Glacier Bay region is located to the west of Haines, Alaska and to the northwest of Juneau, Alaska and had an ice covered area of around 6427 km^2 as of August 2010 (Raup et al., 2007; J. Rich 2011, pers. comm.). The glaciated area is arrowhead shaped and ranges from 58˚ 19' N to 59˚ 45' N and spans from 135˚ 25' W to 138˚ 11' W (Fig. 1). There are two distinct areas of ice coverage: the western icefield glaciers located in the Fairweather Range, which includes Grand Pacific and Brady Glaciers, and the glaciers of the eastern icefield that are located northeast of the West Arm of Glacier Bay in the Alsek and Chilkat Ranges, which includes Carroll and Muir Glaciers. These two separate icefields were previously part of the much more extensive Glacier Bay Icefield that has experienced a massive glacial retreat since the end of the Little Ice Age (LIA) (Larsen et al., 2005).

1.2. Glacial History of Glacier Bay Since the End of the Little Ice Age

During the Last Glacial Maximum the Cordilleran Ice Sheet covered all of Southeast Alaska and advanced out onto the continental shelf (Kaufman and Manley, 2004). This ice sheet melted back approximately 20 kya with the termination of the Fraser glaciation until most of Southeast Alaska was ice-free. Periodic glacier advances have occurred in Alaska during the Holocene (Mann and Streveler, 2008; Connor et al., 2009). The most recent advance occurred during the LIA (Barclay et al., 2009), which was a period of cooling climate that started around the 16^{th} century and persisted until the mid-19^{th} century (Mann, 2002). During the LIA the open water of Glacier Bay had become entirely covered by the Glacier Bay Icefield (Molnia, 2007). Rapid retreat of the tidewater ice front occurred after the maximum ice extent was reached around 1770 (Larsen et al., 2005).

The Glacier Bay area has had documented glacier observations since 1794 when Captain George Vancouver first visited the area. At this time a survey party from Vancouver's expedition recorded that the southern terminus of the Glacier Bay Icefield was located at the mouth of Icy

Strait (the present location of the town of Gustavus). The maximum ice extent during the LIA is documented in time by radiocarbon dating of plant and animal material and in space by terminal moraines and other geomorphologic features (Connor et al., 2009). A submarine terminal moraine shows that the terminus reached into Icy Strait and was adjacent to Lemesurier Island sometime between 1725 and 1794. John Muir visited and documented glacier termini positions within Glacier Bay in 1879 and 1899; Harry Reid made observations in the 1890's, as did Israel Russell and William Field in the 1890's and 1900's. William Cooper and Field also did extensive work from the 1920's through the 1940's. These observations established the terminus location of various glaciers over an extended period of time and help to constrain the magnitude of glacier terminus retreat (Field, 1947), especially for the tidewater retreat of Muir Glacier up the East Arm of Glacier Bay.

Cooper (1937) extensively documented the glacial history of Glacier Bay prior to 1900. Retreat rates of Muir Glacier in the East Arm are recorded since John Muir first visited Glacier Bay in 1879, and Cooper reports a retreat rate of 2.7 km yr^{-1} between 1903 and 1907, after which recession slowed with only 3.2 km of retreat over the next 28 years. Field (1947) reports a recession of around 13 km for Muir Glacier between 1899 and 1913. By 1912 the ice front in the West Arm had retreated back to the present location of Grand Pacific Glacier terminus along the U.S-Canadian border (Clague and Evans, 1994); however the terminus of Muir Glacier was still around 30 km from the present-day terminus at this time.

Field also extensively documented the American Geographical Survey of 1941, which produced a new topographical map of the East Arm that has historic glacier terminus positions. At this time Muir and McBride Glaciers were still connected in a single ice front, but by 1945 Muir had retreated past McBride Glacier towards Riggs Glacier, leaving McBride with its own calving front. In 1945 the terminus of Muir Glacier had retreated back to within 15 km of the present terminus.

In the 1970's the East Arm had become mostly free of ice (Molnia, 2007), and by 1978 the terminus of Muir Glacier was within 2 km of the present terminus. Molnia (2008) summarized the retreat of Muir Glacier, which had an average retreat rate of 400 m yr^{-1} between 1886 and 1968, and in the 1970's the rate of retreat exceeded 1 km yr^{-1}. This makes the retreat of the Glacier Bay Icefield the largest glacier retreat in Alaska over the last 200 years, with a retreat of more than 100 km. This rapid tidewater retreat is a good analogue for glaciers within Alaska that are currently experiencing tidewater retreat like the Stikine Icefield, Icy Bay, and Columbia Glacier

(although on a smaller scale), and the current glaciated area in Glacier Bay is possibly a glimpse of how these retreating glaciers will appear in the future.

It is possible that the glacial retreat dynamics from the recession of the Glacier Bay Icefield are still present today, however it is not currently known if there are any remnant retreat dynamics that are influencing the glacial behavior at the present time. The rapid loss of ice in Glacier Bay since the LIA has also resulted in very high rates of ground uplift, with up to 3 cm per year of glacial isostatic adjustment occurring at the present (Larsen et al., 2005, Elliott et al., 2010).

2. DATA

The University of Alaska Fairbanks (UAF) has acquired laser altimetry data with three different systems since 1995. A scanning laser system was used to acquire the late summer 2009 through 2011 data, and two laser profiler systems were used between 1995 and early summer of 2009. The profiler systems have been described in previous publications (Echelmeyer et al., 1996; Sapiano et al., 1998; Arendt et al., 2002) and the data are treated in the same manner for both profiler systems. All data acquired during earlier missions have been reprocessed to create a consistent dataset for the entire UAF laser altimetry program. All data are now referenced in an Earth centered coordinate frame (ITRF00). The current laser scanner is a Riegl LMS-Q240i that has a sampling rate of 10,000 Hz, an angular range of 60 degrees, and a wavelength of 905 nm. The average spacing of laser returns both along and perpendicular to the flight path at an optimal height above the glacier surface of 500 m is approximately 1 m by 1 m, with a swath width of approximately 500 m. Each laser shot has a footprint diameter of about 20 cm. The current inertial navigation system (GPS-INS) is an Oxford Technical Solutions Inertial+ unit that has an update rate of 100 Hz.

The digital elevation model (DEM) that is used for glacier hypsometries (also known as the area altitude distribution or AAD) is derived from the Shuttle Radar Topography Mission (SRTM) DEM that was acquired in February of 2000. Larsen et al. (2007) found that the SRTM DEM has an accuracy of around ± 5 m over glaciers in Southeast Alaska and has no vertical frame bias. Herein, the SRTM is not used to determine mass balance or surface elevation changes through differencing with altimetry profiles. Rather it is used as the reference AAD. The surface area of each glacier is derived from glacier outlines made by the GLIMS project (Raup et al., 2007). Outlines utilized are based upon Landsat 7 images from August 1999 and August 2010, and on USGS topographic maps based upon air photos from 1948.

Laser altimetry is used in this study to find the mass balance ($\dot{B}$) for the Glacier Bay area. The glaciers located here have been profiled in 1995, 1996, 2000, 2001, 2005, 2009, and 2011 (Table 1). The glaciers were profiled very close to the same dates during the different years, with the difference being up to 11 days between 1995 and 2000. The difference between profile dates is small enough that the data are reported in the fixed date system. The Brady Icefield (Brady, Lamplugh, and Reid Glaciers) has been profiled the largest number of times, and has $\dot{B}$ for four different time periods. These time periods are: 1995 – 2000 (period 1), 2000 – 2005 (period 2),

2005 – 2009 (period 3), and 2009 – 2011 (period 4). A number of other glaciers have two or more time periods, while glaciers with two profiles include Little Jarvis, Tkope, and Konamoxt Glaciers.

Table 1: Date of laser altimetry flights for glaciers located in the Glacier Bay region. Profiles were acquired during the last week of May and the first week of June.

Brady	**Lamplugh**	**Reid**	**Grand Pacific**	**Muir**	**Margerie**
6/4/1995	6/4/1995	6/4/1995	6/6/1996	5/27/2000	6/2/2005
5/24/2000	5/24/2000	5/24/2000	6/6/2001	6/1/2005	6/2/2009
6/1/2005	6/1/2005	6/1/2005	6/2/2009	6/2/2009	5/30/2011
6/2/2009	6/2/2009	6/2/2009	5/30/2011	5/30/2011	
5/30/2011	5/30/2011	5/30/2011			
Riggs	**Casement**	**Davidson**	**Grand Plateau**	**Fairweather**	**Carroll**
6/1/2005	6/1/2005	6/1/2005	6/2/2005	6/2/2005	6/2/2009
6/2/2009	6/2/2009	6/2/2009	6/2/2009	6/2/2009	5/30/2011
5/30/2011	5/30/2011	5/30/2011	5/30/2011	5/30/2011	

This selection of glaciers includes a wide variety of glacier types (tidewater, lake calving, land terminating, and surge type), geometries, and sizes (Table 2). Most of the major glaciers of the Glacier Bay Icefield are included in the profiling. Glaciers with areas over 100 km^2 that are not profiled are Johns Hopkins (254 km^2), Alsek (244 km^2), LaPerouse (124 km^2), and McBride Glaciers (119 km^2). The total area of the profiled glaciers is 3328 km^2, which is 52% of the total glaciated area of the Glacier Bay region.

Table 2: Glaciers profiled with laser altimetry in the Glacier Bay region with attributes for glacier type, August 2010 area, area-weighted mean elevation, and the elevation range. Glacier types are land terminating (L), lake calving (LK), tidewater (T), and surge type (S). Reid Glacier is likely now land terminating, however it appears that high tides do still reach the terminus on occasion. Fairweather Glacier calves into a lake that is located in the middle of the stagnant terminus of the glacier.

Glacier	**Type**	**Area (km^2)**	**Mean Elevation (m)**	**Elevation Range (m)**
Brady	L	512	720	20 - 3640
Lamplugh	T	142	960	0 - 3120
Reid	L / T	70	800	0 - 1420
Casement	L	162	1160	100 - 2420
Davidson	LK	86	1180	20 - 1990
Riggs	L	116	1060	10 - 1910
Muir	L	131	1120	20 - 2020
Carroll	L / S	405	1030	50 - 2190
Tkope	L	117	1260	730 - 2060
Margerie	T / S	182	1680	0 - 4050
Fairweather	L / LK	279	880	10 - 4190
Grand Plateau	LK	403	1310	20 - 4190
Grand Pacific	T	565	1360	0 - 3730
Melbern	LK	82	1150	200 - 2350
Konamoxt	L	73	1310	200 - 2510
Little Jarvis	L	2	1230	840 - 1610

3. METHODS

3.1. Estimating Mass Balance

Glacier surface elevations were derived from the combination of airplane positioning and attitude data from the onboard GPS-INS, and the distance to the laser point returns from the glacier surface. The combination of these data determines the position in 3-dimensional space of the laser point on the glacier surface. The points are referenced in ITRF00 and coordinates are projected to WGS84 / UTM zone 8N. Elevation data are recorded as height above ellipsoid.

The glacier surface elevation profiles from different years are differenced to find the surface elevation change (Δh), and dividing by the time elapsed between profiles gives the rate of thickness change ($\Delta h/\Delta t$). This is determined with slightly different methods depending on whether data from the laser profiler (1995 – early summer 2009) or laser scanner (late summer 2009 – 2011) are being used.

For laser profiler to laser profiler differencing, points that are located within 10 m of each other in the x-y plane are selected as common points between the different years. If more than one point is located within that 10 m grid, then the mode of the elevation is calculated for each grid cell. Using the mode instead of the average elevation helps to filter out laser returns from crevasse bottoms. The elevations of common grid cells are then differenced to find $\Delta h/\Delta t$. Since data points are recorded only at nadir with the laser profiler it is critical that these earlier tracks were repeated as closely as possible to obtain a large number of common points. Sometimes the flights were not repeated closely enough to provide extensive elevation change measurements. For example, the elevation profile of Muir Glacier between 2005 and 2009 only has five common points over a large area between 1275 and 1800 m elevation. This limits the robustness of the interpolated line that is fit to the data, especially if there is variability within the data from surface roughness such as crevasses or snow drifting.

When comparing laser scanner to laser profiler for surface elevation differencing, a grid is made of the laser scanner swath at a resolution of 10 m. This grid is based upon the mode of all the points within each grid cell. Then, the coordinates from each point in the old profile are used to extract an elevation from this grid using bilinear interpolation (for all laser profiler points that fall within the new LiDAR swath extents). This interpolated elevation is then differenced with the laser profiler elevation at that point. The same idea is used for laser scanner to laser scanner

comparisons, but instead of using every point from the older laser scanner swath, the mode of laser return surface elevations on a 10 m by 10 m grid is calculated out of the old swath. A grid to grid subtraction then gives surface elevation differences.

The series of $\Delta h/\Delta t$ values vs. elevation along the entire glacier's flight line is modeled using a moving window that has a default window size of 12 data points. The moving window is used to find the $\Delta h/\Delta t$ quartiles over the elevation range of all the data points. The second quartile (median) values are then interpolated and smoothed, and are used as the modeled line for the $\Delta h/\Delta t$ vs. elevation curve. This method preserves the shape of the $\Delta h/\Delta t$ vs. elevation curve and is able to interpolate through elevations where there are sparse data points. The rate of volume change ($\Delta v/\Delta t$) in $km^3\ yr^{-1}$ is approximated by numerical integration of the modeled $\Delta h/\Delta t$ vs. elevation curve over the glacier specific SRTM AAD. This approximation relies on several assumptions discussed in later sections (3.3.3, 3.3.4, 3.3.5, and 4.7). A similar process is used to calculate $\Delta v/\Delta t$ based upon the lower and upper quartiles. The $\Delta v/\Delta t$ from these two quartiles are used to define the uncertainty of the $\Delta v/\Delta t$ from the interpolated $\Delta h/\Delta t$ that is defined using the median quartile. Elevation steps of 30 m are used for this integration.

$\Delta h/\Delta t$ is tied to zero at both the lower and upper elevation limits. This assumption is based on previous observations that have shown that the thickness changes at a glacier's head are generally near zero over time (Schwitter and Raymond, 1993; Rignot et al., 2003; Arendt et al., 2006). However, the assumption will not hold for a glacier or ice field that has an equilibrium line altitude (ELA) that is higher than the glaciers head, e.g. Yakutat Glacier (Larsen et al., 2007). Fortunately, there are no such glaciers located within Glacier Bay (except for the 6 km^2 Burroughs Glacier Remnant).

A limitation of this method is that winter and summer balances are not recorded and snow density measurements are also not taken, which necessitates invoking Sorge's law (Bader, 1954) to assume constant accumulation rates and a constant glacier density profile in the absence of these data. The mass balance rate ($\dot{B}$) is calculated assuming that the mass changes of the glacier are entirely ice, i.e. by applying Sorge's law. The calculated $\Delta v/\Delta t$ is converted to water equivalent (and therefore mass balance, with units of gigatonne (Gt) yr^{-1}) by assuming a constant glacier density where $\rho_{ice} = 900\ kg\ m^{-3}$. The specific mass balance rate, in units m w.e. yr^{-1}, is found by dividing the $\dot{B}$ of a glacier in Gt yr^{-1} by the total surface area of the glacier in m^2. The specific balance rate is useful in comparing the changes that occur on glaciers of various sizes as opposed to just using the total mass change in Gt yr^{-1}.

3.2. Regionalization

The measured mass balance rate of individual glaciers is extrapolated (a "regionalization") to all the unprofiled glaciers of the Glacier Bay region to estimate the total mass change that has occurred in Glacier Bay over the time period covered by the altimetry measurements. Regionalization is accomplished with two different methods. The first method is a normalized elevation method that normalizes the elevation from the $\Delta h/\Delta t$ vs. elevation curve, while the second is an area-weighted averaged $\dot{B}$ method. The magnitude of glacier surface elevation change is typically greatest at the current glacier terminus. However, the elevations of the terminus and head of individual glaciers are widely variable, as are elevations where greatest thickness change occurs (Table 2). This means that a direct averaging by elevation of thickness change across many glaciers will incorporate different responses for a given elevation. Arendt et al. (2006) built upon the results of Schwitter and Raymond (1993) to develop a normalized regionalization ("method B" in Arendt et al., 2006). Herein, only the elevation difference, which is defined by the glaciers' elevation range, is normalized while Arendt et al. (2006) normalized both the elevation difference and thickness changes. Normalizing the thickness changes would require the terminus elevation of each profiled glacier; any change in terminus elevations over the altimetry time period would also have to be accounted for.

The elevation range is normalized using the equation:

$$h_{norm} = (h - h_{term}) / (h_{head} - h_{term})$$

where h is the binned, interpolated elevation derived from the SRTM AAD, and h_{term} and h_{head} are the elevations of the glacier terminus and head. This normalization is applied to all of the glaciers that have been profiled during a particular time period. An average normalized curve is then calculated for each altimetry time period. This $\Delta h/\Delta t$ vs. average normalized elevation curve is then integrated over the AAD of unprofiled glaciers to find the $\dot{B}$ of those glaciers.

The normalization method is applied individually to the eastern and western glacierized regions of Glacier Bay as shown in Fig. 2. This was done due to the notably different AADs of the two areas (Fig. 3); the peak in glacier area of the eastern region is close to the median elevation, while in the western region a large portion of the glacier area is located at the lower end of the elevation range. The western region also has glaciers that reach a much higher elevation than those in the eastern region. The AADs are so different that applying the $\Delta h/\Delta t$ vs. average normalized elevation curve to the AAD of the entire Glacier Bay region would give mass

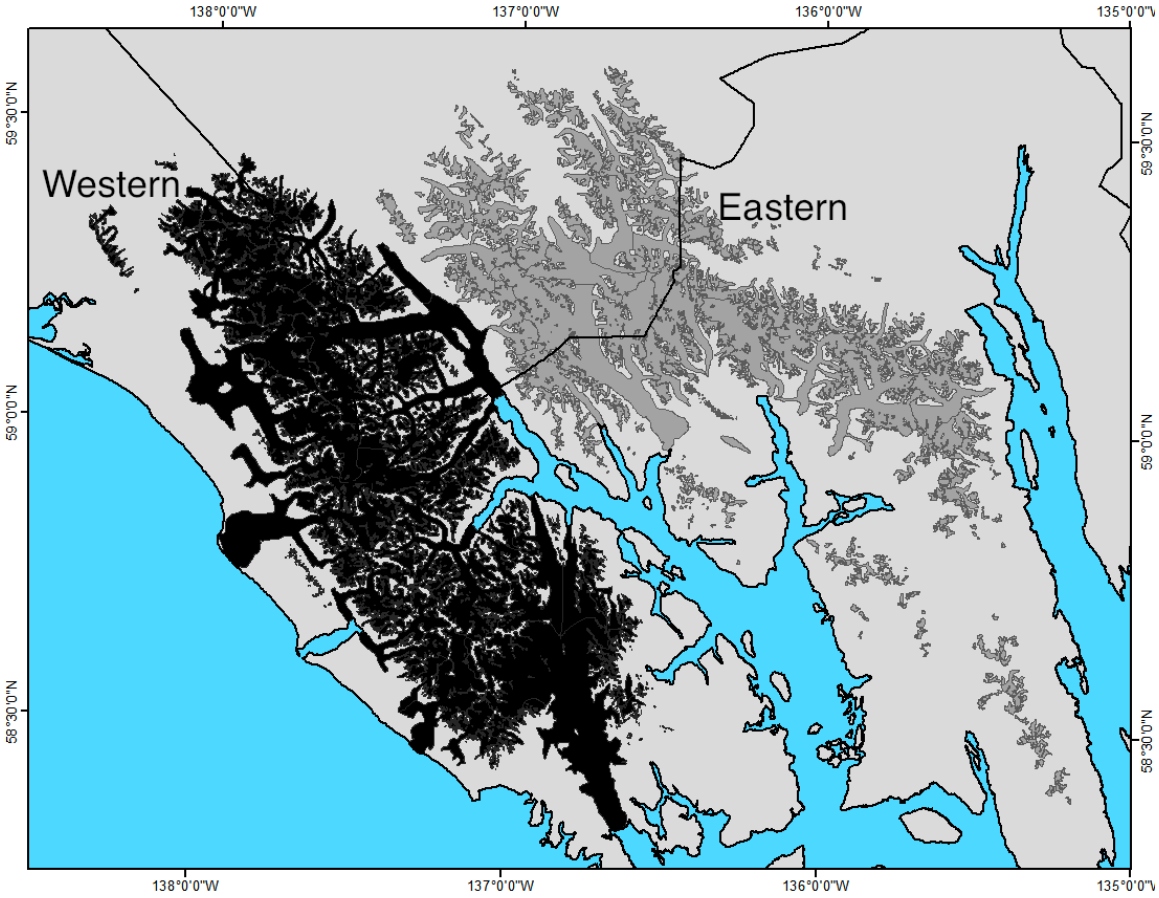

Fig. 2: The two glaciated regions of Glacier Bay. The eastern region glaciers (2,618 km^2 as of August 2010) are in gray and include the glaciers to the northeast of Grand Pacific Glacier and the West Arm of Glacier Bay. The western region glaciers (3,810 km^2, August 2010) are in black and lie to the west of the West Arm.

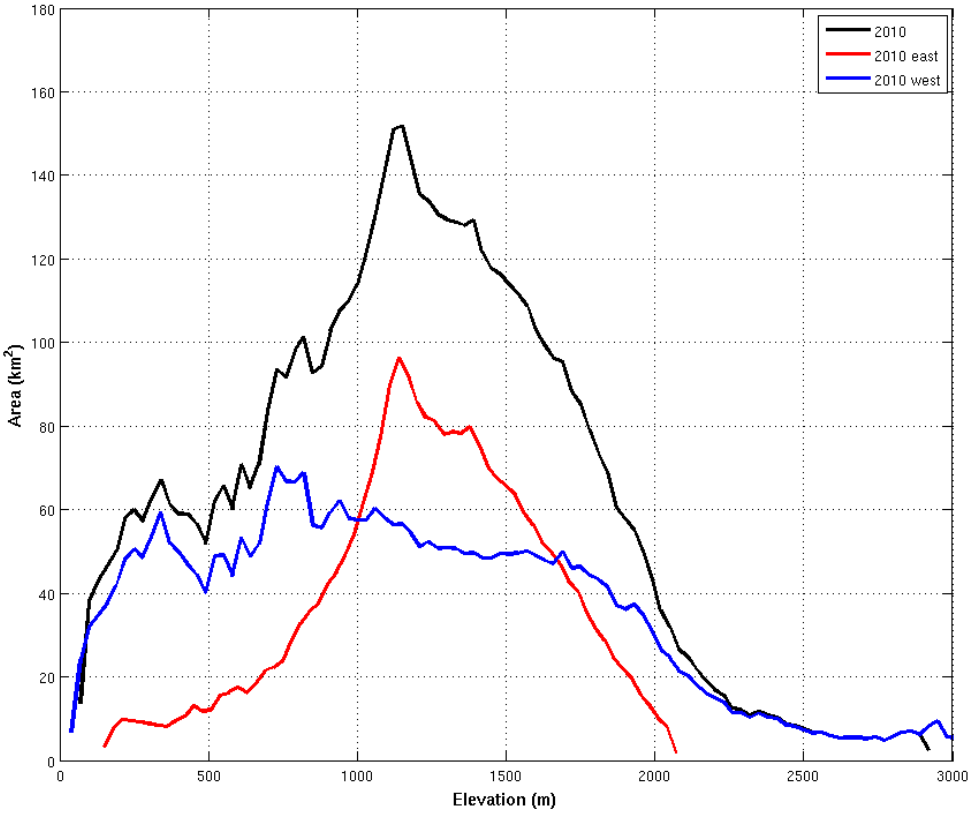

Fig. 3: The area altitude distribution (AAD) of glaciers in the Glacier Bay area is calculated using 2010 glacier outlines and the SRTM DEM from 2000. The black line shows the AAD of the entire Glacier Bay area, while the red and blue lines are the AAD of the eastern and western glaciated regions of Glacier Bay. The eastern region, which includes Carroll and Muir Glaciers, has an AAD that is generally typical of glaciated regions. The peak in glacier area at 1,150 m occurs close to the median elevation (1,110 m) of the eastern region. The western region includes Grand Plateau and Grand Pacific Glaciers and the Brady Icefield, all of which have a large amount of surface area located at lower elevations. This accounts for the much different shape of the AAD of the western region, with the peak in glacier area occurring at the lower end of the elevation range. The glaciers in this region also reach a much higher peak elevation due to the presence of the Fairweather Range.

change results that were not representative for either the eastern or western regions. Theoretically, the average normalized elevation vs. $\Delta h/\Delta t$ curve could be applied to the AAD of each of the unprofiled glaciers within the Glacier Bay region, of which there are more than 1,000. The separation into eastern and western regions is a compromise between not having to extrapolate to each unprofiled glacier (requiring glacier outlines and the AAD for each glacier) while still using an AAD that is broadly representative of the region that is being extrapolated to.

Performing this regionalization gives estimates of the mass change of the unprofiled glaciers during each of the four altimetry time periods of the entire Glacier Bay region. The mass change of the unprofiled glaciers is then added to the measured mass change of the profiled glaciers. This gives an estimate of the mass change and the resulting contribution to SLR of the entire Glacier Bay region for each altimetry time period

The second regionalization method that is used is based on "method C" from Arendt et al. (2006) and applies the area-weighted average of all the profiled glaciers $\dot{B}$ (in m w.e. yr^{-1}) to all of the unprofiled glaciers in Glacier Bay for a particular period. This method is particularly useful if the AAD of the unprofiled glaciers is not well known, and only requires knowledge of the total surface area of the unprofiled glaciers.

A challenge in performing a robust regionalization of the total ice mass change of an area is determining whether the profiled glaciers are representative of the region. To examine this issue, sensitivity analyses are carried out by removing profiled glaciers from the regionalization of a given interval. This simulates what the measured $\dot{B}$ would have been if that particular glacier was never profiled with altimetry. Comparing the amount of variation within the results of the sensitivity analyses to the mass change estimates can give an idea of whether the group of selected glaciers as a whole is representative of the entire glaciated area.

Mass balance has only been recorded for a select few glaciers during periods 1 and 2. The profiles that occurred in 2005, 2009, and 2011 were more complete by encompassing many more glaciers, thus a comprehensive sensitivity analysis is more meaningful for those time periods. In particular, period 3 has $\dot{B}$ recorded for 9 glaciers and period 4 has $\dot{B}$ for 14 glaciers. The Glacier Bay region has a variety of glacier geometries, so applying the most representative thickness change function to the unprofiled glaciers is important to accurately determine the mass balance rate of those glaciers. For instance, as previous authors have shown (e.g., Arendt et al., 2006), it is clearly unwise to apply the thickness change profile of a rapidly calving tidewater glacier to a terrestrial glacier due to tidewater glacier dynamics, even if they have similar geometries.

However, it has to be considered whether the same limitation occurs for tidewater or previously tidewater glaciers that are currently not rapidly retreating.

3.3. Errors and Uncertainties in Mass Balance Estimations

The error in laser altimetry derived mass balance consists of several different components that have been described in previous studies (Echelmeyer et al., 1996; Arendt et al., 2002; Arendt et al., 2008). First, there are instrument errors that include laser ranging errors and GPS-INS errors of the kinematic positioning of the aircraft. Second, there is a curve fitting (model) uncertainty created by the choice of the interpolation that is used to model the $\Delta h/\Delta t$ vs. elevation profile. Third, there are across-glacier $\Delta h/\Delta t$ uncertainties arising from the assumption that the thinning at the centerline is representative of the width of the glacier. Fourth, there are uncertainties that are introduced by using a single glacier outline in the mass change calculations. This outline uncertainty is dependent on whether the surface area of the glacier changes between profile dates. Fifth, the assumption of $\rho_{ice} = 900$ kg m^{-3} creates a density uncertainty. There is assumed to be no seasonal error due to the profile dates being located within a week of each other at the end of May and beginning of June.

3.3.1. Positioning Errors

The dominant error in the positioning of laser shot points is the positioning of the aircraft along its trajectory, which includes measurement errors from the kinematic GPS solution and attitude errors from the onboard GPS-INS. The laser ranging error is quite small at ± 0.002 m for all of the laser systems used by UAF. Aircraft GPS positioning errors are on the order of ± 0.2 m and the effect of attitude errors can lead to a laser shot point coordinate error of ± 0.2 m. Errors were estimated by analyzing repeat profiles that occurred on unchanging surfaces such as paved airport runways. These errors are considered to be independent, resulting in a net positioning error of ± 0.3 m. Attitude errors are larger with the profiler system than with the scanner system. The profiler system has INS attitude errors of ± 0.2° that can lead to laser point-positioning errors of ± 0.2 m, while the scanner system has INS attitude errors of ± 0.02° that can lead to associated positioning errors of ± 0.02 m. A worst-case attitude error would occur when the aircraft's attitude had a steep angle relative to the glacier surface. Typically the profiler system was flown

at an elevation of 250 m above the glacier surface, which could result in an attitude error induced positioning error of the laser return of ± 0.58 m at an attitude of 30° relative to the glacier surface. The scanner system at a typical flight elevation of 500 m has a similarly derived attitude positioning error of ± 0.19 m. The more accurate GPS-INS of the scanner system leads to higher laser point positioning accuracy than the profiler system at the typical flight altitudes of each system. The effects of attitude measurement errors on laser point positioning are minimized when the angle between the aircraft and glacier surface is near zero; for instance the less accurate profiler would have an attitude positioning error of ± 0.002 m under level flight situations over a flat glacier. GPS positioning errors are dependent on a number of variables that change with time and can be difficult to quantify. These variables include atmospheric delays, geometric strength of GPS constellations, variable ionosphere characteristics, and variable distances from the reference station to the kinematic GPS on board the aircraft. A complete error analysis of the coordinates of laser returns would incorporate those variables and the full covariance matrix from the GPS-INS solution. However, this analysis is not done here; rather we adopt the positioning error of ± 0.2 m from Echelmeyer et al. (1996) and Arendt et al. (2008).

3.3.2. Modeled Δh/Δt Uncertainties

The uncertainty of the modeled Δh/Δt vs. elevation curve is estimated using the lower and upper quartiles. These quartiles are determined by using a 12 point window that moves through the elevation range of the Δh/Δt vs. elevation curve. Since the lower and upper quartiles are not always equally spaced from the median the positive and negative uncertainties will not necessarily be the same for each quartile, which means that the plus and minus mass balance errors can be different for a glacier. The Δh/Δt uncertainty for elevations above which there are no Δh/Δt data is determined by applying the full interquartile range of all the Δh/Δt points for all elevations and results in a typical spread of less than ± 1.0 m yr^{-1} at the glacier's head. The individual glacier uncertainties are propagated in quadrature sum along with the positioning errors to estimate the mass change error for the entire Glacier Bay region.

3.3.3. Across Glacier Δh/Δt Uncertainties

The glacier-wide mass balance extrapolation scheme of laser altimetry relies on the assumption that the thinning that is measured along the centerline is constant across the width of the glacier. Berthier et al. (2010) raised a number of points of why this assumption may be flawed. They examined the ice loss from Alaskan glaciers by differencing the elevations of sequential DEMs. Their study indicated that the ice loss had been overestimated with the laser altimetry method of using centerline surface elevation profiles (Arendt et al., 2002) by 34%. Berthier et al. (2010) also compared the DEM derived ice loss to laser altimetry-simulated (simu-laser) ice loss for ten large Alaskan glaciers, wherein the glacier elevation changes along laser altimetry flight lines were extracted from the difference DEM. This was done to test the assumption in the laser altimetry method that the thinning along a glacier's centerline is representative of the width of the glacier. Situations where this assumption may be incorrect include tidewater glaciers that have varying retreat rates in different branches and glaciers that have gently sloping valley walls. However, Alaskan glaciers generally are located in U-shaped valleys with steep valley walls and have cross sections that retain a consistent geometry and shape over time.

The centerline difference DEM profiles were used by Berthier et al. (2010) to simulate the ice loss that would have been estimated from having centerline altimetry profiles. The Δh/Δt values extracted along the simulated profiles were assumed to be representative of the glacier width, and these Δh/Δt values were integrated over the AAD to calculate mass balance ($\dot{B}$), following the same methodology as laser altimetry mass balance estimates. Berthier et al. (2010) found that the simu-laser ice loss for the ten selected Alaskan glaciers exceeded the sequential DEM derived ice loss by 22%, which indicates that the laser altimetry method is overestimating mass loss of Alaskan Glaciers due to centerline thinning not being representative of the width of a glacier. In their analysis they assumed that the glaciers tested with the simu-laser method are representative of the rest of Alaskan Glaciers. However, their results are dominated by Columbia Glacier (a rapidly retreating tidewater glacier) and Bering Glacier (a surge type glacier, which is also the largest glacier in Alaska).

Herein, we similarly examine whether the centerline extrapolation method is overestimating mass loss by comparing DEM differencing to simulated DEM centerline extrapolations. There are no glaciers in Glacier Bay that have geometries and characteristics similar to the Columbia and

Bering Glaciers. This compels an examination of whether centerline thinning is representative across-glacier in the Glacier Bay region. The sequential DEMs that are used for the Glacier Bay area are derived from Larsen et al. (2007). The full results are presented in section 4.6. In summary the DEM and simulated centerline $\dot{B}$ estimations were found to be within 1% over all the altimetry profiled glaciers in the Glacier Bay region, and within 6% over a glacierized area of 5143 km^2, or 80% or the total glaciated area of Glacier Bay.

3.3.4. Outline and AAD Uncertainties

A single outline is used here for determining the glacier surface area. If a glacier's area is changing over time, the extrapolated mass change calculations will either be including area that is no longer glacierized in a retreating glacier, thus having a mass change that is too high, or excluding area that has recently become glaciated if the glacier is advancing. However, using a single outline gives the reference-surface balance (Elsberg et al., 2001; Huss et al., 2012), which has been proposed to be better correlated to variations in climate. The conventional balance is calculated using multiple outlines that are coincident with the mass balance measurements and provides the actual mass change of a glacier (Elsberg et al., 2001).

The effect of using outlines from different dates is tested using outlines from 2010, 1999, and 1948 to determine how the $\dot{B}$ estimates vary by only changing the glacier surface area that is used. This affects both the amount of area over which the mass change is calculated and the spatial extent of the DEM that is used to determine the AAD. The difference in $\dot{B}$ that results from using the most recent glacier outlines from 1999 and 2010 is within the $\dot{B}$ uncertainties for the four different periods. The $\dot{B}$ uncertainty of period 4 is ± 0.47 Gt yr^{-1} for the profiled glaciers, while the $\dot{B}$ of the profiled glaciers was only 0.15 Gt yr^{-1}, or 3%, more negative when using 1999 outlines as compared to using 2010 outlines. This error is not propagated to the mass balance error; however, it does show that using different outlines during the period of altimetry measurements has little effect on the mass balance estimates and thus a minimal effect on both conventional and reference-surface balances. A worst case scenario would be using outlines from topographic maps that were based upon air photos from 1948, which is 47 years before the first altimetry profiles. In this case, the $\dot{B}$ for period 4 using 1948 outlines was 0.54 Gt yr^{-1}, or 13%, more negative than using 2010 outlines.

3.3.5. Density Assumption

There are no density measurements recorded on the glaciers that are profiled. The density profile of the snow, firn, and ice is thus assumed to remain constant by invoking Sorge's Law (Bader, 1954), which assumes a glacier has a constant density structure. A change in the density structure of a glacier (particularly in the accumulation area) could be recorded as change in ice mass, when in fact there was no change in ice mass. The effect on $\dot{B}$ of changing the overall glacier density is examined by using different ice densities (ρ_{ice} = 830 kg m^{-3} and 917 kg m^{-3}) in the same manner as previous studies, e.g. Arendt et al. (2008), in the place of the assumption used here of 900 kg m^{-3}. The effect on $\dot{B}$ of using these minimum and maximum densities is well within the $\dot{B}$ uncertainties and the percent difference between $\dot{B}$ estimates is around 10%. For example, period 4 had an uncertainty of $\pm$ 0.47 Gt yr^{-1} for the profiled glaciers, while using the different densities of 830 kg m^{-3} and 917 kg m^{-3} produces $\dot{B}$ estimates for the same period that only vary by 0.36 Gt yr^{-1}. This error estimate is also not propagated to the final mass balance error. The density error does show that the effect of using different ice densities is small when compared to the total mass change and the error in the mass change estimates. Additionally, the majority of a glacier's mass loss occurs in the ablation area where variations in glacier density are reduced.

4. RESULTS AND DISCUSSION

4.1. Brady Icefield

The mass balance ($\dot{B}$) for Brady, Lamplugh, and Reid Glaciers between 1995 and 2000 (period 1) was -1.01 ± 0.13 m w.e. yr^{-1}, -0.31 ± 0.21 m w.e. yr^{-1}, and -0.30 $^{+0.21}_{-0.22}$ m w.e. yr^{-1} respectively (the different plus/minus estimates are not systematic errors but are a result of the method that is used to calculate the quartiles that are used to define the uncertainty). The $\dot{B}$ was then more negative between 2000 and 2005 (period 2), with $\dot{B}$ of -1.83 $^{+0.19}_{-0.15}$ m w.e. yr^{-1}, -0.53 $^{+0.22}_{-0.21}$ m w.e. yr^{-1}, and -0.93 $^{+0.15}_{-0.16}$ m w.e. yr^{-1} respectively. The more negative mass balance was likely caused by higher than average temperatures during the 2004 summer melt season (Truffer et al., 2005), which would increase the rate of ablation through increased melting. Brady Glacier had a rate of thickness change ($\Delta h/\Delta t$) of -3 to -4 m yr^{-1} at the terminus during both periods; however the major contributing factor to the more negative $\dot{B}$ during period 2 was increased thinning at higher elevations. For example, the $\Delta h/\Delta t$ of Brady Glacier during period 2 is more negative than period 1 at elevations above 300 m (Fig. 4).

The time period from 2005 to 2009 (period 3) had substantially less negative mass balances than period 2, with $\dot{B}$ of -0.73 $^{+0.22}_{-0.17}$ m w.e. yr^{-1} (Brady), -0.10 $^{+0.25}_{-0.28}$ m w.e. yr^{-1} (Lamplugh), and -0.10 $^{+0.16}_{-0.17}$ m w.e. yr^{-1} (Reid). The $\dot{B}$ of period 3 was less negative than both periods 1 and 2. The $\Delta h/\Delta t$ was significantly less negative for elevations below 400 m on Brady Glacier, with $\Delta h/\Delta t$ changing from -3 m yr^{-1} during periods 1 and 2 to -1 m yr^{-1} during period 3 (Fig. 4).

The time period from 2009 to 2011 (period 4) had $\dot{B}$ magnitudes that were similar to period 3 for Lamplugh and Reid, with a $\dot{B}$ of -0.06 $^{+0.22}_{-0.16}$ m w.e. yr^{-1} and -0.14 $^{+0.25}_{-0.31}$ m w.e. yr^{-1} respectively. However, the $\dot{B}$ for Brady was -1.44 $^{+0.16}_{-0.21}$ m w.e. yr^{-1}, which is twice as negative as the $\dot{B}$ of period 3 (this period had the least negative $\dot{B}$) and close to the $\dot{B}$ of period 2 (which had the most negative $\dot{B}$).

4.2. Muir Glacier

The Muir Glacier had a $\dot{B}$ of -0.47 $^{+0.28}_{-0.29}$ m w.e. yr^{-1} during period 2. The glacier had some thickening of around 0.5 m yr^{-1} at elevations between 600 m and 1200 m (Fig. 5). There was also

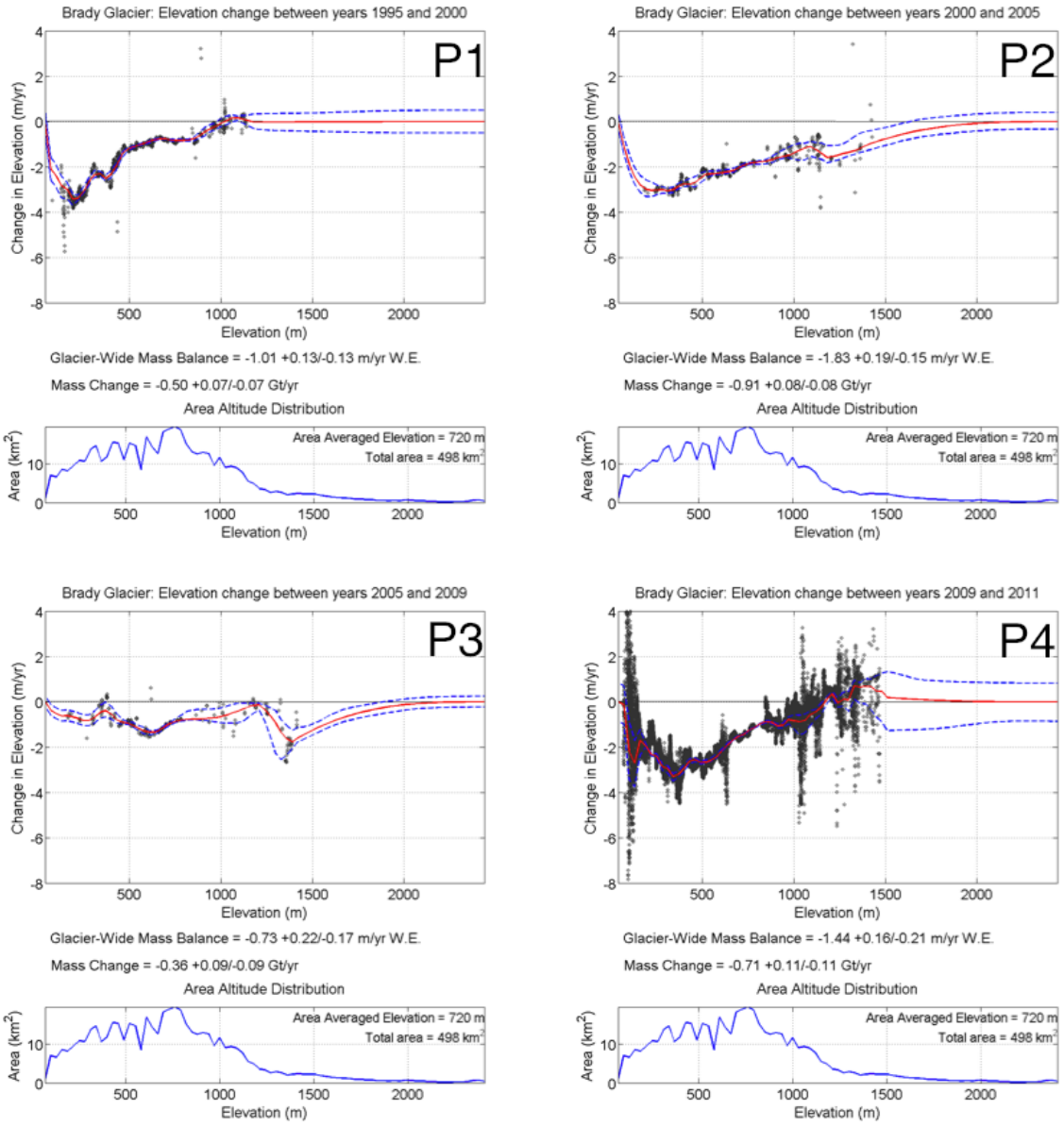

Fig. 4: Rate of thinning profile for Brady Glacier during periods 1 through 4. Red line is the modeled $\Delta h/\Delta t$ vs. elevation curve that is determined from the middle quartile of the moving window, while the dashed blue lines are the lower and upper quartiles that are used to estimate uncertainty. The smaller plots show the area altitude distribution of the glacier in solid blue lines. The period 2 profile shows the increased thinning rates and the surface drawdown at elevations above 300 m as compared to period 1. The period 3 profile shows the less negative $\dot{B}$ as compared to period 2, with lower rates of thinning below 1000 m during period 3. Period 4 had the same magnitude of maximum thinning rates as periods 1 and 2 along with slight thickening at higher elevations.

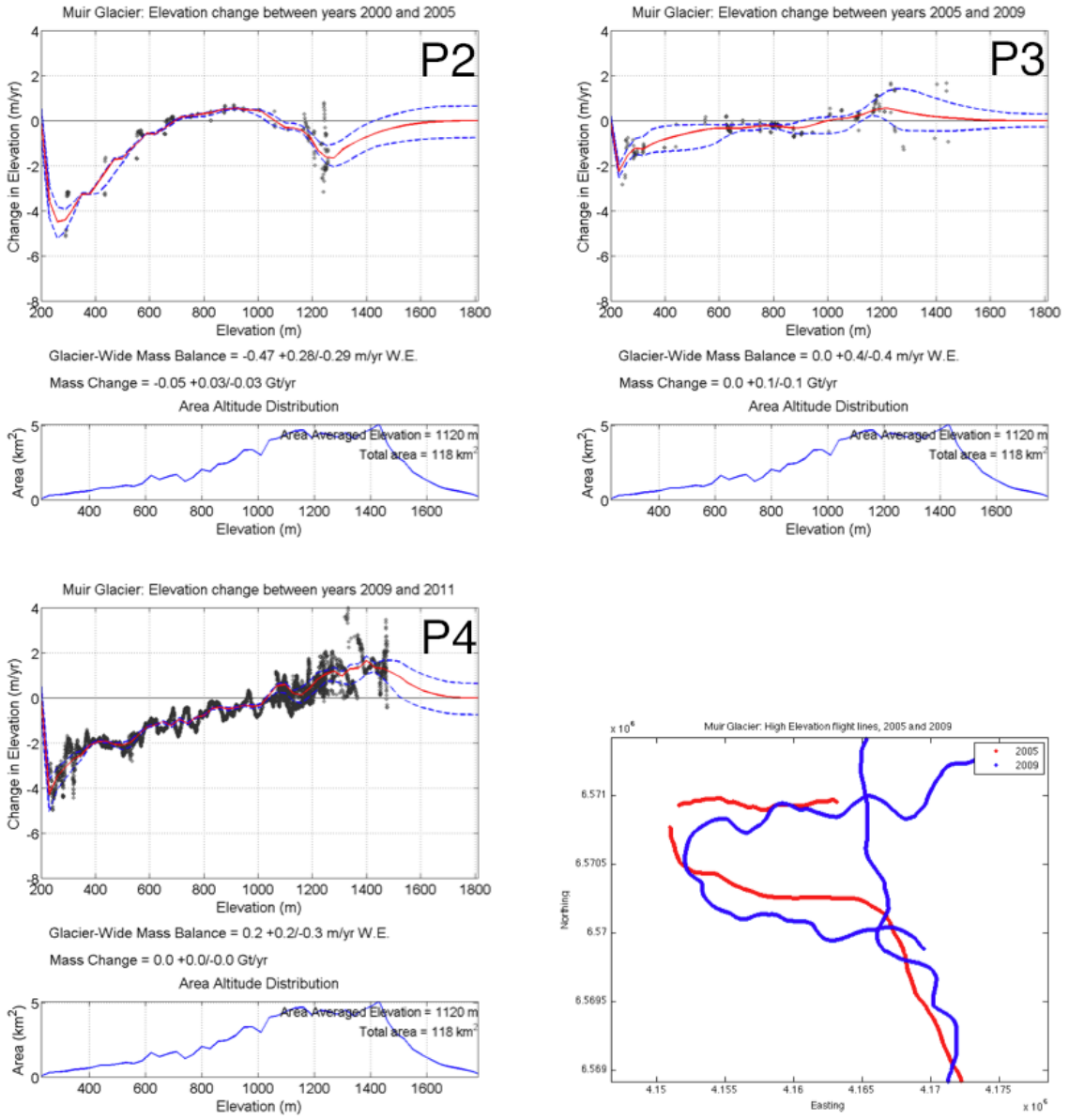

Fig. 5: Rate of thinning profile for Muir Glacier during periods 2 through 4 shows the thickening at higher elevations. The sparse distribution of points up high during period 3 shows how crucial it was to have the repeated flight lines flown as accurately as possible. This results in a large error envelope between 1200 and 1400 m due to the small number of points and the large variability in the $\Delta h/\Delta t$ of those points. The bottom right panel shows the period 3 flight lines from 2005 (red) and 2009 (blue) and demonstrates the lack of overlap between the two flight lines.

some thickening at higher elevations during period 3 that approaches 1 m yr^{-1} between 1000 m and 1300 m (Fig. 5), however the magnitude of thinning at lower elevations was decreased during period 3 when compared to period 2. The slight thickening up high resulted in the glacier being near balance during period 3, with a $\dot{B}$ of 0.05 ± 0.43 m w.e. yr^{-1}. This response seems to be consistent with the results from periods 2 and 3 for the Brady Icefield, with a more negative $\dot{B}$ during period 2 compared to period 3. During period 4 Muir had a $\dot{B}$ of $0.22\ ^{+0.18}_{-0.30}$ m w.e. yr^{-1}, and also had thickening above 1000 m (same as periods 2 and 3) which approaches 1.75 m yr^{-1} at 1400 m (Fig. 5). There is significant thinning that occurred at the terminus during period 4 with a $\Delta h/\Delta t$ of -4 myr^{-1}, which is consistent with the response of Brady Glacier (reduced thinning during period 3 compared the periods 2 and 4). However, the thickening during period 4 at higher elevations is located where the glacier has a lot surface area and results in the glacier having an overall positive $\dot{B}$.

4.3. Other Glaciers

A number of other glaciers have mass balances for multiple time periods, including Grand Pacific Glacier, which had a mass balance ($\dot{B}$) of -0.47 ± 0.34 m w.e. yr^{-1} during period 1. There is a small area of thickening around 500 m, above which $\Delta h/\Delta t$ was around -1 m yr^{-1} (Fig. 6, which shows the spatial distribution of thinning derived from centerline extrapolation). Below this elevation $\Delta h/\Delta t$ approached -4 m yr^{-1}. There is no period 2 or period 3 as Grand Pacific was not profiled in 2005 (see absence in Fig. 7), however the combined period from 2000 to 2009 had a more negative $\dot{B}$ of $-1.16\ ^{+0.80}_{-0.36}$ m w.e. yr^{-1}, with a maximum $\Delta h/\Delta t$ of around -4 m yr^{-1}. Period 4 had a $\dot{B}$ of $-1.63\ ^{+0.48}_{-0.51}$ m w.e. yr^{-1}, which is the second most negative $\dot{B}$ during period 4, and had a terminus $\Delta h/\Delta t$ that approaches -7 m yr^{-1}.

During period 3 Riggs Glacier had a $\dot{B}$ of $-0.41\ ^{+0.17}_{-0.18}$ m w.e. yr^{-1}. The thinning profile is similar to Muir Glacier below 1100 m. However, Riggs had no thickening above this elevation whereas Muir did (Fig. 8). This response is intriguing as the accumulation areas of the two glaciers are directly adjacent to each other. The $\dot{B}$ during period 4 was more negative at $-0.92\ ^{+0.19}_{-0.22}$ m w.e. yr^{-1}, with increased thinning below 800 m compared to period 3. The same spatial pattern during period 3 is present during period 4, with Muir and Riggs having similar thinning profiles below 1000 m; above 1000 m Riggs had no thickening whereas Muir had thickening around 1.75 m yr^{-1} (Fig. 9).

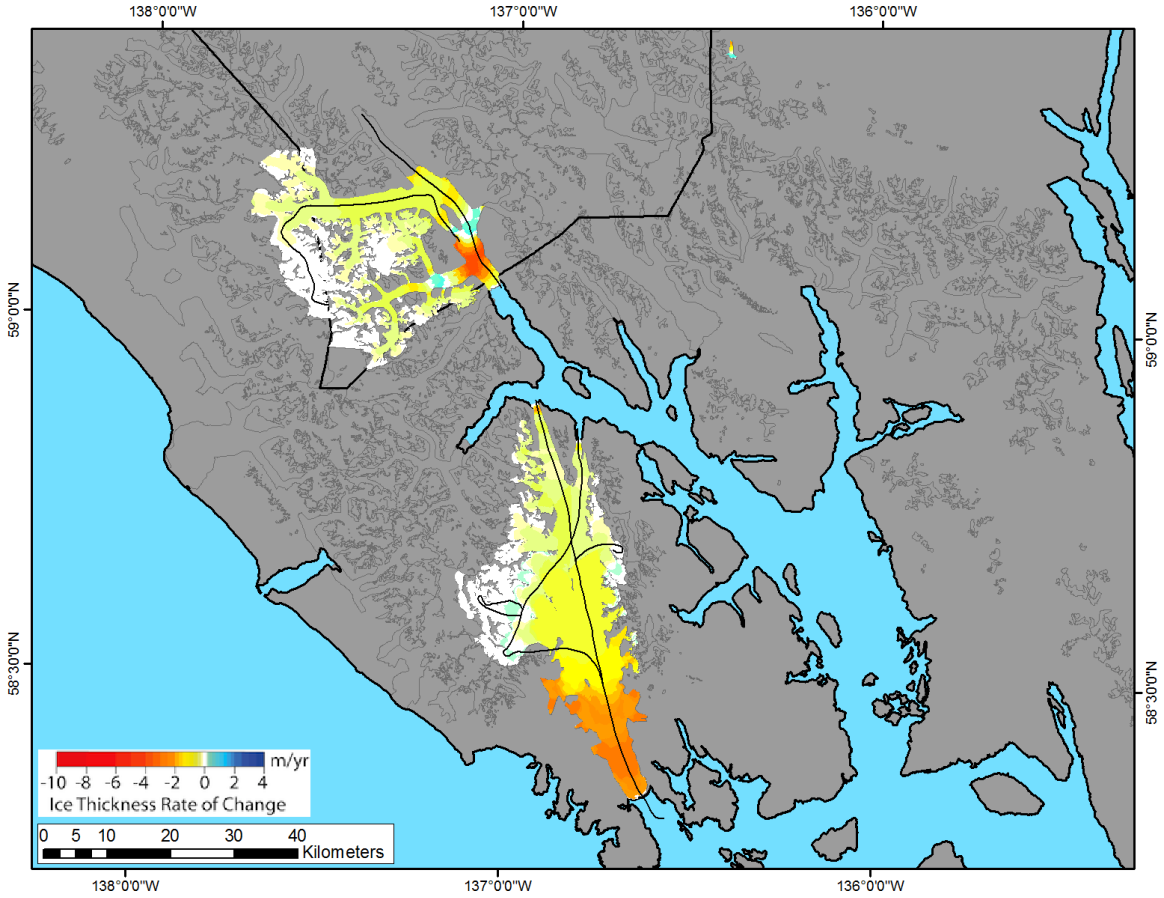

Fig. 6: Change in glacier surface elevation between 1995 and 2000 (period 1) for 5 glaciers in the Glacier Bay area. The black lines lying over glacier surfaces are the laser altimetry flightlines used to calculate surface thinning rates. These flightlines generally follow glacier centerlines. The centerline thinning rates are then extrapolated across the width of entire glacier to obtain the spatial distribution of thinning shown here that is used to estimate the mass balance of the entire glacier. Little Jarvis Glacier is small glacier at top center. Brady Icefield is at the bottom and Grand Pacific is at top left; Grand Pacific had a small area of thickening up glacier from the terminus.

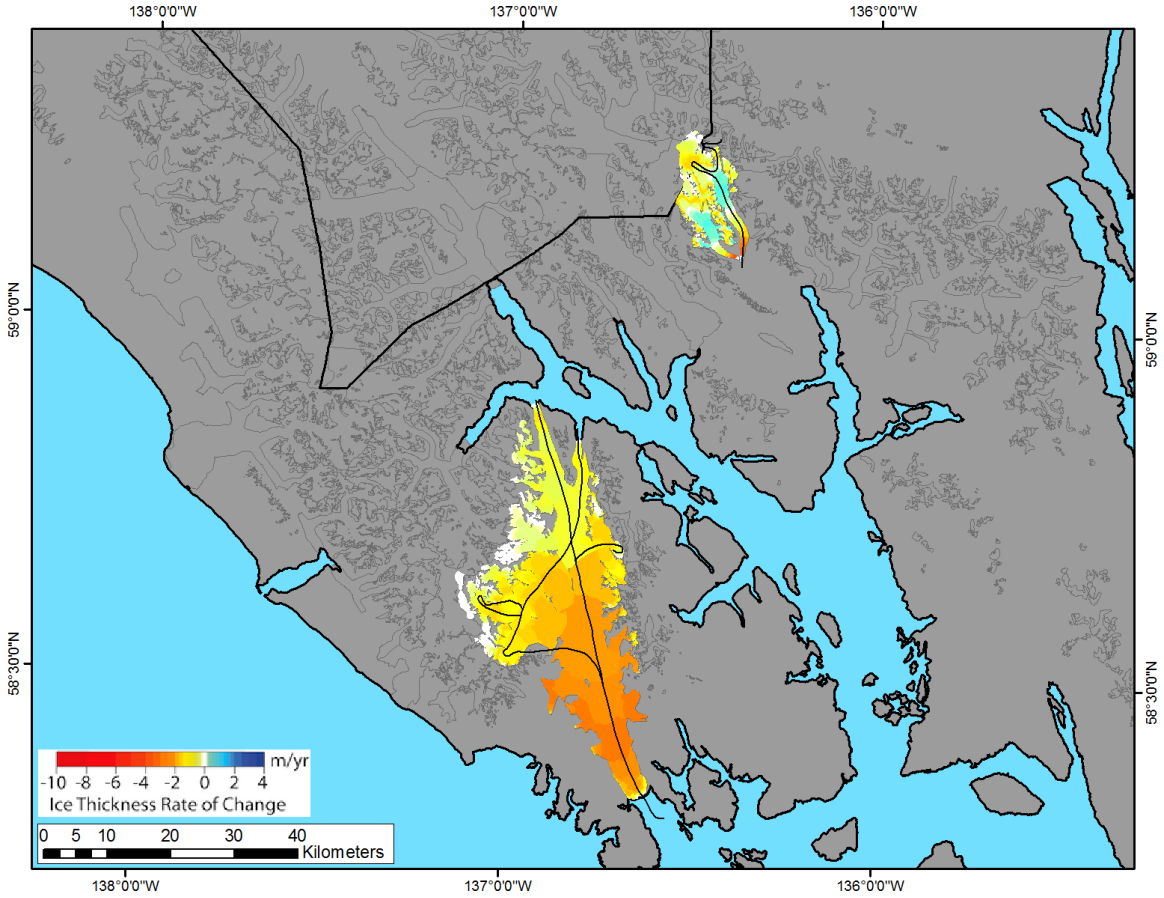

Fig. 7: Change in glacier surface elevation between 2000 and 2005 (period 2) for 4 glaciers in the Glacier Bay area. Brady Glacier (southern part of Brady Icefield) had increased thinning over a large area compared to the earlier period 1. Muir Glacier is at top right-center and had thickening at the middle elevations of the glacier. Note the absence of Grand Pacific Glacier as it was not profiled in 2005.

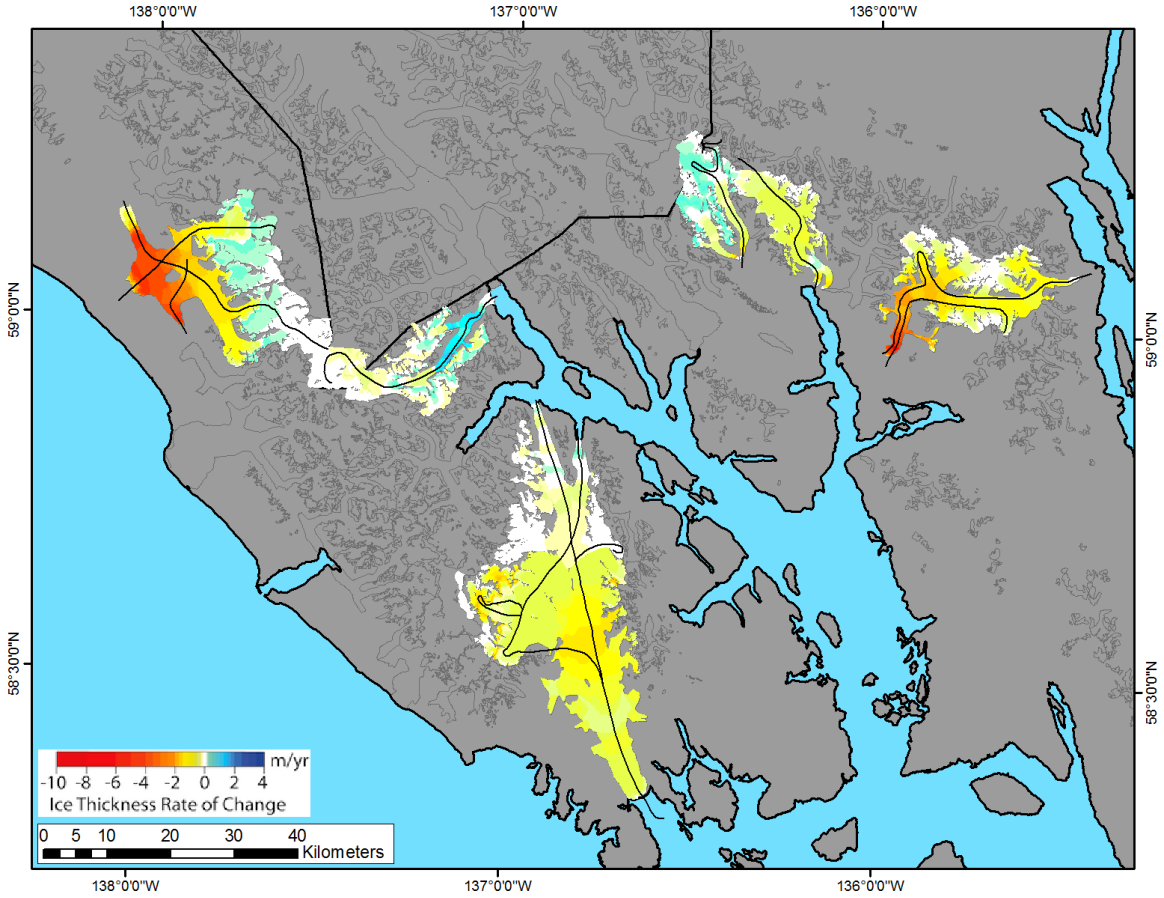

Fig. 8: Change in glacier surface elevation between 2005 and 2009 (period 3) for 9 glaciers in the Glacier Bay area. Brady Glacier had a large area of reduced thinning compared to period 2. Riggs Glacier, located just east of Muir Glacier, had no thickening at higher elevations while Muir did. Casement and Davidson Glaciers are at the far right; Casement had an area of much higher thinning at its terminus than Davidson. Margerie Glacier calves into the northern-most portion of the West Arm and had thickening over much of its area. The glacier at the far left with an extensive area of high thinning is the lake calving Grand Plateau Glacier.

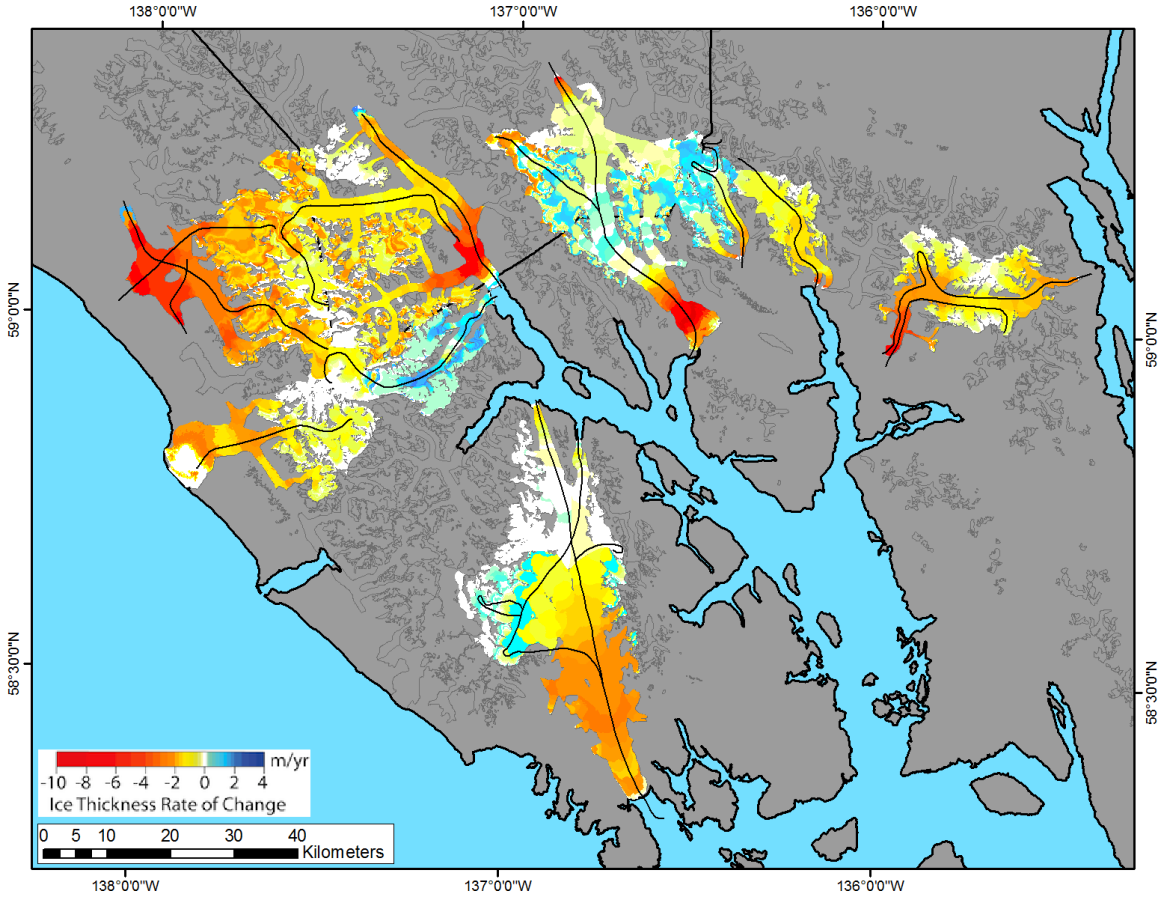

Fig. 9: Change in glacier surface elevation between 2009 and 2011 (period 4) for 14 glaciers in the Glacier Bay area. Increased thinning is observed over most of the glaciers, with the highest thinning rates at the termini of Grand Plateau, Grand Pacific, Carroll, and Casement Glaciers. There are indications of a small surge occurring at the upper region of Carroll Glacier, with a drawdown of around 3 m yr^{-1} at higher elevations and thickening of around 2 m yr^{-1} over middle elevations.

During period 3 Casement Glacier had a $\dot{B}$ of -1.11 $^{+0.20}_{-0.25}$ m w.e. yr^{-1}, which is more negative than the $\dot{B}$ of adjoining Davidson Glacier (-0.68 $^{+0.23}_{-0.22}$ m w.e. yr^{-1}). Both glaciers had a rate of thickness change ($\Delta h/\Delta t$) of around -1 m yr^{-1} at the flow divide that separates them at an elevation of around 1200 m, but Casement had a much higher $\Delta h/\Delta t$ below 600 m. It had the highest terminus thinning of the profiled glaciers during period 3, with a $\Delta h/\Delta t$ of -6 m yr^{-1} at the terminus of Casement (Fig. 8). For comparison, Davidson had a terminus $\Delta h/\Delta t$ close to 0 m yr^{-1} during period 3. Casement then had a more negative $\dot{B}$ of -1.50 $^{+0.25}_{-0.44}$ m w.e. yr^{-1} during period 4 along with a $\Delta h/\Delta t$ that was greater than -8 m yr^{-1} at the terminus, which was again among the most negative measured terminus $\Delta h/\Delta t$ (Fig. 9). Davidson also had a more negative $\dot{B}$ of -1.18 $^{+0.15}_{-0.14}$ m w.e. yr^{-1} in period 4, with a more negative $\Delta h/\Delta t$ below 1100 m compared to period 3. As with period 3, both glaciers have a similar $\Delta h/\Delta t$ at the flow divide of -1.5 m yr^{-1}.

During period 3 Grand Plateau Glacier had a $\dot{B}$ of -1.02 $^{+0.36}_{-0.40}$ m w.e. yr^{-1}. The $\Delta h/\Delta t$ at the broad and relatively flat terminus of this lake calving glacier was around -5 m yr^{-1} during period 3 (Fig. 8). The $\dot{B}$ for period 4 was -2.77 $^{+0.56}_{-0.61}$ m w.e. yr^{-1}, which is by far the most negative $\dot{B}$ of all the profiled glaciers for any period. Maximum $\Delta h/\Delta t$ at the terminus was around -8 m yr^{-1} and thinning rates were greater than -1.5 m yr^{-1} up to 3400 m during period 4 (Fig. 9). It is possible that the high elevation thinning is due to variable snowfall. However, there is no data on snowfall amounts in this area so constant accumulation rates and ice density profiles are assumed; this example shows why Sorge's Law is applied in the absence of density and snowfall data.

Margerie Glacier had a $\dot{B}$ of 0.07 $^{+0.48}_{-0.50}$ m w.e. yr^{-1} during period 3. There was thickening of around 2 m yr^{-1} at the terminus during this period (Fig. 8), which is not consistent with the other profiled glaciers. However, Margerie is a calving tidewater glacier, so the glacier doesn't necessarily respond in response to changing climate conditions. Margerie is also a surge type glacier that last surged during the 1980's, so it probably has different ice flow dynamics than a non-surge type glacier. During period 4 Margerie had a $\dot{B}$ of 0.36 $^{+0.81}_{-1.11}$ m w.e. yr^{-1}, with thickening that is sustained from the terminus up to 1200 m (Fig. 9). During both periods there are no data between 1300 m and 2200 m, which is caused by an icefall with a slope steeper than the aircraft can descend or climb up.

4.4. Regionalization

The two different regionalization methods gave differing results for periods 1 through 4. To review, in method one (normalized elevation method), the Δh/Δt vs. average normalized elevation is applied separately to the AAD of the unprofiled glaciers in the eastern and western regions to find the $\dot{B}$ of those glaciers (Δh/Δt vs. normalized elevation curves for periods 1 through 4 are in Fig. 10). For method two (average $\dot{B}$ regionalization), the area-weighted average glacier $\dot{B}$ in m w.e. yr^{-1} is applied to the area of unprofiled glaciers during a particular period. The area of the unprofiled glaciers (i.e. the area of extrapolation) varies significantly between periods; period 1 has an unprofiled glacier area of 5136 km^2, period 2 is 5572 km^2, period 3 is 4624 km^2, and period 4 is 3174 km^2. With a total glaciated area in Glacier Bay of 6427 km^2, the percent of extrapolated area for periods 1 through 4 are: 80, 87, 74, and 49%.

Applying the Δh/Δt vs. average normalized elevation curve from period 1 to the AAD of unprofiled glaciers during period 1 results in a $\dot{B}$ of -0.21 ± 0.04 m w.e. yr^{-1} for the eastern unprofiled glaciers and -0.56 ± 0.11 m w.e. yr^{-1} for the western region. This corresponds to a $\dot{B}$ for all of the unprofiled glaciers of -1.84 ± 0.45 Gt yr^{-1}, and adding this to the measured total $\dot{B}$ of -0.82 ± 0.20 Gt yr^{-1} (Table 3) results in a total estimated $\dot{B}$ of -2.66 ± 0.49 Gt yr^{-1} for the Glacier Bay region between 1995 and 2000. Converting this to SLR gives 0.007 ± 0.001 mm yr^{-1} during this period. The area-weighted average $\dot{B}$ for the period 1 profiled glaciers was -0.66 ± 0.13 m w.e. yr^{-1}. Applying this to the unprofiled glacier area results in a $\dot{B}$ of -3.39 ± 0.82 Gt yr^{-1}. Adding this value to the measured total gives a total estimated $\dot{B}$ of -4.21 ± 0.85 Gt yr^{-1}, with a resulting SLR of 0.012 ± 0.002 mm yr^{-1}. The two regional $\dot{B}$ estimates differ by 58% and 1.55 Gt yr^{-1}.

During period 2, the normalized $\dot{B}$ was -4.05 ± 0.33 Gt yr^{-1}, and adding this to the measured total $\dot{B}$ of -1.09 ± 0.09 Gt yr^{-1} results in a total estimated $\dot{B}$ of -5.14 ± 0.35 Gt yr^{-1} for the Glacier Bay region between 2000 and 2005. Converting this to SLR gives 0.014 ± 0.001 mm yr^{-1} during this period. The area-weighted average $\dot{B}$ for the profiled glaciers was -1.33 ± 0.11 m w.e. yr^{-1}. Applying this to the unprofiled glacier area results in a $\dot{B}$ of -7.41 ± 0.70 Gt yr^{-1}. The total estimated $\dot{B}$ is -8.50 ± 0.71 Gt yr^{-1}, with a corresponding SLR of 0.024 ± 0.002 mm yr^{-1}. These two $\dot{B}$ estimates have the largest difference of the four periods (3.36 Gt yr^{-1}, or 65%).

In period 3, the normalized $\dot{B}$ was -1.91 ± 0.40 Gt yr^{-1}, and adding this to the measured total $\dot{B}$ of -1.05 ± 0.22 Gt yr^{-1} results in a total estimated $\dot{B}$ of -2.96 ± 0.46 Gt yr^{-1} for the Glacier Bay

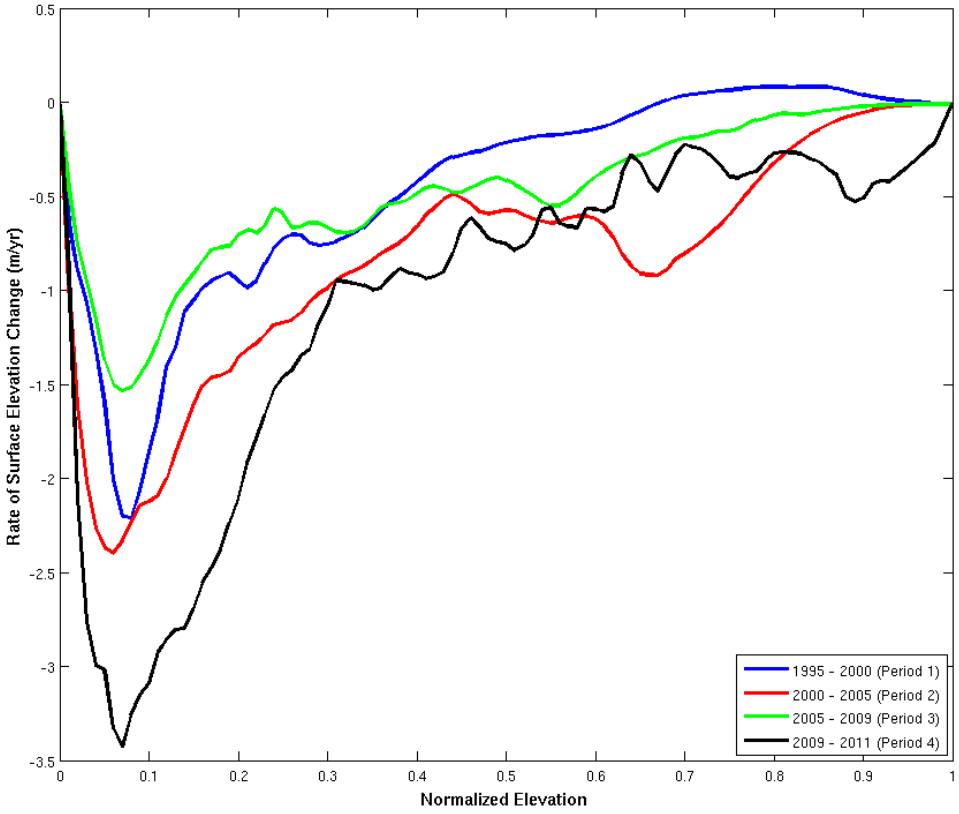

Fig. 10: The Δh/Δt vs. average normalized elevation curves for periods 1 through 4 are shown. Period 2 (red line) is more negative than both period 1 (blue line) and period 3 (green line) over the whole normalized elevation range. Period 4 (black line) is the most negative at lower normalized elevations and is similar to period 2 at higher normalized elevations. However, periods 3 and 4 include glaciers that were not profiled in earlier periods so these comparisons are not over the same amount of glacier surface area.

area between 2005 and 2009. Converting this to SLR gives 0.008 ± 0.001 mm yr^{-1} during this period. The area-weighted average $\dot{B}$ for the profiled glaciers was -0.59 ± 0.10 m w.e. yr^{-1}. Applying this to the unprofiled glacier area results in a $\dot{B}$ of -2.73 ± 0.57 Gt yr^{-1}, for a total estimated $\dot{B}$ of -3.78 ± 0.61 Gt yr^{-1}, with a corresponding SLR of 0.010 ± 0.002 mm yr^{-1}. The two regional $\dot{B}$ estimates vary by 28% and 0.82 Gt yr^{-1}.

During period 4, the normalized $\dot{B}$ was -2.43 ± 0.31 Gt yr^{-1}, and adding this to the measured total $\dot{B}$ of -3.63 ± 0.47 Gt yr^{-1} (Table 3) results in a total estimated $\dot{B}$ of -6.06 ± 0.56 Gt yr^{-1} for the Glacier Bay area between 2009 and 2011. Converting this to SLR gives 0.017 ± 0.002 mm yr^{-1} during this period. The area-weighted average $\dot{B}$ for the profiled glaciers was -1.18 ± 0.12 m w.e. yr^{-1}. Applying this to the unprofiled glacier area results in a $\dot{B}$ of -3.75 ± 0.49 Gt yr^{-1}, giving a total estimated $\dot{B}$ of -7.38 ± 0.68 Gt yr^{-1}, with a corresponding SLR of 0.020 ± 0.002 mm yr^{-1}. The two regional $\dot{B}$ estimates vary by 22% and 1.32 Gt yr^{-1}.

Table 3: Mass balance rates of the Glacier Bay region. Profiled Glaciers m w.e. yr^{-1} is an area-weighted average mass balance that is used in the average balance regionalization method. The average normalized elevation curves from Fig. 10 are used in the normalized regionalization method. Numbers in bold italics are ice mass change for the entire Glacier Bay region using the two different regionalization methods.

	Period 1	**Period 2**
Profiled Glaciers m w.e. yr^{-1}	-0.66 ± 0.13	-1.33 ± 0.11
Profiled Glaciers Gt yr^{-1}	-0.82 ± 0.20	-1.09 ± 0.09
Unprofiled Glaciers: Normalized Gt yr^{-1}	-1.84 ± 0.45	-4.05 ± 0.33
Profiled + Normalized Gt yr^{-1}	***-2.66 ± 0.49***	***-5.14 ± 0.35***
Unprofiled Glaciers: Average Balance Gt yr^{-1}	-3.39 ± 0.82	-7.41 ± 0.70
Profiled + Average Balance Gt yr^{-1}	***-4.21 ± 0.85***	***-8.50 ± 0.71***

	Period 3	**Period 4**
Profiled Glaciers m w.e. yr^{-1}	-0.59 ± 0.10	-1.18 ± 0.12
Profiled Glaciers Gt yr^{-1}	-1.05 ± 0.22	-3.63 ± 0.47
Unprofiled Glaciers: Normalized Gt yr^{-1}	-1.91 ± 0.40	-2.43 ± 0.31
Profiled + Normalized Gt yr^{-1}	***-2.96 ± 0.46***	***-6.06 ± 0.56***
Unprofiled Glaciers: Average Balance Gt yr^{-1}	-2.73 ± 0.57	-3.75 ± 0.49
Profiled + Average Balance Gt yr^{-1}	***-3.78 ± 0.61***	***-7.38 ± 0.68***

In summary, periods 1 and 3 have around the same total estimated $\dot{B}$ magnitude, with a normalized mass change of slightly less than -3 Gt yr^{-1}. Periods 2 and 4 have a total normalized $\dot{B}$ that is around twice as negative as the other two periods (Fig. 11). The total $\dot{B}$ estimates vary depending on whether the normalized elevation or average $\dot{B}$ regionalization is used. The large difference in $\dot{B}$ between the two methods during periods 1 and 2 is likely due to the small number of glaciers that was profiled and the large area of Brady Glacier compared to the other glaciers, which means that Brady dominates the area-weighted average $\dot{B}$. The total mass change in Glacier Bay between 1995 and 2011 can be found by summing the $\dot{B}$ rates during each altimetry time period. We estimate that the normalized mass loss over that 16 year time span was 62.9 ± 7.1 Gt, which is equivalent to an average $\dot{B}$ of -3.93 ± 0.44 Gt yr^{-1}, resulting in a total SLR of 0.174 ± 0.020 mm over the altimetry period.

4.5. Temporal Variability of Mass Balance

Previous studies have demonstrated that the rate of ice loss of glaciers in Alaska has been increasing. Arendt et al. (2002) found that the mass loss between the mid-1950s and the mid-1990s was -52 ± 15 Gt yr^{-1}. The mass loss then accelerated between the mid-1990s to 2000-2001, with an annual mass loss of -96 ± 55 Gt yr^{-1} during the more recent period. To investigate whether ice loss is also accelerating in the Glacier Bay area, we compare mass loss results from laser altimetry to sequential DEM differencing. Larsen et al. (2007) differenced the 2000 SRTM DEM from an older composite DEM based on air photos from 1948 and 1987 to estimate glacier mass change in southeast Alaska. Here we sample the surface elevation change grid of Larsen et al. (2007) over the glaciers located in the Glacier Bay region and find that the $\dot{B}$ was -4.62 ± 1.22 Gt yr^{-1}, with the highest rate of thinning occurring at Muir Glacier (Fig. 12), which experienced a rapid tidewater retreat during this period. This is more negative than the altimetry $\dot{B}$ of -3.93 ± 0.44 Gt yr^{-1} between 1995 and 2011. The decrease in the mass loss rate is likely due to the termination of the rapid tidewater retreat of Muir Glacier up to West Arm, with the rapid retreat ending around 1980. There was also rapid retreat of Melbern and Konamoxt Glaciers, which had created the 20 km long Lake Melbern by around 2000. Additionally, Grand Plateau and Alsek Glaciers, which are both lake calving, have also experienced rapid retreat that continues at the present.

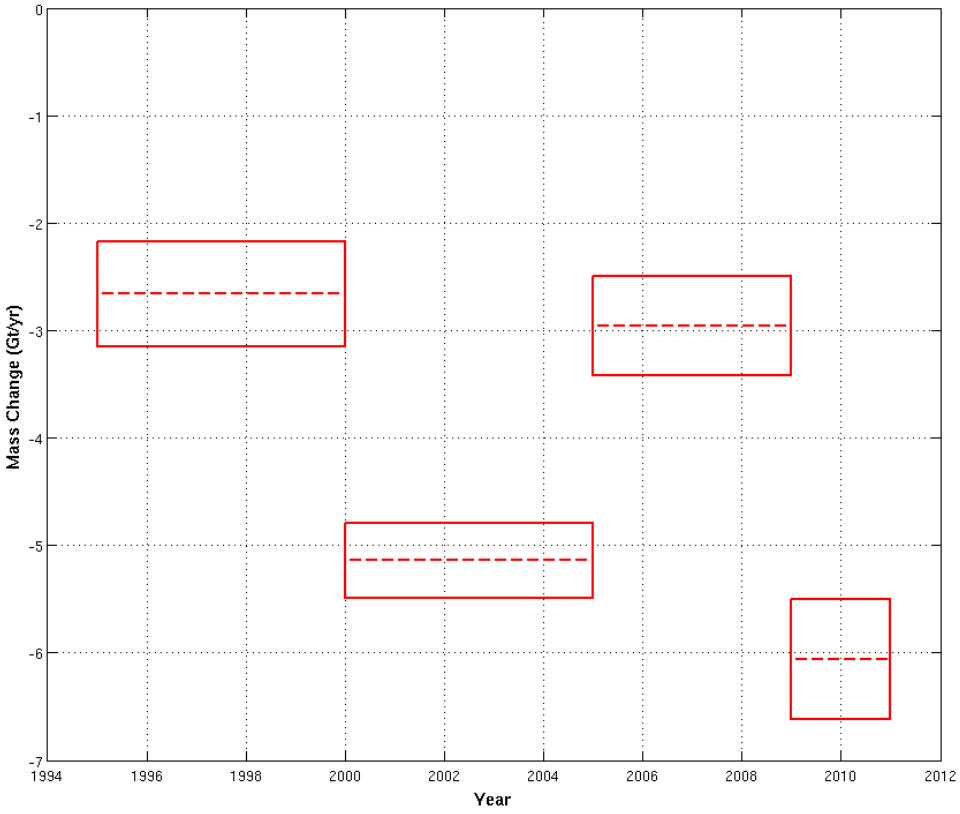

Fig. 11: The total regional mass change in Glacier Bay between 1995 and 2011. Results are presented for the normalized method; the average balance method has a similar mass change pattern with slightly higher mass change magnitudes. Width of the box is the time span of each period, while height is the uncertainty of the mass balance estimate. The mass change during periods 2 and 4 (around -5 and -6 Gt yr^{-1}, respectively) is around twice as negative as periods 1 and 3 (less than -3 Gt yr^{-1}).

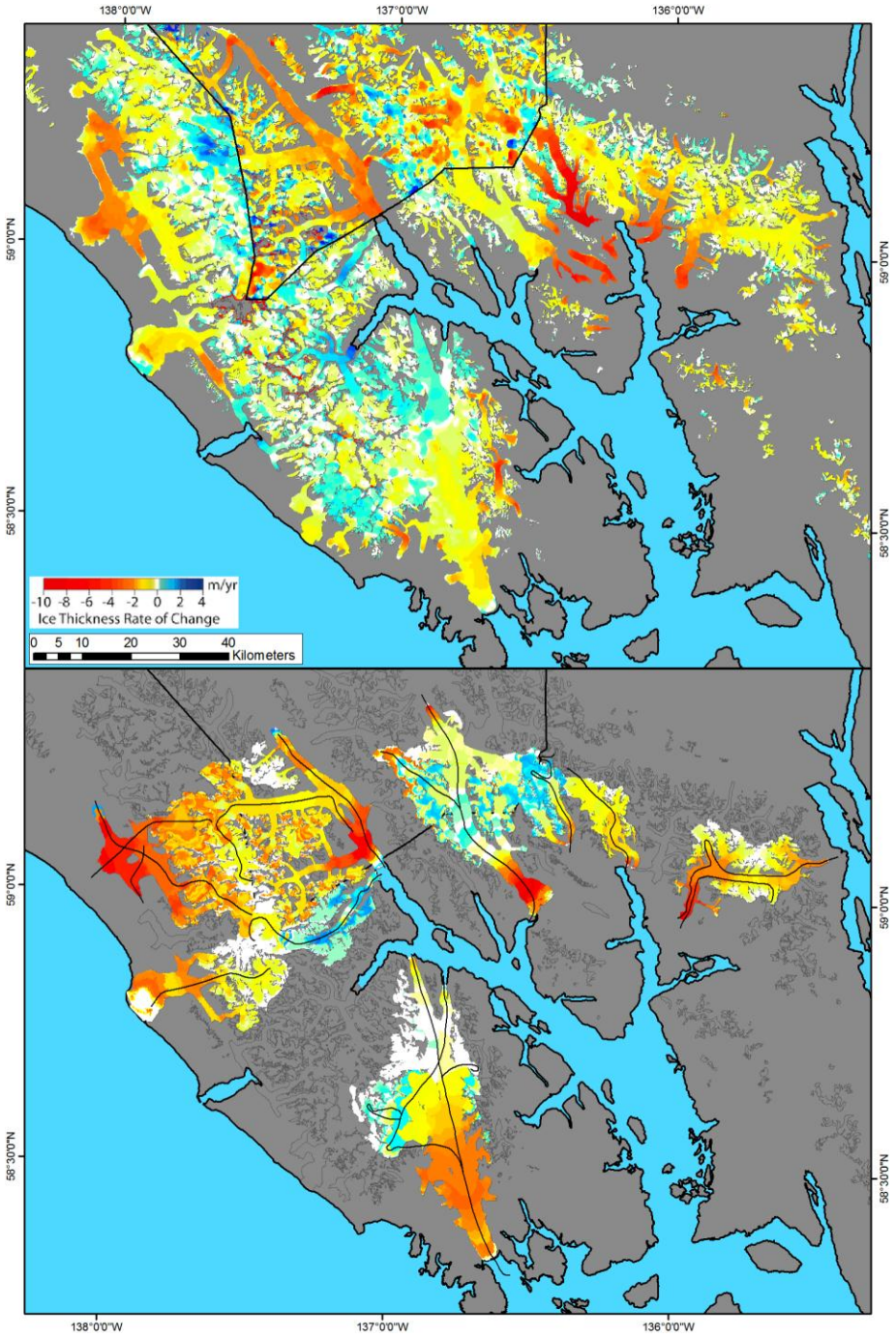

Fig. 12: Rate of thinning from differencing of DEMs from 2000 and 1948 / 1987 is shown in the top map, with the period 4 thinning rates provided on the bottom for comparison. Although the magnitude of thinning is different during the two time periods, the spatial patterns are similar with the exception of Muir Glacier. For example, Brady Glacier had higher thinning rates than the adjacent Lamplugh and Reid Glaciers during both periods, Casement Glacier had higher terminus thinning rates than the terminus of the adjacent Davidson Glacier, and Margerie Glacier had thickening over much of the glacier.

The $\dot{B}$ of -4.62 ± 1.22 Gt yr^{-1} from DEM differencing is equivalent to a total mass loss of 240.2 ± 63.4 Gt over the 52 years between 1948 and 2000, using the assumption that the area in Canada which is covered by the 1987 DEM had been experiencing a mass loss rate between 1948 and 1987 that was the same as the rate between 1987 and 2000. Adding this to the altimetry normalized mass loss of 49.6 ± 4.7 Gt between 2000 and 2011 gives a total regional mass loss of 289.8 ± 68.1 Gt since 1948 and an equivalent total SLR of 0.801 ± 0.188 mm. To put this into perspective, the total ice mass loss since 1770 has been estimated at around 3030 Gt, which is equivalent to a total SLR of 8.37 mm (Larsen et al. 2005).

Arendt et al. (2002) used map to profile comparisons to obtain $\dot{B}$ for their "early period". In Glacier Bay they used profiles from 1995 and a topographic map that was based upon 1948 air photos. The Brady Icefield glaciers were the only glaciers within Glacier Bay that had map to profile calculations performed. Arendt et al. (2002) estimated the early period $\dot{B}$ for Brady Glacier (-0.39 ± 0.09 m w.e. yr^{-1}), Lamplugh Glacier (0.36 ± 0.10 m w.e. yr^{-1}), and Reid Glacier (0.40 ± 0.10 m w.e. yr^{-1}). These early period $\dot{B}$ are less negative than those estimated by differencing altimetry profiles from 1995 and 2011: -1.18 ± 0.11 m w.e. yr^{-1} for Brady; -0.41 ± 0.10 m w.e. yr^{-1} for Lamplugh; and -0.35 ± 0.09 m w.e. yr^{-1} for Reid.

4.6. Sensitivity Analysis

A sensitivity analysis was carried out to examine the effect that removing a single glacier from the normalized elevation regionalization had on the $\dot{B}$ of unprofiled glaciers. The results of the sensitivity analyses for period 3 are generally within 0.1 m w.e. yr^{-1} and 0.20 Gt yr^{-1} (Table 4), with the exception of the case where Casement Glacier was excluded. Casement had the most negative $\Delta h/\Delta t$ vs. elevation curve during this period. Its removal meant the $\dot{B}$ in Gt yr^{-1} was 0.44 Gt yr^{-1} lower than any of the other estimates and was the only case where $\dot{B}$ was outside of the estimated error. The results from period 4 are generally within 0.05 m w.e. yr^{-1} and 0.15 Gt yr^{-1} (Table 5). As with period 3, the removal of Casement Glacier had a large impact on the $\dot{B}$ estimates, second only to the impact of Grand Plateau Glacier. However, both cases were still within the estimated error of the calculated $\dot{B}$ for period 4.

Table 4: Results of sensitivity analysis on period 3 through the exclusion of one glacier from the normalized regionalization. Mass balance values are calculated over the total area of the unprofiled glaciers.

Glacier Removed	Remaining Glaciers: m w.e. yr^{-1}	Gt yr^{-1}
None Removed	-0.46	-2.01
Brady	-0.43	-1.88
Lamplugh	-0.51	-2.22
Reid	-0.51	-2.23
Casement	-0.32	-1.40
Davidson	-0.42	-1.84
Riggs	-0.45	-1.99
Muir	-0.50	-2.20
Margerie	-0.52	-2.28
Grand Plateau	-0.46	-2.02

Table 5: Results of sensitivity analysis on period 4 through the exclusion of one glacier from the normalized regionalization. Mass balance values are calculated over the total area of the unprofiled glaciers.

Glacier Removed	Remaining Glaciers: m w.e. yr^{-1}	Gt yr^{-1}
None Removed	-0.80	-2.41
Brady	-0.83	-2.50
Lamplugh	-0.85	-2.58
Reid	-0.85	-2.56
Casement	-0.71	-2.16
Davidson	-0.74	-2.25
Riggs	-0.77	-2.33
Muir	-0.85	-2.56
Carroll	-0.83	-2.49
Tkope	-0.82	-2.48
Margerie	-0.88	-2.66
Fairweather	-0.78	-2.38
Grand Plateau	-0.69	-2.09
Grand Pacific	-0.75	-2.26
Melbern	-0.82	-2.47

4.7. Simu-Laser From DEM Difference Map

The simu-laser methodology is applied here to the Glacier Bay region to examine whether the laser altimetry method overestimates ice loss when compared to sequential DEMs for this area. This methodology attempts to determine if centerline changes are representative of the entire

glacier or if new approaches are needed to scale centerline elevation changes from altimetry. The DEM difference map used in this analysis is derived from Larsen et al., 2007. Glacier centerlines follow altimetry flight paths in Glacier Bay, generally as flown in 2009. Glacier outlines are derived from August 2010 Landsat images. This analysis is performed for all of the 16 glaciers that have multiple laser altimetry profiles in Glacier Bay. These 16 glaciers have a total area of 3328 km^2 that represents 52% of the total ice covered area of the Glacier Bay region. The analysis was also done for 24 additional unprofiled glaciers with simulated flightlines that generally followed the glacier's centerline, resulting in a total of 40 glaciers with simu-laser results. These 24 additional glaciers include all unprofiled glaciers with August 2010 surface areas larger than 25 km^2 and have a total area of 1815 km^2. The distribution of the 16 profiled glaciers is biased toward the larger glaciers, with11 glaciers that have areas larger than 100 km^2. In contrast, the 24 unprofiled glaciers only have four glaciers with areas larger than 100 km^2. The total simu-laser glacier area is 5143 km^2, which represents 80% of the total glaciated area of the Glacier Bay region.

Although the magnitude and sign of the relative difference between $\dot{B}_{\text{DEM}}$ and $\dot{B}_{\text{SIMU-LASER}}$ is variable for individual glaciers, we find that on average the simu-laser method underestimates the DEM derived ice loss by only 6% for the 40 glaciers that were tested. Overall, $\dot{B}_{\text{DEM}}$ and $\dot{B}_{\text{SIMU-LASER}}$ cumulative mass changes were -2.84 Gt yr^{-1} and -2.68 Gt yr^{-1} (glacier specific results are summarized in Appendix B, table 13). The relative difference between $\dot{B}_{\text{DEM}}$ and $\dot{B}_{\text{SIMU-LASER}}$ is generally more variable for the 24 unprofiled glaciers than for the 16 profiled glaciers; however the actual difference between $\dot{B}_{\text{DEM}}$ and $\dot{B}_{\text{SIMU-LASER}}$ is generally smaller due to the smaller sizes of the unprofiled glaciers. The agreement between the DEM and simu-laser methods (Fig. 13) lends strong support to the validity of scaling centerline altimetry-derived elevation changes to an entire glaciated region, in particular to the entire Glacier Bay area, provided that a number of glaciers are profiled within a glaciated area. Further work will be required to extend this type of comprehensive analysis to other glaciated areas of Alaska.

4.8. GRACE Mass Balance Record

Gravity data from the GRACE mission provide another mass change estimate that can be compared to the laser altimetry mass change. The GRACE mission uses tandem satellites to map temporal variations in the Earth's geoid and senses all components of the atmosphere, ocean, and

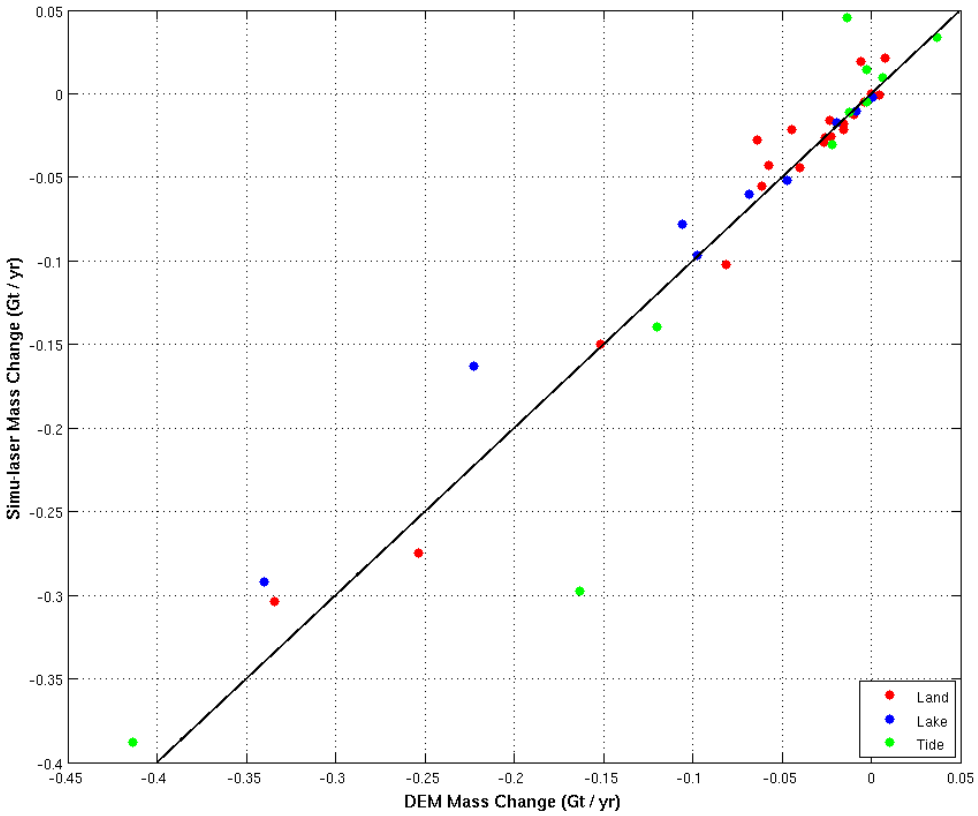

Fig. 13: Comparison of mass change from DEM differencing and simu-laser method for 40 different glaciers in Glacier Bay. Simu-laser mass change is on y-axis and DEM mass change is on x-axis. Different colors distinguish between glacier type (tidewater, lake calving, and land terminating) and solid black line is a one to one mass change, i.e. DEM mass change equals simu-laser mass change. There appears to be no bias in the simu-laser results for land terminating, lake calving, or tidewater glaciers.

Earth systems. The geophysical signal of interest (e.g. change in ice mass) is separated out using models and observations. The fundamental resolution is limited by the orbital height of the satellite, accelerometer accuracy, etc. GRACE cumulative mass balances are currently available from the middle of 2003 through late 2010, which coincides with all of altimetry period 3, the end of period 2, and most of period 4. In previous studies the Glacier Bay area was represented by two degree by two degree mascons that included both the Yakutat and Juneau Icefields (Luthcke et al., 2008). These two icefields are experiencing mass loss, and in particular the Yakutat Icefield is currently experiencing rapid retreat of lake calving glaciers.

Mascon solutions from the GRACE mission have recently been refined to higher resolutions. Current mascons from Luthcke et al. (2008) are calculated over a grid size of approximately one degree by one degree and are based upon updated solutions from Pritchard et al. (2010). The equal-area mascons are used as the domain over which spatial and temporal constraints are applied on the gravity signal that is recorded from GRACE. The mass change is estimated over successive time intervals of 10 days (Pritchard et al., 2010). The errors for individual mascon solutions can potentially be large due the smearing of the signal between neighboring mascons, however this error is not quantified here.

The current mascon that that includes the Glacier Bay region covers most of the region's glaciated area, with parts of the eastern glaciers and the southern part of Brady Glacier located in neighboring mascons that also include glaciers outside of Glacier Bay (Fig. 14). Cumulative mass balances are estimated for those areas by finding the percentage of ice in the adjoining mascons that is located within the Glacier Bay region, and then adjusting the mass balance of the adjoining mascons by the same percentage. The time period covered is from April, 2003 through December, 2010 (Fig. 15). The trend in the Glacier Bay GRACE signal over this period was -3.05 Gt yr^{-1}, which includes parts of laser altimetry periods 2, 3, and 4. The trend is -2.47 Gt yr^{-1} when the GRACE signal is restricted to period 3 from altimetry. This is much closer to the period 3 normalized $\dot{B}$ estimate of -2.96 ± 0.46 Gt yr^{-1} than the area-weighted average $\dot{B}$ of -3.78 ± 0.61 Gt yr^{-1}. Selecting the GRACE cumulative mass balance from the end of May during each year allows for the GRACE derived mass loss to be calculated over the annual balance year that is used here in laser altimetry. 2009 - 2010 had the most negative annual mass change at -6.34 Gt yr^{-1}, while 2006 - 2007 and 2008 - 2009 had much lower annual mass changes at -0.99 Gt yr^{-1} and -1.16 Gt yr^{-1} (Table 6). The wide variability in GRACE annual mass balances echoes the variability that is seen in the various laser altimetry periods and appears to be dominated by winter accumulation.

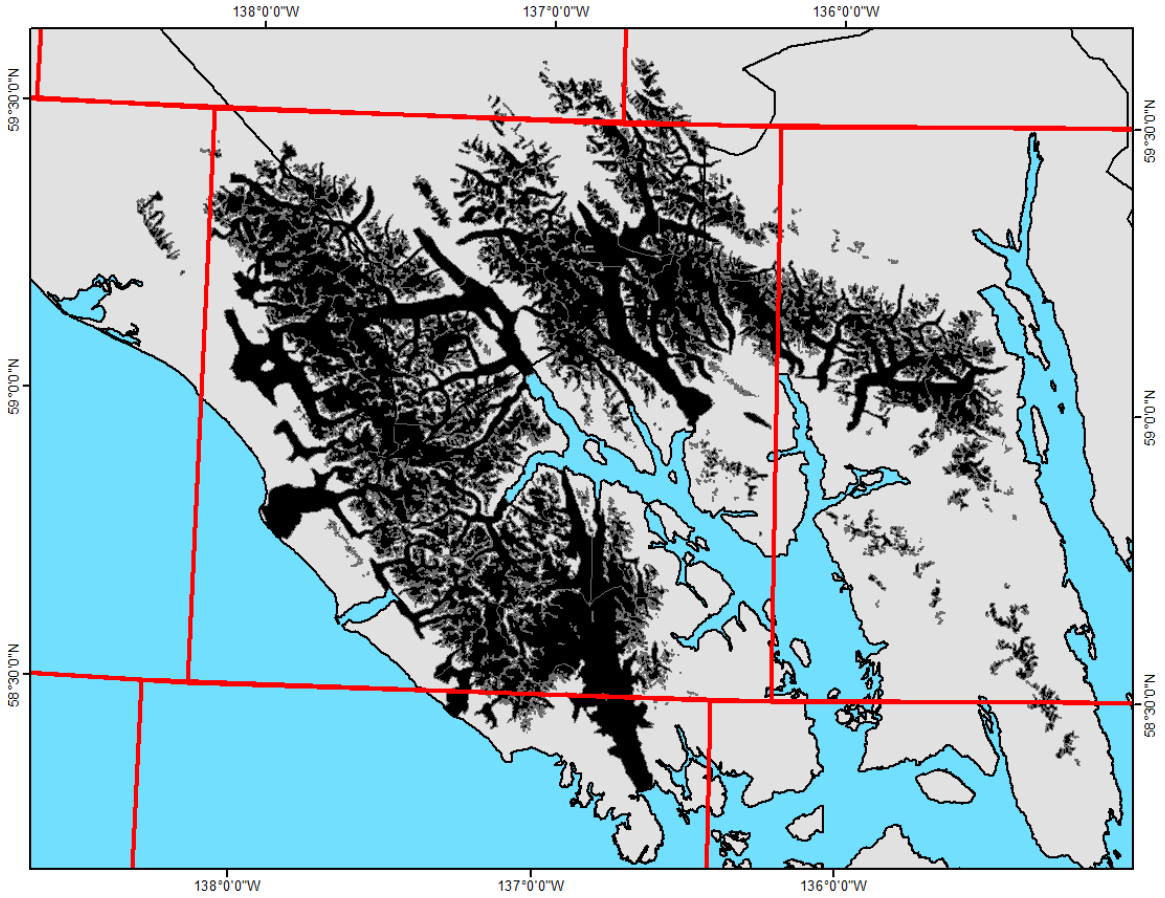

Fig. 14: Grid cells used to calculate gravity signal changes from GRACE data. A single GRACE mascon covers most of Glacier Bay, except for those glaciers located east of the terminus of Riggs Glacier, the southern half of Brady Glacier, and minor outlying glaciers.

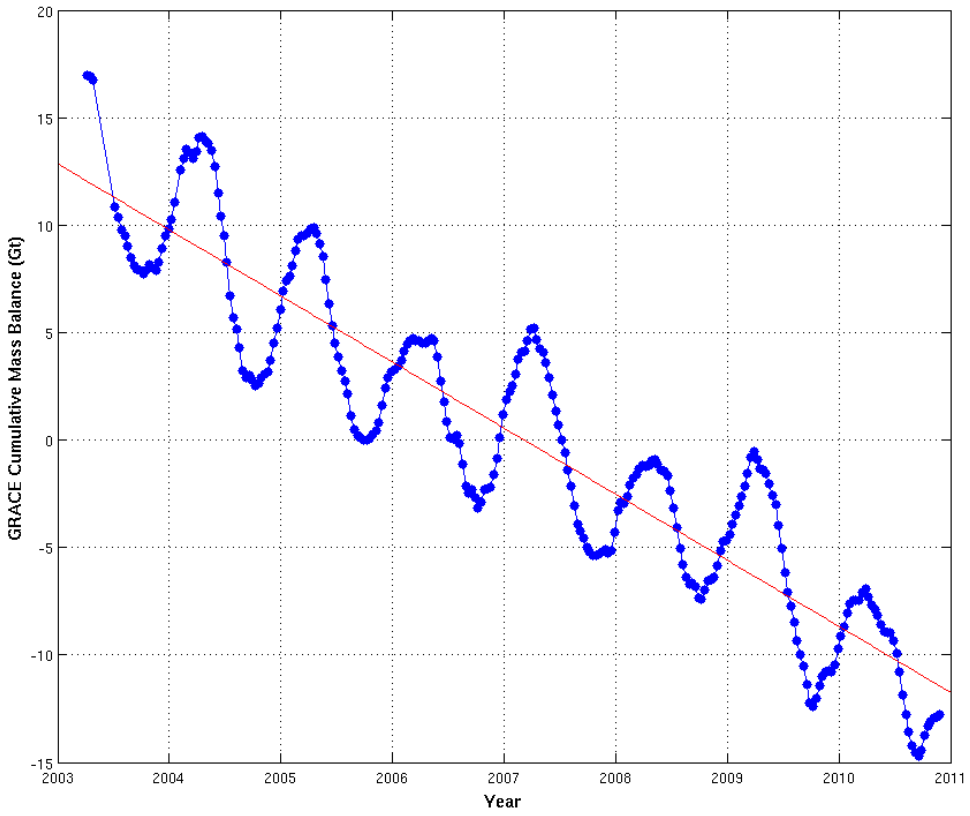

Fig. 15: GRACE cumulative mass balance, 2003 - 2010. Red line represents the mass change trend for the entire period of GRACE observations. The trend is calculated through simultaneous estimations of tidal aliasing period and bias, trend, annual, and semi-annual sinusoids.

Table 6: GRACE mass loss over each annual balance year that coincides with laser altimetry. Cumulative GRACE mass balances for each year are from May 28th to coincide with the laser altimetry profile dates.

Balance Year	GRACE mass loss Gt yr^{-1}
2004 - 2005	-5.27
2005 - 2006	-3.60
2006 - 2007	-0.99
2007 - 2008	-4.29
2008 - 2009	-1.16
2009 - 2010	-6.34

4.9. Patterns in the Mass Balance Record

The laser altimetry mass balance record shows large temporal and spatial variations in $\dot{B}$. However, the dominant signal for the profiled glaciers is increased ice loss during periods 2 and 4 when compared to periods 1 and 3. Previous studies have demonstrated that alpine glaciers are sensitive to small changes in climate, and are able to respond quickly to short-term changes in climate (Oerlemans, 1998). This suggests that there should be a relationship between a glacier's $\dot{B}$ and the local climate conditions, in particular to air temperatures greater than 0˚C which mainly occurs during summer. It is investigated here whether the temporal variation in mass balance can be linked to positive degree days (a proxy for melt energy availability) and winter precipitation (a proxy for snowfall) within the Glacier Bay area or to some other variable such as glacier area or area averaged elevation.

4.9.1. Relationship to Climate

There is a dearth of long-term climate stations within the study area, with the closest sites located in Juneau, Yakutat, and Sitka. Arendt et al. (2009) suggest that the Yakutat station has the best fit with glacier changes derived from the GRACE data. However, climate data can be examined on a wider scale by utilizing a gridded climate data set that has been produced by an Oregon State team led by Dave Hill (Hill and Calos, 2011). This climate model provides a monthly resolution record of temperature and precipitation between 1961 and 2009 that can possibly be linked to the behavior of the profiled glaciers.

The model uses PRISM climate data to define the spatial trends in a 30-year climatology record of temperature and precipitation (Daly et al., 1997). A monthly, gridded data set of the temporal variability of temperature and precipitation was obtained by using data from weather stations to calculate anomalies (departures) from the PRISM climatology record on a monthly resolution. A cubic spline interpolation was performed on the anomalies to calculate a gridded dataset of average monthly temperature and total monthly precipitation at a resolution of 2 km by 2 km. We then utilized the gridded dataset in this study to obtain monthly temperature and precipitation in Glacier Bay by sampling the dataset separately for the entire Glacier Bay region, eastern Glacier Bay, and western Glacier Bay (eastern and western glaciated regions in Fig. 2).

The gridded average monthly temperature was used to calculate annual, spatially averaged, positive degree months, which were converted to positive degree days (PDD) that can be more directly related to melt than mean temperature (Hock, 2005). The PDD were summed over the entire region that is being examined using a temperature threshold of 0˚C and then normalized by the number of grid cells. Here, the average PDD does not have a direct physical interpretation; however it can be used to examine temporal and spatial trends in the amount of energy that is available to contribute to the melting of snow and ice (ablation). Winter precipitation, or the amount of precipitation that fell as solid precipitation or snow in water equivalent (mm w.e. m^{-2}), was calculated by extracting grid cells that had temperatures below 0˚C, summing the amount of precipitation over those grid cells, and normalizing by the number of grid cells. Here we use the assumption that any precipitation that fell when the average monthly temperature was lower than 0˚C was solid, and any precipitation at temperatures above 0˚C was liquid. Different temperature thresholds can be used in the PDD and winter precipitation calculations to examine the sensitivity to different temperature cut-offs, however this analysis is not performed here.

The average annual PDD in Glacier Bay was calculated over the time span of the four altimetry mass balance periods. The annually averaged PDD during each altimetry period over three different spatial domains is presented in Table 7. The average PDD for periods 2 through 4 corresponds to the $\dot{B}$ record as PDD increased during periods 2 and 4 compared to period 3. This would correlate to increased ablation during periods 2 and 4 than in period 3, which is reflected in the $\dot{B}$ record (periods 2 and 4 had a mass loss rate that was twice as high as period 3). The summer of 2004 had the highest PDD during periods 2 through 4 (Fig. 16), which correlates with the high summer temperatures that were measured in Alaska during 2004 (Truffer et al., 2005) and the increased mass loss during period 2. However, the relationship between annually

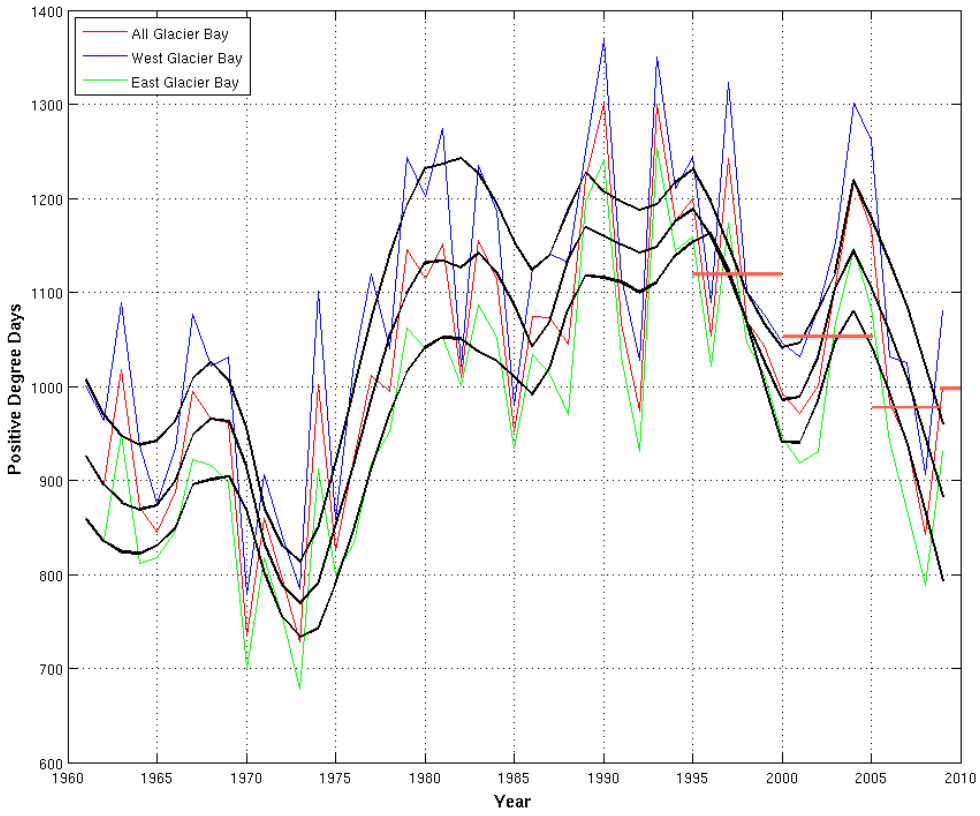

Fig. 16: Spatially averaged annual positive degree days in Glacier Bay. Blue is the western glaciated region, green is the eastern glaciated region, and red is over both regions together. Solid black line is a 10-year running average. Average annual PDD during each altimetry time period for the entire Glacier Bay region is indicated by horizontal red lines.

averaged PDD and mass balance does not hold for period 1 (which had a similar mass loss rate as period 3), as period 1 had an average PDD that was significantly higher than the other 3 periods (and was particularly high in 1997). This suggests that period 1 would have the most ablation of all the periods, which is contrary to the altimetry $\dot{B}$ record. The patterns described above are similar for each of the three spatial domains (Table 7), although the average PDD is higher in the western region.

Table 7: Annual average of positive degree days (PDD) during each altimetry time period. All is calculated over the entire Glacier Bay domain, while East and West were sampled separately over the two distinct glaciated regions of Glacier Bay.

	All	**East**	**West**
Period 1	1121.6	1082.8	1166.8
Period 2	1057.9	1001.9	1123.0
Period 3	983.4	920.1	1056.2
Period 4	999.9	930.8	1079.8

The change in annual average temperature over time was calculated using a linear regression method. The temperature record shows that the annual temperature has increased around 1.7˚C since 1961 in Glacier Bay, with summer temperatures increasing by 1.4˚C and winter temperatures by 1.9˚C.

The winter precipitation record does not appear to be correlated at all with the altimetry $\dot{B}$ measurements. The average winter precipitation during each period was steadily increasing over time (Table 8), which does not correspond with the fluctuations that are seen in the $\dot{B}$ record. If winter precipitation was directly related to $\dot{B}$ we would expect to see decreased winter precipitation during the periods with the most negative $\dot{B}$ (periods 2 and 4) and increased winter precipitation during period with less negative $\dot{B}$ (period 1 and 3). The pattern of increasing winter precipitation over time is similar for each of the three spatial domains, although there is significantly more winter precipitation in the western region, which is located in the coastal Fairweather Range (the western region also had higher average PDD). Interestingly, there appears to be a 10 to 15 year cycle in the amount of winter precipitation (Fig. 17).

Looking at both PDD and winter precipitation together, the correlation with the $\dot{B}$ record becomes even more tenuous. For instance, based upon the lower mass loss that is observed with altimetry during period 1, we would expect to see the high average PDD during period 1 being

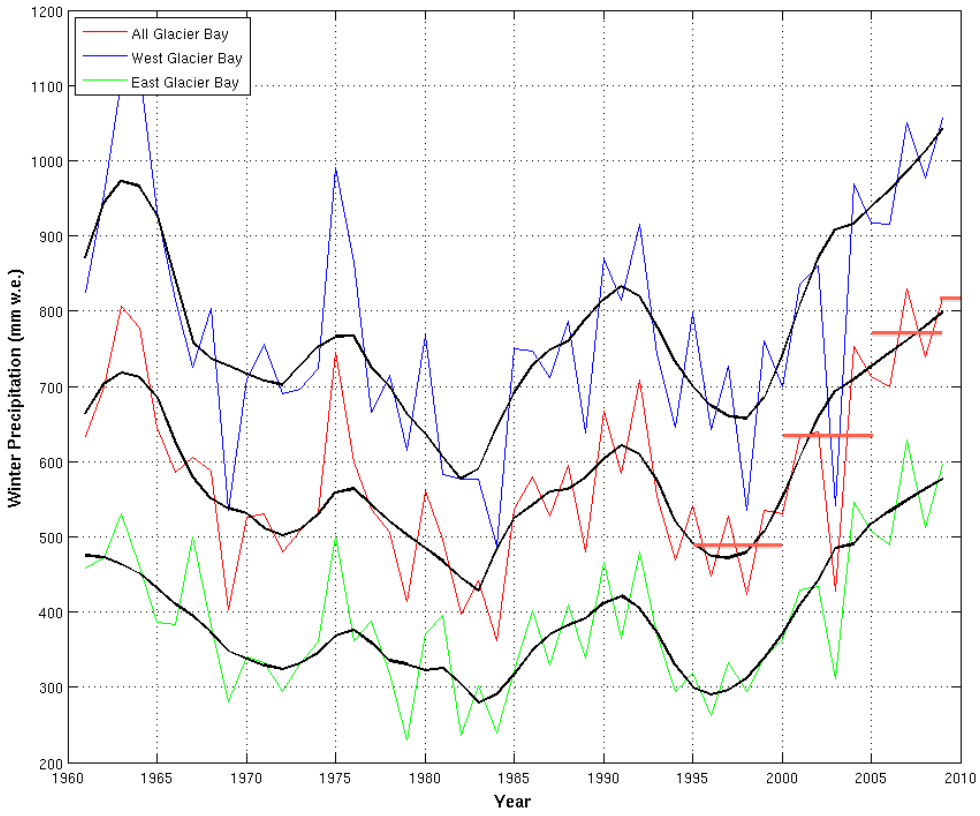

Fig. 17: Spatially averaged total winter precipitation (mm w.e. m^{-2}) in Glacier Bay. Blue is the western glaciated region, green is the eastern glaciated region, and red is over both regions together. Solid black line is a 10-year running average. Average annual winter precipitation during each altimetry time period for the entire Glacier Bay region is indicated by horizontal red lines.

balanced by higher winter precipitation. The exact opposite response is seen, with period 1 having the lowest winter precipitation.

Table 8: Annual average of precipitation that fell when the average monthly temperature was below 0˚C (in mm w.e. m^{-2}). Data is averaged over the entire spatial domain, which is the same as the PDD domains.

	All	**East**	**West**
Period 1	492.9	318.6	673.2
Period 2	633.3	445.4	824.3
Period 3	771.1	556.2	1000.2
Period 4	817.5	596.0	1057.1

There are a number of possible explanations for the discrepancy between the climate record and mass balance. First, Glacier Bay is located in a maritime, temperate climate which results in precipitation being very sensitive to freezing thresholds (here we assume a freezing threshold of 0˚C). Second, precipitation is very difficult to measure, particularly in high mountain areas. The climate model used here only employs a limited number of low altitude weather stations in Southeast Alaska, thus the model may not be correctly interpolating temperature and precipitation in the mountainous Glacier Bay region. Third, temperature and precipitation are calculated at a monthly resolution, which likely is not capturing shorter term variability. This variability will have the largest affect during spring and fall, when the temperature is close to the freezing point. Finally, it is possible that the variable mass balance record in Glacier Bay is related to dynamic mass losses, in which case there would be no correlation between mass balance and climate.

4.9.2. Other Relationships

The glaciers that have been profiled are mostly larger glaciers. Are these glaciers really representative of the rest of the Glacier Bay area? This is tested by examining the relationship between $\dot{B}$ and glacier area for the profiled glaciers. Fig. 18 shows that the larger glaciers generally have a more negative specific $\dot{B}$, although the relationship does not appear to be very robust. This indicates the larger glaciers that have been profiled may not be truly representative of the entire Glacier Bay area, especially for the smaller glaciers. There appears to be no relationship with the area averaged elevation of the profiled glaciers (Fig. 19). There is also no relationship between $\dot{B}$ and glacier type i.e. land terminating, lake calving, and tidewater. The same analysis

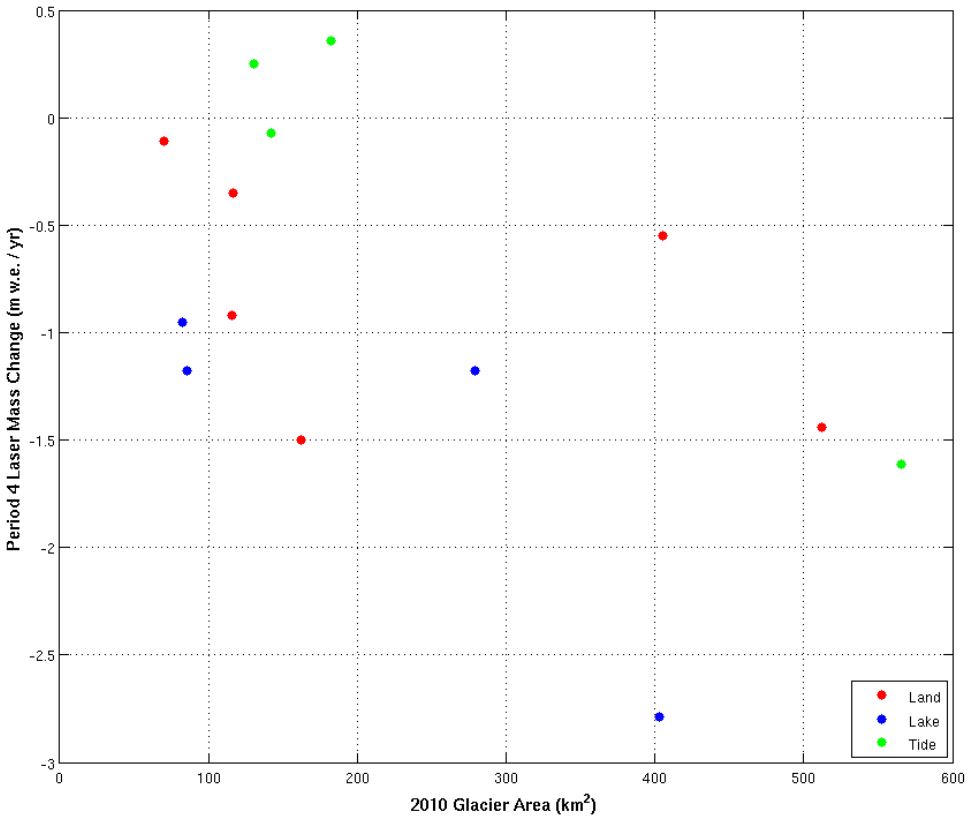

Fig. 18: Mass change vs. glacier size for glaciers profiled in Glacier Bay between 2009 and 2011. Altimetry mass change is in m w.e. yr^{-1} and is compared to the August 2010 glacier surface areas.

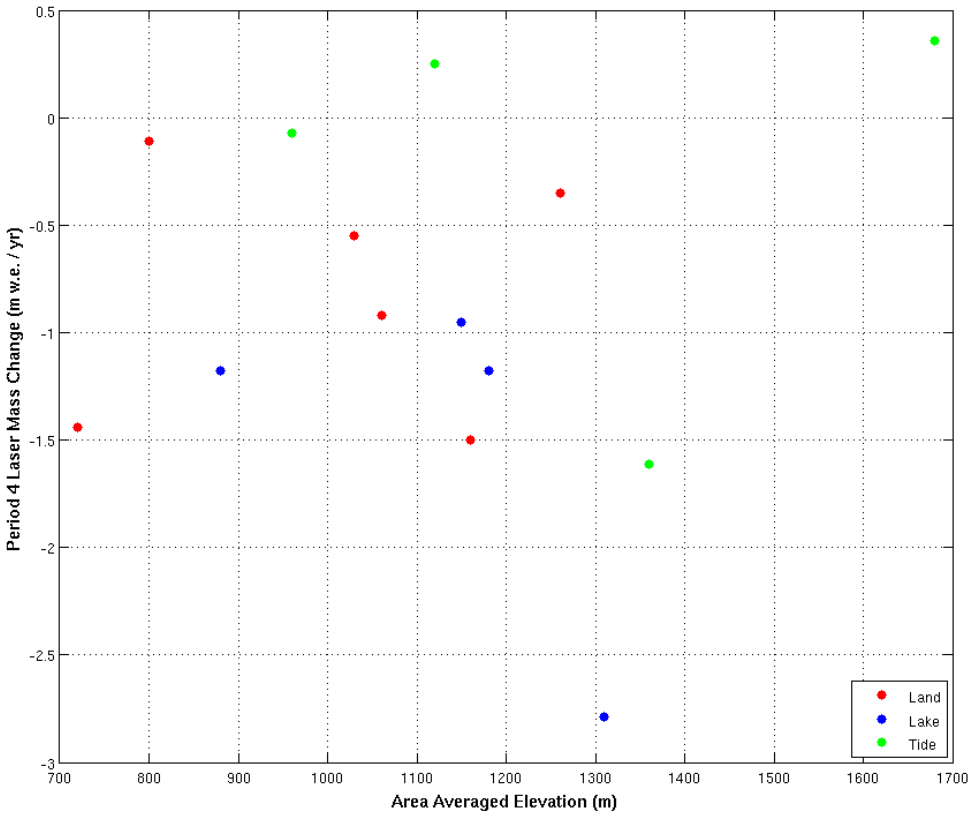

Fig. 19: Mass change vs. area averaged elevation for glaciers profiled in Glacier Bay between 2009 and 2011. Altimetry mass change is in m w.e. yr^{-1} and is compared to the August 2010 glacier area averaged elevations.

was performed on the eastern and western regions, and there was no significant difference between the glaciated regions.

The mass balance regime of tidewater glaciers is strongly controlled by the ice dynamics of the tidewater glacier cycle (Meier and Post, 1987). In many cases calving glaciers don't respond concurrently with variations in climate. These glaciers may be contributing markedly to a region's overall ice loss, especially if they are in a state of rapid calving. It is important to monitor as many tidewater glaciers as possible, including advancing, retreating, and stable tidewater glaciers, to determine present mass change rates. With as many tidewater glaciers monitored as possible, the complications of regionalizing tidewater glaciers as raised in Arendt et al. (2006) can be avoided.

The tidewater glaciers of the Glacier Bay area are relatively stable when compared to other dramatically retreating Alaska tidewater glaciers, e.g. Columbia and South Sawyer Glaciers. This raises the question whether the tidewater glaciers in Glacier Bay can be included in a regionalization without adversely affecting the estimated ice loss. The sensitivity analysis that was carried out in section 4.5 shows that removing individual tidewater glaciers from the regionalization does not have an anomalous effect on the mass balance of the remaining glaciers when compared to removing a non-tidewater glacier. The rapid tidewater retreat that Glacier Bay experienced after the Little Ice Age has ended, and the fastest retreating glaciers are now mostly lake calving glaciers like Grand Plateau Glacier.

4.9.3. Comparison to Wolverine and Gulkana Glaciers

The USGS has been using the glaciological method to monitor the mass balance of two Alaskan glaciers since 1966: Gulkana Glacier in the eastern Alaska Range and Wolverine Glacier on the Kenai Peninsula (Van Beusekom et al., 2010). Wolverine is located in in a maritime setting that is similar to Glacier Bay, while Gulkana is located in an interior continental setting. Reference-surface mass balance data from the USGS was used to find the average $\dot{B}$ of these glaciers during the altimetry time periods (Table 9). The average $\dot{B}$ for both of these two glaciers is the most negative during the altimetry period 2 and the least negative during periods 1 and 3. This pattern corresponds to the regional $\dot{B}$ record in Glacier Bay, which had around twice as much mass loss during period 2 compared to periods 1 and 3. Additionally, the $\dot{B}$ for both

glaciers was the most negative during 1997 and 2004, which corresponds to the years that had the highest annually averaged PDD in the Glacier Bay region.

Table 9: Average mass balance rates in m w.e. yr^{-1} for Wolverine and Gulkana glaciers during each altimetry time period. The Glacier Bay mass balance is the regional total in m w.e. yr^{-1} using the normalized elevation method.

Period	**Wolverine**	**Gulkana**	**Glacier Bay**
1	-0.60	-0.89	-0.41
2	-1.00	-1.15	-0.80
3	-0.68	-0.75	-0.46

5. CONCLUSIONS

Airborne laser altimetry has been used herein to estimate mass balance rates for glaciers located in the Glacier Bay area of Alaska and Canada. Mass balances are estimated by differencing glacier surface elevations acquired during repeat laser altimetry flights in 1995, 2000, 2005, 2009, and 2011.The mass balance record generally shows a more negative mass balance for the periods from 2000 to 2005 (period 2) and 2009 to 2011 (period 4) as compared to periods from 1995 to 2000 (period 1) and 2005 to 2009 (period 3).

The estimated regional mass change for the entire Glacier Bay glaciated area with the normalization method was -2.66 ± 0.49 Gt yr^{-1} during period 1, -5.14 ± 0.35 Gt yr^{-1} during period 2, -2.96 ± 0.46 Gt yr^{-1} during period 3, and -6.06 ± 0.56 Gt yr^{-1} during period 4. The area weighted mass balance method yields mass balance estimates that are more negative than those estimated with the normalization method. The difference was around 60% more negative for period 2, while periods 3 and 4 are around 25% more negative. This difference is likely due to the influence that the larger glaciers have in the area weighted method. Periods 3 and 4 had more glaciers profiled, including many smaller glaciers, which likely accounts for the smaller difference between the two regionalization methods.

There appears to be a weak relationship between the climate of Glacier Bay and the mass balance record. The positive degree day record corresponds to the altimetry mass balance during periods 2 through 4, however there is no correlation with period 1. There appears to be no correlation with winter precipitation, which is steadily increasing over the time period covered by altimetry measurements. The altimetry mass balance of the Glacier Bay region does correspond to the mass balance of Gulkana and Wolverine Glaciers over the same time periods as altimetry, suggesting an Alaska-wide pattern. All three areas had a more negative mass balance during period 2 as compared to periods 1 and 3.

Finally, the laser altimetry method has been validated against DEM differencing for glaciers located in the Glacier Bay area. The simu-laser method, wherein surface elevation changes along laser altimetry flightlines are extracted from a difference DEM, shows good agreement with DEM differencing. Berthier et al. (2010) found that the simu-laser ice loss was overestimated by 22% when compared to DEM differencing for ten Alaskan glaciers; here we find the simu-laser method underestimates ice loss in Glacier Bay by 6% when compared to DEM differencing.

REFERENCES

Abdalati, W., W. Krabill, E. Frederick, S. Manizade, C. Martin, J. Sonntag, R. Swift, R. Thomas, J. Yungel, and R. Koerner. 2004. *Elevation changes of ice caps in the Canadian Arctic Archipelago*. Journal of Geophysical Research, 109, F04007

Arendt, A.A., K.A. Echelmeyer, W.D. Harrison, C.S. Lingle, and V.B. Valentine. 2002. *Rapid wastage of Alaska glaciers and their contribution to rising sea level*. Science, 297, 382-386

Arendt, A, K. Echelmeyer, W. Harrison, C. Lingle, S. Zirnheld, V. Valentine, B. Ritchie, and M. Druckenmiller. 2006. *Updated estimates of glacier volume changes in the western Chugach Mountains, Alaska, and a comparison of regional extrapolation methods.* Journal of Geophysical Research, 111, F03019

Arendt, A.A, S.B. Luthcke, C.F. Larsen, W. Abdalati, W.B. Krabill, and M.J. Beedle. 2008. *Validation of high-resolution GRACE mascon estimates of glacier mass changes in the St Elias Mountains, Alaska, USA, using aircraft laser altimetry*. Journal of Glaciology, 54 (188), 778-787

Arendt, A.A, S.B. Luthcke, and R. Hock. 2009. *Glacier changes in Alaska: can mass-balance models explain GRACE mascon trends?* Annals of Glaciology, 50, 148-154

Bader, H. 1954. *Sorge's Law of densification of snow on high polar glaciers.* Journal of Glaciology, 2 (15), 319-323

Barclay, D.J., G.C. Wiles, and P.E. Calkin. 2009. *Holocene glacier fluctuations in Alaska*. Quaternary Science Reviews, 28, 2034-2048

Berthier, E., E. Schiefer, G.K.C. Clarke, B. Menounos, and F. Remy. 2010. *Contribution of Alaskan glaciers to sea-level rise derived from satellite imagery*. Nature Geoscience, 3, 92-95

Clague, J.J and S.G. Evans. 1994. *Historic retreat of Grand Pacific and Melbern Glaciers, Saint Elias Mountains, Canada: an analogue for decay of the Cordilleran ice sheet at the end of the Pleistocene?* Journal of Glaciology, 40 (134), 205-210

Connor, C., G. Streveler, A. Post, D. Monteith, and W. Howell. 2009. *The Neoglacial landscape and human history of Glacier Bay, Glacier Bay National Park and Preserve, southeast Alaska, USA*. The Holocene, 19, 381-393

Cooper, W.S. 1937. *The Problem of Glacier Bay, Alaska: A Study of Glacier Variations*. Geographical Review, 27, 37-62

Daly, C., G. Taylor, and W. Gibson. 1997. *The PRISM approach to mapping precipitation and temperature*. Preprints, 10th Conference on Applied Climatology, Reno, NV, American Meteorological Society, 10-12

Dyurgerov, M. 2002. *Glacier Mass Balance and Regime: Data of Measurements and Analysis*. University of Colorado Occasional Paper 55, 268 pp.

Echelmeyer, K.A., W.D. Harrison, C.F. Larsen, J. Sapiano, J.E. Mitchell, J. DeMallie, B. Rabus, G. Adalgeirsdottir, and L. Sombardier. 1996. *Airborne surface profiling of glaciers: a case-study in Alaska*. Journal of Glaciology, 42 (142), 538-547

Elliott, J.L., C.F. Larsen, J.T. Freymueller, and R.J. Motyka. 2010. *Tectonic block motion and glacial isostatic adjustment in southeast Alaska and adjacent Canada constrained by GPS measurements*. Journal of Geophysical Research, 115, B09407

Elsberg, D.H., W.D. Harrison, K.A. Echelmeyer, and R.M. Krimmel. 2001. *Quantifying the effects of climate and surface change on glacier mass balance*. Journal of Glaciology, 47 (159), 649-658

Field, W.O. 1947. *Glacier recession in Muir Inlet, Glacier Bay, Alaska*. Geographical Review, 37, 369-399

Foy, N., L. Copland, C. Zdanowicz, M. Demuth, and C. Hopkinson. 2011. *Recent volume and area changes of Kaskawulsh Glacier, Yukon, Canada*. Journal of Glaciology, 57 (203), 515-525

Geist, T., H. Elvehoy, M. Jackson, and J. Stotter. 2005. *Investigations on intra-annual elevation changes using multitemporal airborne laser scanning data: case study Engabreen, Norway*. Annals of Glaciology, 42, 195-201

Heinrichs, T.A., L.R. Mayo, K.A. Echelmeyer, and W.D. Harrison. 1996. *Quiescent-phase evolution of a surge type glacier: Black Rapids Glacier, Alaska, U.S.A*. Journal of Glaciology, 42 (140), 110-122

Hill, D.F. and S.E. Calos. 2011. *High-resolution gridded monthly precipitation and temperature data for Alaska*. Submitted, Journal of Hydrology

Hock, R. 2005. *Glacier melt: a review of processes and their modeling*. Progress in Physical Geography, 29, 362-391

Hodge, S. M., D.C. Trabant, R.M. Krimmel, T.A. Heinrichs, R.S. March, and E.G. Josberger. 1998. *Climate variations and changes in mass of three glaciers in western North America*. Journal of Climate, 11, 2161-2179

Huss, M., R. Hock, A. Bauder, M. Funk. 2012. *Conventional versus reference-surface mass balance*. Journal of Glaciology, 38 (208), 278-286

Jacob, T., J. Wahr, W.T. Pfeffer, and S. Swenson. 2012. *Recent contributions of glaciers and ice caps to sea level rise*. Nature, 10847

Kaufman, D.S. and W.F. Manley. 2004. *Pleistocene Maximum and Late Wisconsinan glacier extents across Alaska, U.S.A.* Developments in Quaternary Science, 2, 9-27

Krabill, W., W. Abdalati, E.B. Frederick, S.S. Manizade, C.F. Martin, J.G. Sonntag, R.N. Swift, R.H. Thomas, J.G. Yugel. 2002. *Aircraft laser altimetry measurement of the Greenland ice sheet: Techniques and accuracy assessment*. Journal of Geodynamics, 34, 357-376

Larsen, C.F., R.J. Motyka, J.T. Freymueller, K.A. Echelmeyer, and E.R. Ivins. 2005. *Rapid Viscoelastic uplift in southeast Alaska caused by post-Little Ice Age glacial retreat.* Earth and Planetary Science Letters, 237, 548-560

Larsen, C.F., R.J. Motyka, A.A. Arendt, K.A. Echelmeyer, and P.E. Geissler. 2007. *Glacier changes in southeast Alaska and northwest British Columbia and contribution to sea level rise*. Journal of Geophysical Research, 112, F01007

Luthcke, S.B., A.A. Arendt, D.D. Rowlands, J.J McCarthy, and C.F. Larsen. 2008. *Recent glacier mass changes in the Gulf of Alaska region from GRACE mascon solutions*. Journal of Glaciology, 54 (188), 767-777

Mann, D.H. and G.P. Streveler. 2008. *Post-glacial relative sea level, isostasy, and glacial history in Icy Strait, Southeast Alaska, USA*. Quaternary Research, 69, 201-216

Mann, M. E. 2002. *Little Ice Age*. Encyclopedia of Global Environmental Change, edited by M. C. MacCracken and J. S. Perry, 504-509

Meier, M.F. and A. Post. 1987. *Fast Tidewater Glaciers*. Journal of Geophysical Research, 92, 9051-9058

Meier, M.F., M.B. Dyurgerov, U.K. Rick, S. O'Neel, W.T. Pfeffer, R.S. Anderson, S.P. Anderson, and A.F. Glazovsky. 2007. *Glaciers dominate eustatic sea-level rise in the 21st century*. Science 317, 1064-1067

Miller, M.M. and M.S. Pelto. 1999. *Mass balance measurements on the Lemon Creek Glacier, Juneau Icefield, Alaska 1953–1998*. Geografiska Annaler 81A, 671-681

Molnia, B.F. 2007. *Late nineteenth to early twenty-first century behavior of Alaskan glaciers as indicators of changing regional climate.* Global and Planetary Change, 56, 23-56

Molnia, B. F. 2008. *Glaciers of North America - Glaciers of Alaska, in Satellite Image Atlas of Glaciers of the World*. R. S. Williams, Jr. and J. G. Ferrigno, eds. U.S. Geological Survey. Professional Paper 1386-K, 525 pp.

Nolan, M., A. Arendt, B. Rabus, and L. Hinzman. 2005. *Volume change of McCall Glacier, Arctic Alaska, USA, 1956-200*. Annals of Glaciology, 42, 409-416

Nuth, C., G. Moholdt, J. Kohler, J.O. Hagen, and A. Kaab. 2010. *Svalbard glacier elevation changes and contribution to sea level rise*. Journal of Geophysical Research, 115, F01008

Oerlemans, J., B. Anderson, A. Hubbard, P. Huybrechts, T. Johannesson, W.H. Knap, M. Schmeits, A.P. Stroeven, R.S.W. van de Wal, J. Wallinga, and Z. Zuo. 1998. *Modeling the response of glaciers to climate warming*. Climate Dynamics, 14, 267-274

Pelto, M. S. and M.M. Miller. 1990. *Mass balance of the Taku Glacier, Alaska, from 1946 to 1986*. Northwest Science, 64, 121-130

Pritchard, H. D., R. J. Arthern, D. G. Vaughan, and L. A. Edwards. 2009. *Extensive dynamic thinning on the margins of the Greenland and Antarctic ice sheets*. Nature, 461, 971-975

Pritchard, H.D., S.B. Luthcke., A.H. Fleming. 2010. *Understanding ice-sheet mass balance: progress in satellite altimetry and gravimetry*. Journal of Glaciology, 56 (200), 1151-1161

Raup, B., A. Racoviteanu, S.J.S. Khalsa, C. Helm, R. Armstrong, and Y. Arnaud. 2007. *The GLIMS geospatial glacier database: A new tool for studying glacier change*. Global and Planetary Change, 56, 101-110

Rignot, E., A. Rivera, and G. Casassa. 2003. *Contribution of the Patagonia Icefields of South America to Sea Level Rise*. Science 302, 434-437

Sapiano, J.J., W.D. Harrison, and K.A. Echelmeyer. 1998. *Elevation, volume and terminus changes of nine glaciers in North America*. Journal of Glaciology, 44 (146), 119-135

Schwitter, M.P. and C.F. Raymond. 1993. *Changes in the longitudinal profiles of glaciers during advance and retreat*. Journal of Glaciology, 39 (133), 582-590

Truffer, M., W.D. Harrison, and R.S. March. 2005. *Record negative glacier balances and low velocities during the 2004 heatwave in Alaska, USA: implications for the interpretation of observations by Zwally and others in Greenland.* Journal of Glaciology, 51 (175), 663-664

Van Beusekom, A.E., S.R. O'Neel, R.S. March, L.C. Sass, and L.H. Cox. 2010. *Re-analysis of Alaskan benchmark glacier mass-balance data using the index method*. U.S. Geological Survey Scientific Investigations Report 2010-5247, 16 pp.

Wu, X. P., M.B. Heflin, H. Schotman, B.L.A Vermeersen, D.A. Dong, R.S. Gross, E.R. Ivins, A. Moore, and S.E. Owen. 2010. *Simultaneous estimation of global present-day water transport and glacial isostatic adjustment.* Nature Geoscience, 3, 642-646

Walter, F., S. O'Neel, D. McNamara, W.T. Pfeffer, J.N. Bassis, H.A. Fricker. 2010. *Iceberg calving during transition from grounded to floating ice: Columbia Glacier, Alaska*. Geophysical Research Letters, L15501

APPENDIX A

Terminus Retreat of Muir Glacier

The tidewater retreat of Muir Glacier since 1890 has been documented through the analysis of satellite images and topographic maps that have historical glacier terminus locations. Muir Glacier is currently a slowly retreating, land-terminating glacier, however as recently as 1993 Muir was a tidewater glacier that had experienced rapid terminus retreat since the LIA glacier maximum. The main objective in this case study is to determine how far the terminus has retreated since 1892 and the rate at which the retreat has occurred. Additionally, time periods that have similar behaviors are identified, especially instances where the retreat rates are higher.

Satellite images acquired by the Landsat program between 1972 and 2010 were used to map glacier extent and terminus locations over time. Mapping was done through manual digitization within a GIS using the visual contrast between ice and water (during periods when Muir Glacier was a tidewater, calving glacier) to identify the position of the terminus. However, identification of the terminus can be complicated by the presence of a thick mélange of icebergs at the calving front. During 1993 the glacier transitioned into a land-terminating glacier, at which point the visual contrast between ice and rock / sediment is used to identify the terminus location. The glacier boundaries are outlined south of where the two 2010 branches of Muir Glacier merge together (one of which is named Morse Glacier) for simplicity purposes (Fig. 20). These two branches have almost separated, however they appear to still be contributing to the same terminus as of 2010. Debris-covered parts of the glacier, i.e. medial moraines, debris covered lateral moraines, and the debris-covered terminus are included as part of the glacier.

Historical terminus positions from topo maps were manually digitized after the maps were georeferenced. Most of the historic terminus positions on the topo maps only have the terminus locations drawn over the current surface of Muir Inlet. The terminus locations are simply digitized following the terminus position lines that are located on the georeferenced topo maps. There are two instances, in 1892 and 1942, where full glacier areal extents are recorded on the maps and outlined.

The amount of terminus retreat that has occurred was determined by measuring how far previous terminus locations were from the August 2010 terminus location. This measurement is made along the centerline of the present Muir Inlet fjord. This fjord confined the centerline flow of Muir Glacier and is considered here to be representative of the centerline of the glacier during

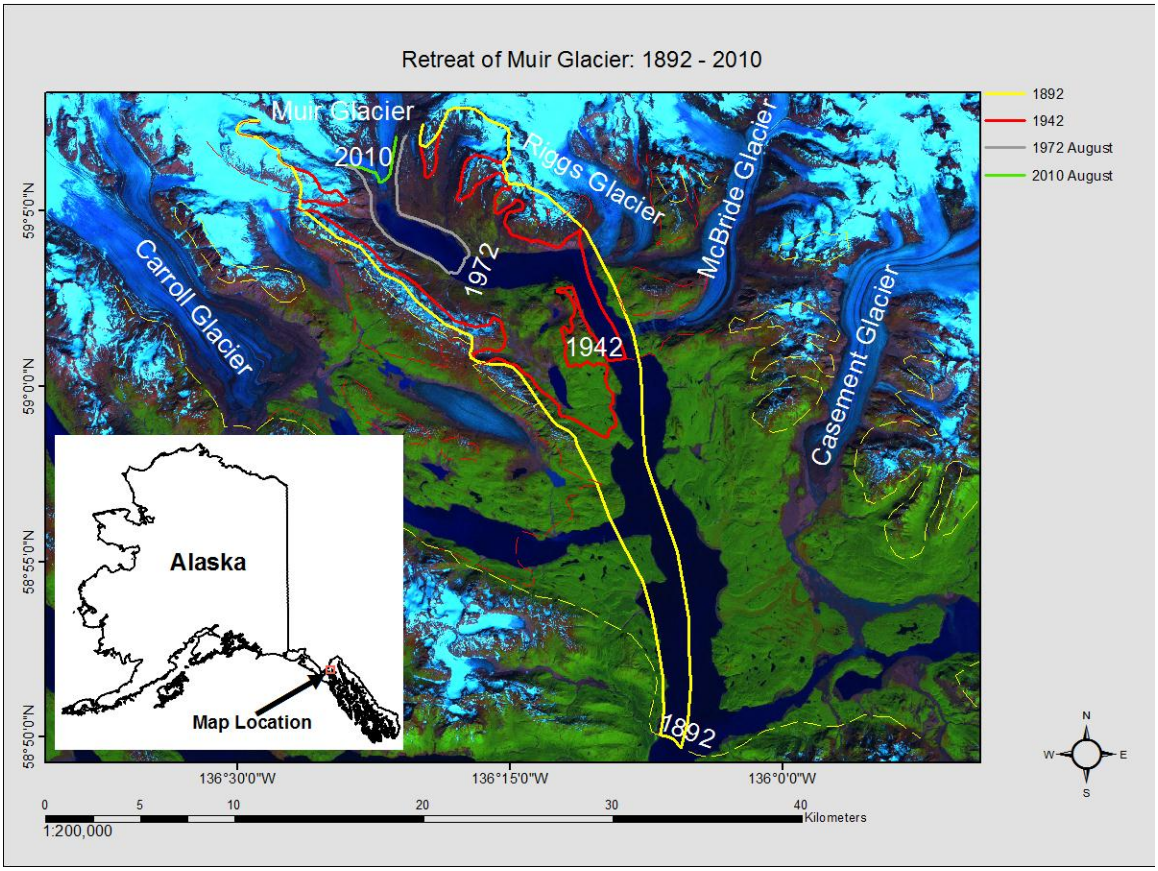

Fig. 20: Historic glacier extent of Muir Glacier during 1892, 1942, and 1972. Dashed lines for 1892 and 1942 are total glacier extent, and solid lines are an attempt to identify only the contribution of Muir Glacier based on the indicated positions of medial moraines on the topo maps. All of the labeled glaciers were part of or connected to Muir Glacier in 1892. This shows the massive amount of glacier loss that has occurred since 1892. The overall surface area loss between 1892 and 2010 is on the order of 700 km^2, and between 1942 and 2010 is around 250 km^2.

the past. The retreat rate can be calculated by dividing the amount of retreat (or advance in some cases) that occurred between subsequent terminus locations by the time elapsed between those terminus locations.

The change in terminus location is examined on an annual to biannual time span between 1972 and 2010 as cloud free Landsat images have been acquired for almost every year since 1972. Years not represented are 1991, 1992, 1996-1998, 2005, and 2008, which all happen to be after the rapid tidewater retreat had ceased. Terminus locations prior to 1972 are derived from topo maps that have historic terminus positions dating back to 1892. Additionally, the transition of Muir Glacier from a tidewater glacier to a land-terminating (or terrestrial) glacier is examined by analyzing the increase in the size of the outwash plain at the terminus of Muir Glacier.

In total 87 Landsat images were used that are multiband, geolocated TIF files (Table 10). For Landsat one, two, and three bands 7, 5, and 4 were used to create a false color image, for Landsat four bands 4, 2, and 1 were used, and for Landsat five and seven bands 5, 4, and 2 were used. With this combination of Landsat bands glacier ice appears as a distinct blue color. Additionally, these specific band combinations have been used almost exclusively in past studies of glaciers that used Landsat images.

Table 10: Number of Landsat images used to monitor Muir Glacier terminus retreat for each Landsat mission.

Landsat	Period	Number of Images
1	Aug 1972 - Mar 1976	10
2	May 1977 - June 1981	5
3	July 1978 - Aug 1982	9
4	July 1983 - Aug 1983	2
5	July 1984 - Sept 2011	39
7	Aug 1999 - Sept 2010	22

A USGS topographic map with terminus positions between 1948 and 1964 was acquired from the web service AlaskaMapped. Earlier mapped terminus positions were acquired from a 1947 topographic map by the American Geographical Society (AGS) titled *Muir Inlet: Glacier Bay, Alaska, 1941 – 1946* (located in Field, 1947).

The transition to a terrestrial glacier was initiated by the accumulation of sediment at the calving front of Muir Glacier. The calving of the glacier into the East Arm fjord rapidly ceased once sediment began to accumulate and a sediment outwash plain began to build up at the

terminus. The sediment debris that has accumulated there are visually distinct from the glacier and from the ocean, thus the area of the outwash plain can be examined and its change in size over time can be estimated. The now-terrestrial glacier terminus continues to retreat and sediment has accumulated in the growing outwash plain. The location of the outwash plain and ocean interface has remained relatively stationary over time as the terminus has retreated.

Retreat since 1892, which is the earliest terminus location on the topo maps, has totaled around 41 km. The bulk of the terminus retreat occurred prior to the acquisition of Landsat images starting in 1972, at which time the terminus was around 7 km down-glacier from the 2010 terminus. During the Landsat era the majority of the terminus retreat occurred between May 1975 and August 1977. The retreat during this two-year time span totaled over 4 km, which is over 60% of the total terminus retreat between 1972 and 2010. Retreat rates during this period were up to 4.5 km yr^{-1}, while the overall retreat rate between 1892 and 1977 was 0.46 km yr^{-1}. The retreat rate between 1977 and 2010 was 0.05 km yr^{-1}, which includes a period of tidewater terminus advancement that occurred between 1984 and 1989.

A.1. Results

A.1.1. Terminus Retreat Determined From Historical Topo Maps

The retreat of the Muir Glacier terminus between 1892 and 1972 accounts for the majority of retreat since 1892. During this time period, the terminus retreated 34 km with an average retreat rate of 0.43 km yr^{-1}. However, this includes a period of no recorded terminus positions between 1892 and 1907 (Fig. 21). Including the more complete record between 1907 and 1972 (Fig. 22) gives a retreat of 21 km (Fig. 23) and an average retreat rate of 0.32 km yr^{-1} (Fig. 24) for that time period. From this data I infer that there was a period of faster retreat that occurred between 1892 and 1907 that was not recorded on the topo maps. During those 15 years the terminus retreated 13 km. This also corresponds with Cooper's (1937) reported retreat rates of 2.69 km yr^{-1} in the few years prior to 1907. There are a few years where there is very little retreat occurring, including 1926-1931 and 1940-1942 (Fig. 22 and 23). These two time periods had retreat rates around 0.05 km yr^{-1}.

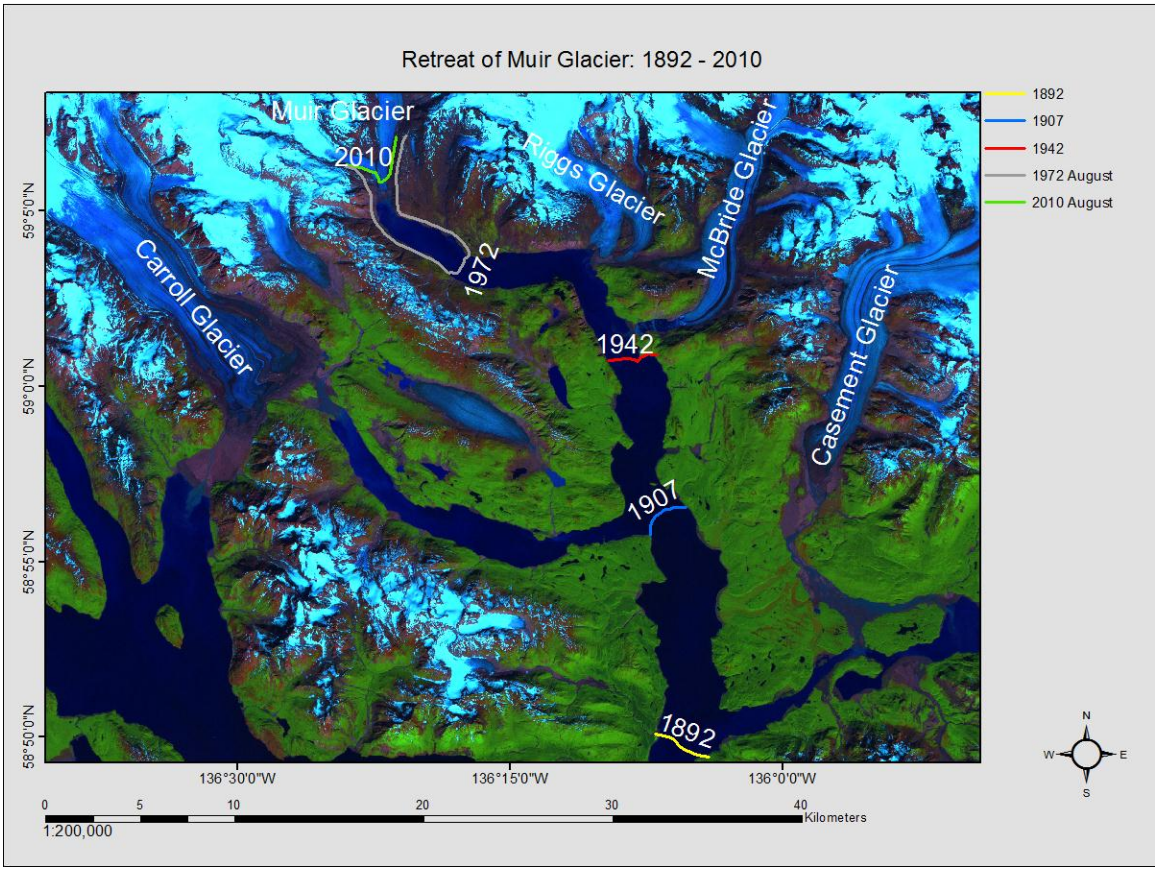

Fig. 21: Retreat of Muir Glacier between 1892 and 2010 with terminus locations indicated for 1892, 1907, 1942, and 1972. Between 1892 and 1907 there are no recorded terminus positions, during which time a large retreat occurred.

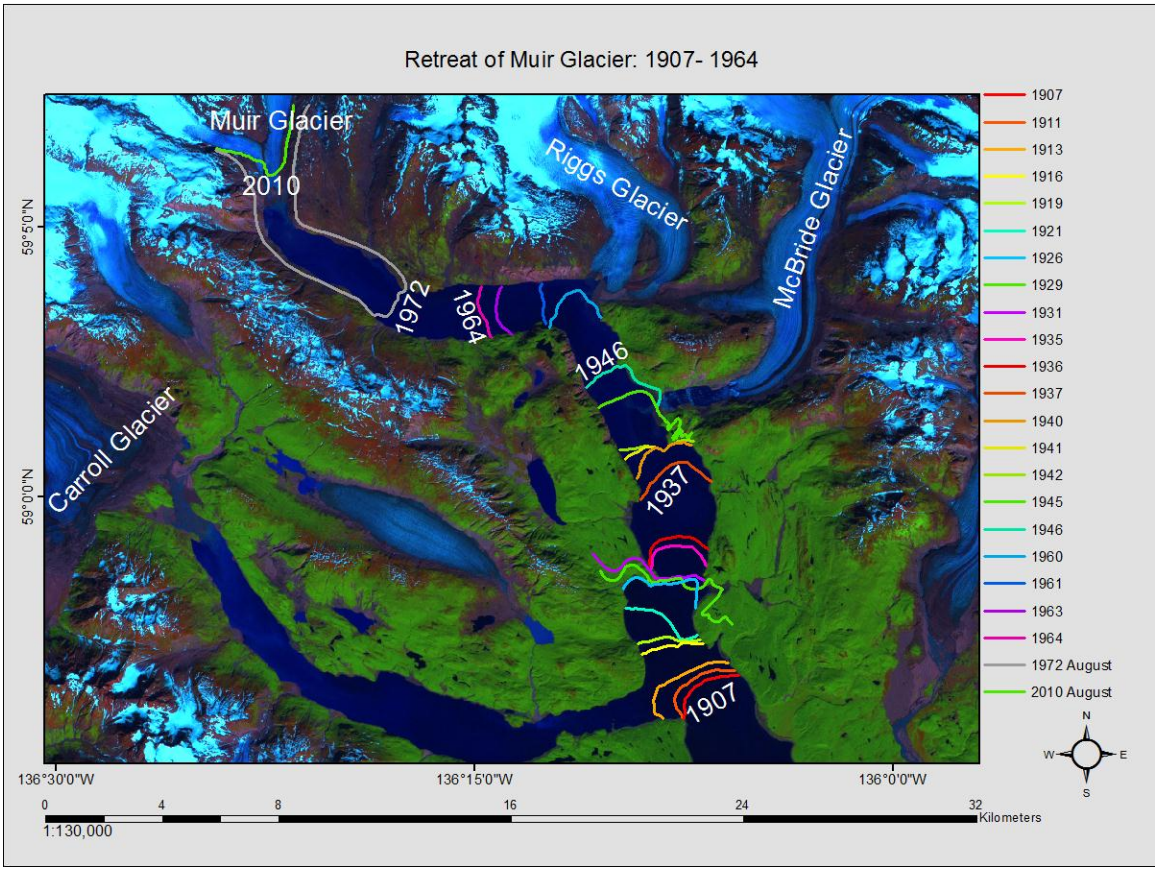

Fig. 22: Retreat of Muir Glacier between 1907 and 1964 showing all historical terminus positions from the topo maps, except for 1892. Visible here are the locations where retreat had almost ceased between 1926-1931 and 1940-1942. In 1930 the ice front was stopped at a peninsula adjacent to The Nunatak, and in 1940 the ice front was at a peninsula of Van Horn Ridge and was also still connected to McBride Glacier.

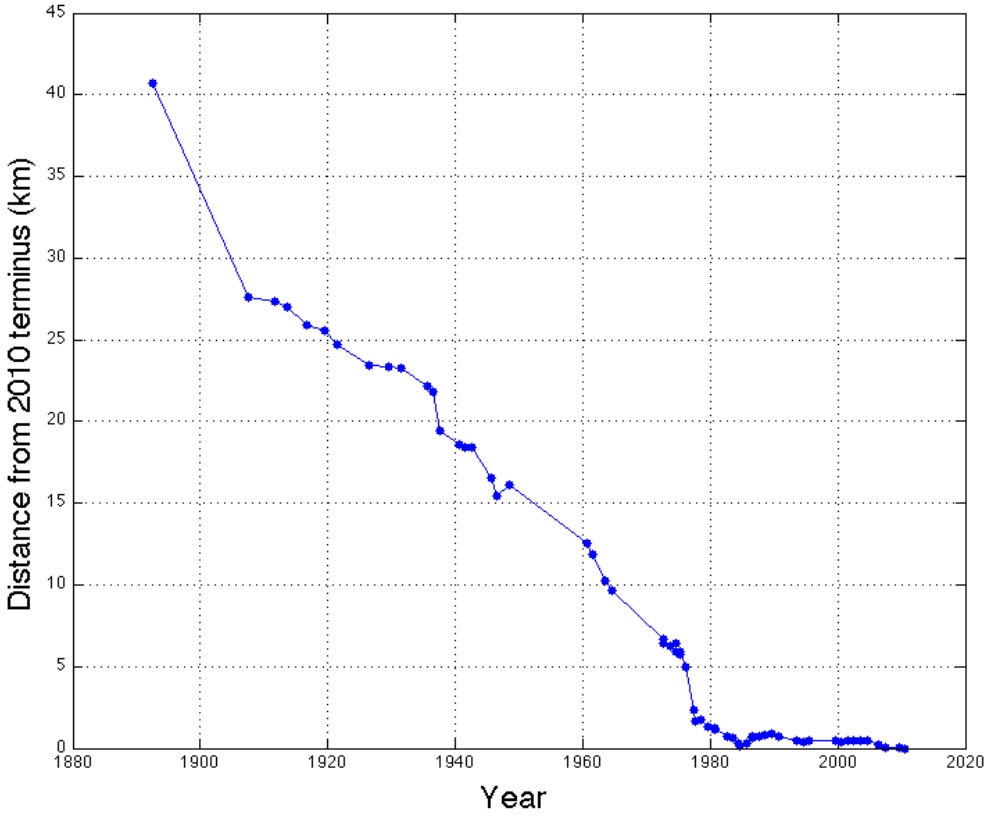

Fig. 23: The retreat distance of Muir Glacier for all digitized terminus positions. Distances are calculated from the August 2010 terminus. The overall record is marked by consistently fast retreat prior to 1977 and the period of retreat between 1975 and 1977 is especially noticeable.

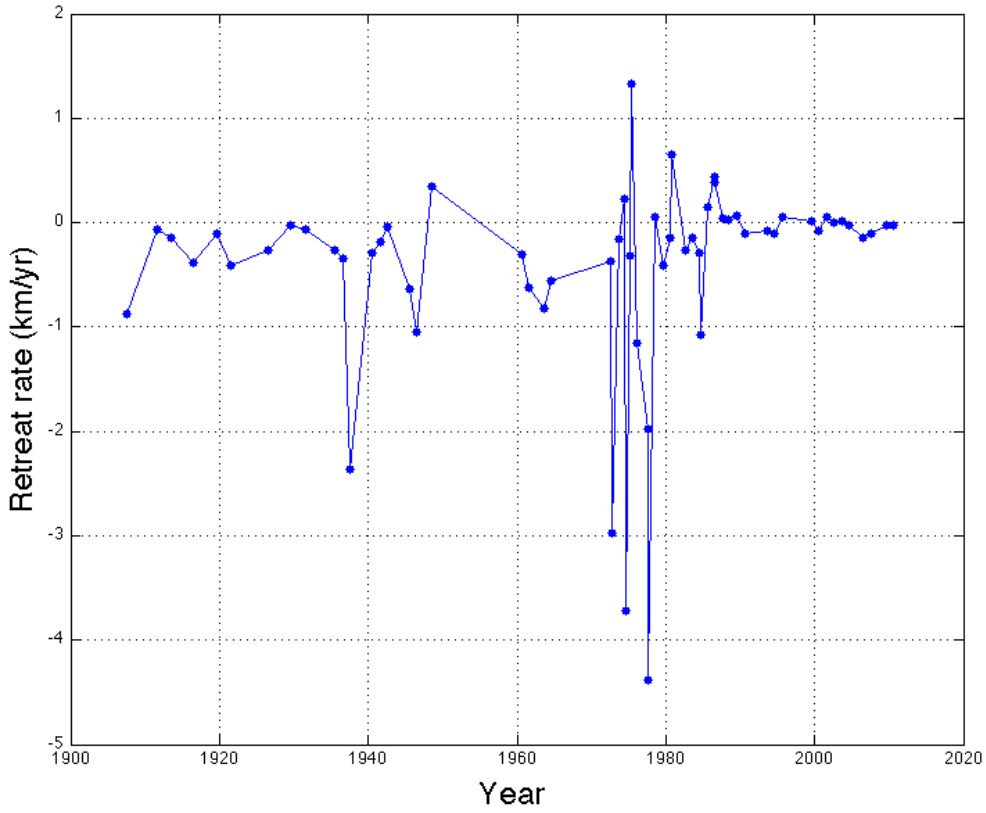

Fig. 24: Muir Glacier rate of retreat between 1892 and 2010 derived from all of the digitized terminus positions. The rapid retreat during the 1970's is visible as the large variations in retreat rate. Prior to 1970 retreat rates fluctuated up and down, with the fastest rate occurring in 1937.

A.1.2. Terminus Retreat During the Landsat Era

There are four distinct periods of glacial behavior between 1972 and 2010. The first period is from 1972 to 1977 (Fig. 25) and is characterized by rapid retreat rates (Fig. 24). At this time the terminus was around 7 km downstream from the 2010 terminus, with the bulk of the retreat occurring between May 1975 and August 1977 (Fig. 23). Total retreat from 1972-1977 totaled around 5 km with an average retreat rate of 1.0 km yr^{-1}. The retreat between 1975 and 1977 totaled over 4.2 km, which is over 60% of the total retreat since 1972. Retreat rates during this period were up to 4.5 km yr^{-1} with an average retreat rate of 1.84 km yr^{-1}. This is significantly higher than the overall retreat rate between 1892 and 1977 of 0.46 km yr^{-1}. There were also a few periods of terminus advance occurring in late spring / early summer prior to the height of the summer melt season.

The second period is from 1978 to 1984 (Fig. 26) and is characterized by slower but sustained retreat. Total retreat was around 1.6 km (Fig. 23) with average retreat rates of 0.26 km yr^{-1} (Fig. 24). The September 1984 terminus position was located remarkably close to the 2010 terminus position, being only 0.14 km down-glacier.

The third period is from 1984 to 1989 (Fig. 27) and is characterized by a period of terminus advance. The total advance was around 0.7 km (Fig. 23) with average advance rates of 0.14 km yr^{-1} (Fig. 24). However, most of the advance occurred between 1984 and 1986, with around 0.58 km of advance taking place with an average advance rate of 0.30 km yr^{-1}. The terminus position advanced to a maximum distance of 0.87 km down-glacier the 2010 terminus.

The fourth period is from 1989 to 2010 (Fig. 28) and is characterized by a period of very slow retreat. Between 1993 and 2004 the terminus position was relatively stable (Fig. 23), with some periods of slight advance occurring. The overall retreat during this time period was 0.05 km for a retreat rate of 0.005 km yr^{-1}. There was some drawback of the Morse Glacier arm during this time period as its contribution to the terminus declined. The terminus then retreated more rapidly from 2004 to 2010 (Fig. 23), with 0.46 km of retreat occurring with a retreat rate of 0.08 km yr^{-1}.

A.1.3. Outwash plain buildup

The outwash plain at the terminus of Muir Glacier has built up steadily since sediment first began to accumulate at the calving front in 1990. The size of the plain has fluctuated on a yearly

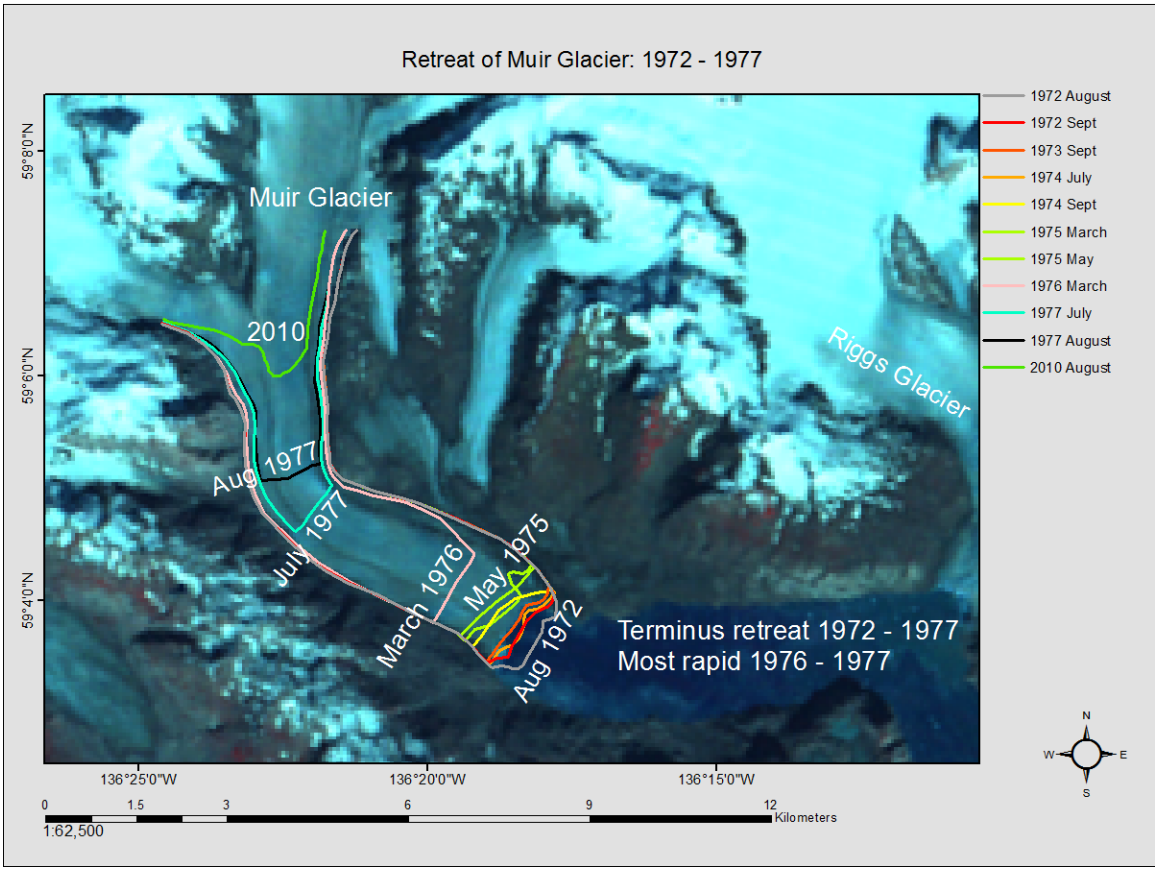

Fig. 25: Retreat of Muir Glacier between 1972 and 1977 derived from Landsat terminus positions. The retreat between 1972 and 1975 appeared to have caused little change in glacier surface elevation based on the location of the glacier surface on the fjord walls and was also marked by some advances in terminus position. However, there was also a significant change in the position of the glacier along the steep fjord walls during the rapid retreat from 1975 to 1977, which indicates a substantial surface lowering.

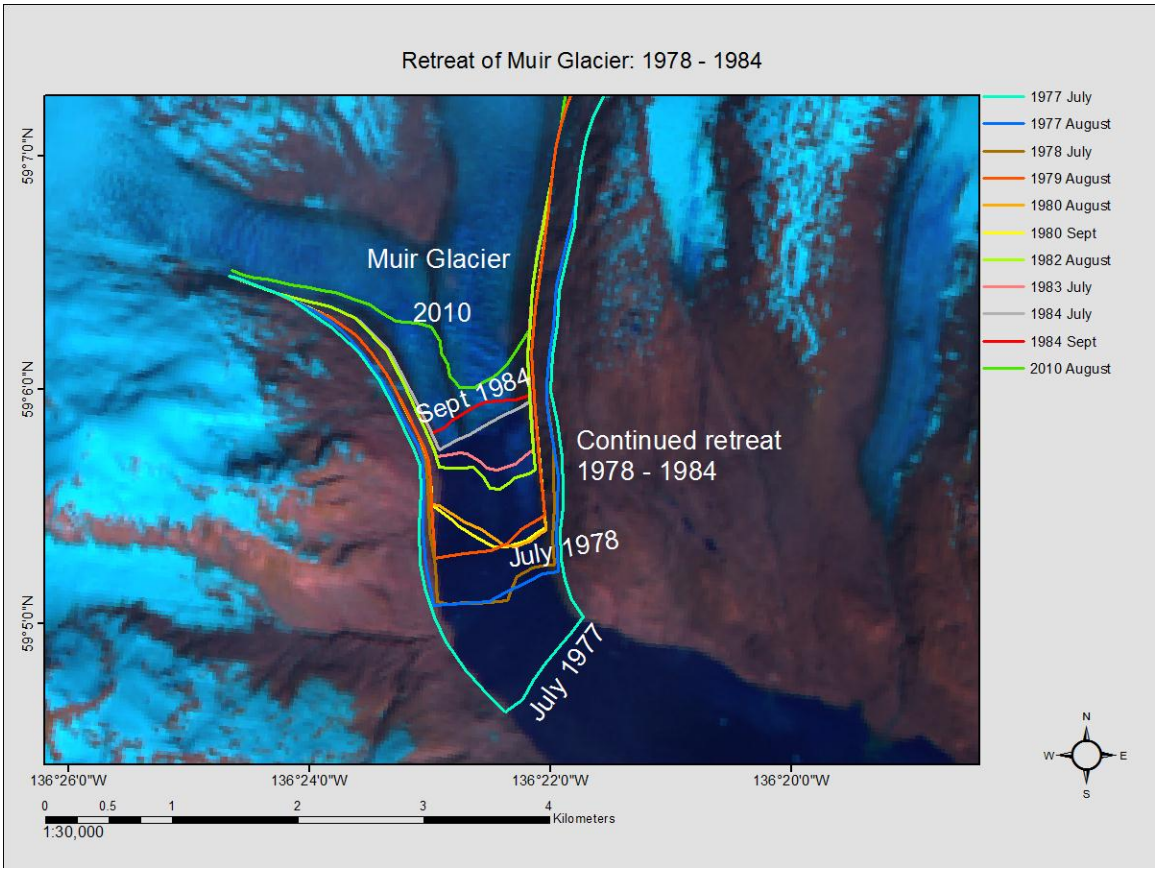

Fig. 26: Retreat of Muir Glacier between 1977 and 1984 derived from Landsat terminus positions. The September 1984 calving front is located very close to the position of the 2010 terminus, being only around 150 m away. This gives some insight into the geometry of the outwash plain that has built up since then. As before, there is significant lowering of the glacier surface that has occurred during this period.

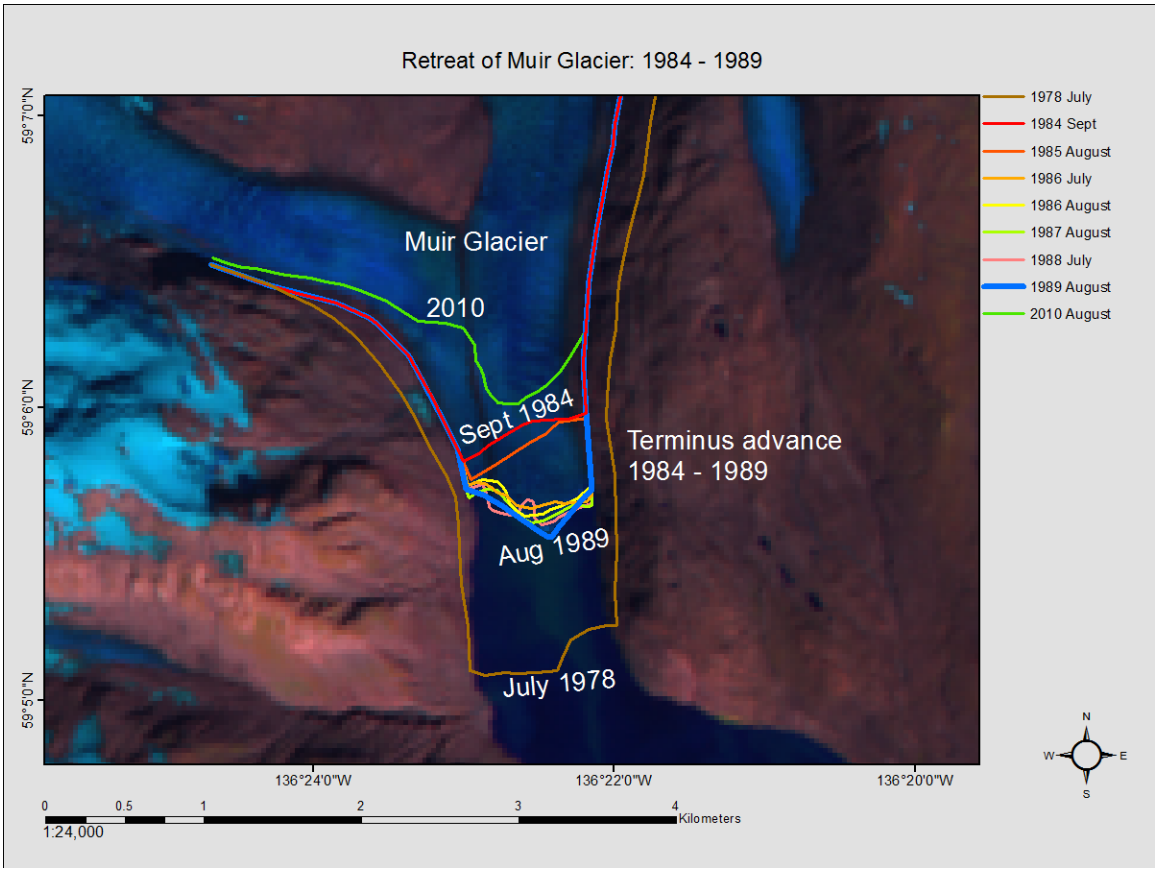

Fig. 27: Advance of Muir Glacier between 1984 and 1989 derived from Landsat terminus positions. The surface elevation appeared to be relatively stable during this period of advance of the terminus. Most of the advance occurred between 1984 and 1986.

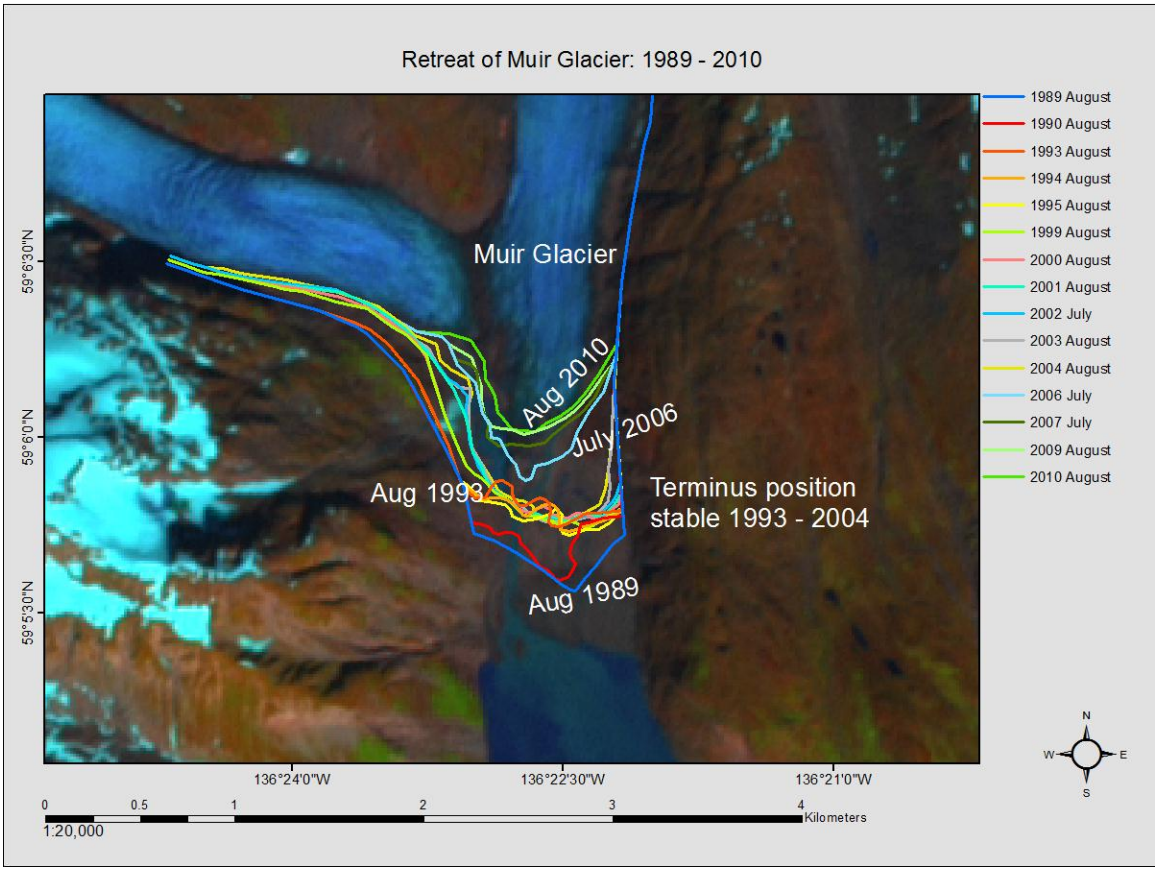

Fig. 28: Retreat of Muir Glacier between 1989 and 2010 derived from Landsat terminus positions. Visible here is the declining contribution of the western branch (Morse Glacier) as it pulled back while the main terminus position of Muir was stable between 1993 and 2004. After 2004 both branches were retreating and they have almost separated as of 2010. The outwash plain has also built up to sizeable extent and is preventing the ocean from reaching the present terminus.

basis and has built up to around 110 hectares as of August 2010 (Fig. 29). However, with this method there is no way to account for the effect of tides on the area. Additionally, the location of the September 1984 terminus provides a clue about the geometry of the outwash plain. Looking at the outwash plain in the August 2010 images, there is no way to tell the depth of the bedrock below the outwash plain. However, since it is known that in 1984 the calving terminus was 140 m from the 2010 terminus, it is also known that bedrock has to be below sea level at the location of the 1984 terminus. This information could provide minimum constraints for the volume of the outwash plain.

A.2. Using Landsat to Monitor Glacier Changes

Using this method to determine glacier terminus positions has a number of advantages. Landsat images are widely available for download through the USGS and date back to the launch of Landsat 1 in 1972. Different images can be easily compared within a GIS, and a working knowledge of how to use a GIS makes creating glacier outlines simple. Rapid changes in terminus position are easily detected, however in some glaciers this change occurs very slowly. This situation can still be easily studied due to the almost 40-year Landsat record, and a high-resolution record of terminus positions can be found if a suitable number of cloud free images are available.

The use of Landsat images for glacier outlining depends on finding cloud-free images. This can be a challenge as glaciers are typically located in mountainous areas, which are prone to having lots of cloud cover. Generally glacier outlining is done on images that are acquired during the end of the melt season, because snowfall will make determining the extent of the glacier difficult. Thus, using images that don't have recent snowfall is preferred. The accuracy of the digitized terminus depends on the resolution of the image; so earlier Landsat images will have larger errors in the accuracy of terminus positions. The geomorphology of the glacier can also have an effect on the ability to determine glacier extent. A debris-covered terminus can be hard to distinguish from the surrounding moraine features and sediment outwash. Also, differentiating between a tidewater glacier and a thick mélange of icebergs can be difficult, especially for earlier images that have lower resolution.

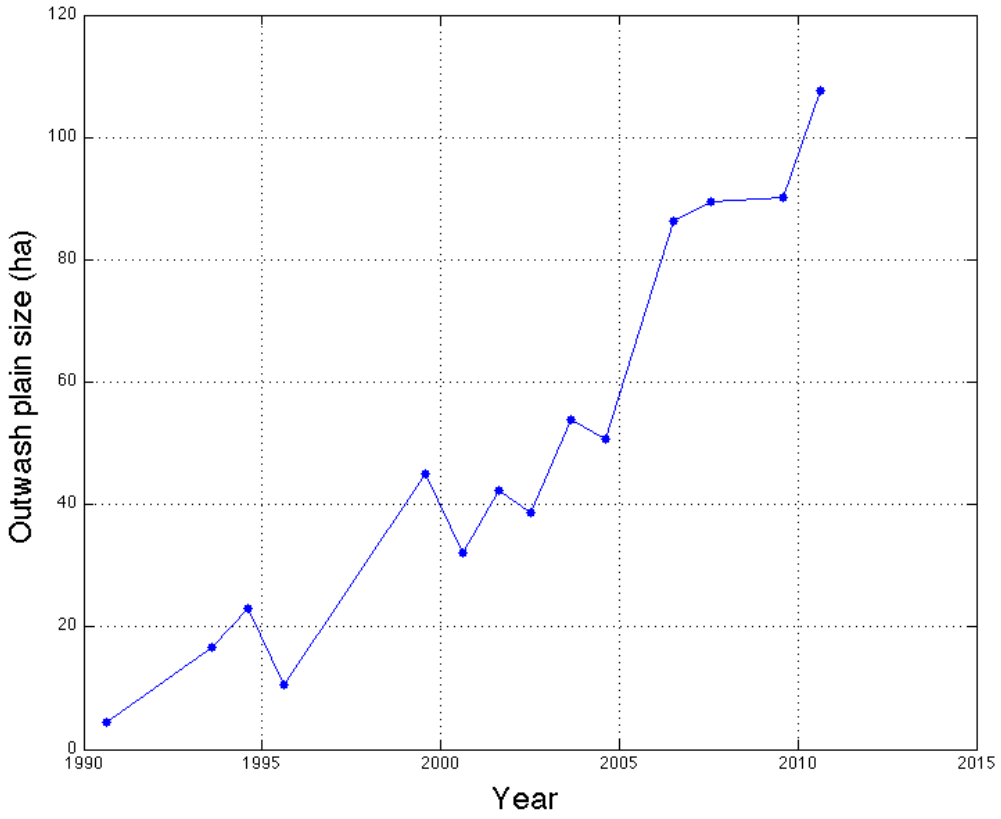

Fig. 29: Growth of Muir outwash plain between 1990 and 2010. Sediment started to build up at the tidewater terminus around 1990 and by 1993 Muir was no longer a tidewater glacier. Whether the fluctuations within the increasing overall trend are due to erosional processes or the effect of tidal variation is unknown.

A.3. Conclusion

Retreat since 1892 has totaled around 41 km. The majority of the terminus retreat occurred prior to the acquisition of Landsat images starting in 1972. Overall, the history of the retreat of Muir Glacier shows a couple of different time periods with consistent behavior. First, there is a steady and fast retreat occurring between 1892 and 1977 with an average retreat of around 0.4 km yr^{-1}. However, there are also a couple of instances where the retreat almost stops for a few years (1926-1931 and 1940-1942). These slower periods had terminus positions that were located at points where peninsulas jut out into Muir Inlet at Van Horn Ridge and The Nunatak. These peninsulas likely acted as "sticking points" or an "anchor position" for Muir Glacier's calving front. This would cause a decrease in the amount of the terminus that was exposed to direct calving into the ocean and could have potentially have caused a reduction in the rate of calving during these years. A similar situation occurred more recently at Columbia Glacier, which experienced slower retreat during the time that the terminus was located at the inlet constriction near the Great Nunatak. The rate of retreat of Columbia increased substantially after the glacier retreated back into the broader bay north of the Great Nunatak during 2005, mirroring what had previously occurred at Muir Glacier.

During the Landsat era the majority of the terminus retreat occurred between May 1975 and August 1977. The retreat during this two-year time span totaled over 4 km, which is over 60% of the total retreat since 1972. Retreat rates during this period were up to 4.5 km yr^{-1}, while the overall retreat rate between 1892 and 1977 was 0.46 km yr^{-1}. The fastest calculated rates of retreat during the observed time period occurs during the 1970's with retreat rates in 1977 reaching almost 5 km yr^{-1}. This is likely due to having multiple terminus positions recorded per year in the 1970's, which is able to capture the faster retreat that occurs during the spring and summer. The majority of a retreating tidewater glacier's calving happens during the spring and summer, with little change or even terminus advance happening during winter. This means that the recorded terminus positions from the topographic maps can basically be considered to be a smoothed yearly average that fails to isolate the seasonal retreat.

Slower and sustained retreat occurred between 1978 and 1984, after which a period of terminus advance lasted until 1989. The 1984 calving terminus was located only 140 m from the 2010 terminus, which is now the location of the outwash plain. Slow retreat began again after 1989 and coincided with the formation of the outwash plain at the glacier terminus. After the

glacier transitioned to a land terminating state the terminus position was mostly stable between 1993 and 2004, with some retreat of the western arm (Morse Glacier). After 2004 the terminus began to retreat again at a higher rate.

APPENDIX B

Supplementary Tables

Table 11: Specific mass balances rates in m w.e. yr^{-1}.

Glacier Name	'95/'96 – '00/'01	'00 – '05	'05 – '09
Brady	-1.01 ± 0.13	-1.83 + 0.19 /– 0.15	-0.73 + 0.22 /– 0.17
Lamplugh	-0.31 ± 0.21	-0.53 + 0.22 /– 0.21	-0.10 + 0.25 /– 0.28
Reid	-0.30 + 0.21 /– 0.22	-0.93 + 0.15 /– 0.16	-0.10 + 0.16 /– 0.17
Casement			-1.11 + 0.20 /– 0.25
Davidson			-0.68 + 0.23 /– 0.22
Riggs			-0.41 + 0.17 /– 0.18
Muir		-0.47 + 0.28 /– 0.29	0.05 ± 0.43
Carroll			
Tkope			
Margerie			0.07 + 0.48 /– 0.50
Fairweather			
Grand Plateau			-1.02 + 0.36 /– 0.40
Grand Pacific	-0.47 ± 0.34		
Melbern			
Konamoxt			
Little Jarvis	-0.39 ± 0.26		
Measured Avg.	-0.50 ± 0.11	-0.94 ± 0.11	-0.45 ± 0.10

Glacier Name	'09 – '11	'01 – '09	'95 – '11
Brady	-1.44 + 0.16 /– 0.21		
Lamplugh	-0.06 + 0.22 /– 0.16		
Reid	-0.14 + 0.25 /– 0.31		
Casement	-1.50 + 0.25 /– 0.44		
Davidson	-1.18 + 0.15 /– 0.14		
Riggs	-0.92 + 0.19 /– 0.22		
Muir	0.22 + 0.18 /– 0.30		
Carroll	-0.55 + 0.21 /– 0.19		
Tkope	-0.35 + 0.23 /– 0.21		
Margerie	0.36 + 0.83 /– 1.11		
Fairweather	-1.31 + 0.72 /– 0.86		
Grand Plateau	-2.77 + 0.56 /– 0.61		
Grand Pacific	-1.63 + 0.48 /– 0.51	-1.16 + 0.28 /– 0.36	
Melbern	-0.67 + 0.62 /– 0.50		
Konamoxt			-1.25 + 0.31 /– 0.35
Little Jarvis			
Measured Avg.	-0.85 + 0.11 /– 0.13		

Table 12: Mass balances rates in Gt yr^{-1}.

Glacier Name	**'95/'96 – '00/'01**	**'00 – '05**	**'05 – '09**
Brady	-0.50 ± 0.07	-0.91 ± 0.08	-0.36 ± 0.09
Lamplugh	-0.04 ± 0.03	-0.07 ± 0.03	-0.02 ± 0.04
Reid	-0.02 ± 0.02	-0.06 ± 0.01	-0.01 ± 0.01
Casement			-0.18 ± 0.04
Davidson			-0.06 ± 0.02
Riggs			-0.05 ± 0.02
Muir		-0.05 ± 0.03	0.01 ± 0.05
Carroll			
Tkope			
Margerie			0.01 ± 0.09
Fairweather			
Grand Plateau			-0.39 ± 0.16
Grand Pacific	-0.25 ± 0.18		
Melbern			
Konamoxt			
Little Jarvis	-0.001 ± 0.0004		
Measured Total	-0.82 ± 0.19	-1.09 ± 0.09	-1.05 ± 0.22

Glacier Name	**'09 – 11**	**'01 – '09**	**'95 – '11**
Brady	-0.71 ± 0.11		
Lamplugh	-0.01 ± 0.02		
Reid	-0.01 ± 0.02		
Casement	-0.24 ± 0.07		
Davidson	-0.10 ± 0.01		
Riggs	-0.10 ± 0.02		
Muir	0.03 ± 0.04		
Carroll	-0.22 ± 0.08		
Tkope	-0.04 ± 0.02		
Margerie	0.06 ± 0.19		
Fairweather	-0.31 ± 0.20		
Grand Plateau	-1.07 ± 0.24		
Grand Pacific	-0.86 ± 0.27	-0.61 ± 0.23	
Melbern	-0.05 ± 0.04		
Konamoxt			-0.09 ± 0.02
Little Jarvis			
Measured Total	-3.63 ± 0.47		

Table 13: Simu-laser and difference DEM mass balance rates in Gt yr^{-1}.

Glacier	km^2 2010	$\dot{B}_{DEM}$ Gt yr^{-1}	$\dot{B}_{SIMU}$ Gt yr^{-1}	Simu - DEM Gt yr^{-1}
Brady	512.1	-0.253	-0.274	-0.021
Lamplugh	142.1	0.037	0.034	-0.003
Reid	70.1	0.004	-0.001	-0.005
Casement	162.5	-0.152	-0.150	0.002
Davidson	85.8	-0.069	-0.060	0.009
Riggs	115.9	-0.081	-0.102	-0.021
Muir	130.6	-0.164	-0.298	-0.134
Carroll	405.4	-0.334	-0.304	0.030
Tkope	116.9	-0.040	-0.044	-0.004
Margerie	182.0	-0.003	-0.005	-0.002
Fairweather	279.1	-0.222	-0.163	0.060
Grand Plateau	402.6	-0.340	-0.292	0.048
Grand Pacific	565.2	-0.414	-0.388	0.026
Melbern	82.7	-0.106	-0.078	0.028
Konamoxt	73.5	-0.047	-0.052	-0.005
Little Jarvis	1.8	0.000	0.000	0.000
Alsek	243.8	-0.097	-0.097	0.001
Johns Hopkins	253.6	-0.014	0.046	0.059
LaPerouse	123.6	-0.022	-0.030	-0.008
McBride	118.6	-0.120	-0.140	-0.019
Bucknell	92.4	-0.061	-0.055	0.006
Crillon	91.3	-0.003	0.014	0.017
Tsirku	87.5	-0.023	-0.016	0.007
Lituya	84.6	-0.012	-0.011	0.001
Sea Otter	69.3	-0.026	-0.027	-0.001
Rendu	67.2	0.008	0.021	0.013
South Netland	60.5	-0.019	-0.018	0.002
Tikke	59.1	-0.064	-0.028	0.036
Jarvis	59.0	-0.057	-0.043	0.014
Peshak	53.0	-0.045	-0.021	0.023
Cushing	45.9	-0.015	-0.018	-0.003
North Alsek	42.0	-0.008	-0.010	-0.002
Tenas Tikke	41.7	-0.006	0.020	0.025
Finger	37.6	0.001	-0.002	-0.003
South Davidson	36.2	-0.023	-0.025	-0.003
Garrison	33.0	-0.010	-0.013	-0.003
Netland	33.0	-0.015	-0.021	-0.006
North Bucknell	28.9	-0.027	-0.029	-0.002
Towagh	27.6	-0.004	-0.005	-0.001
Gilman	25.6	0.006	0.010	0.003
Profiled glaciers	3328.3	-2.18	-2.18	0.01
Unprofiled glaciers	1815.0	-0.66	-0.50	0.16
Total	5143.3	-2.84	-2.67	0.16

APPENDIX C

Supplementary Mass Balance Figures

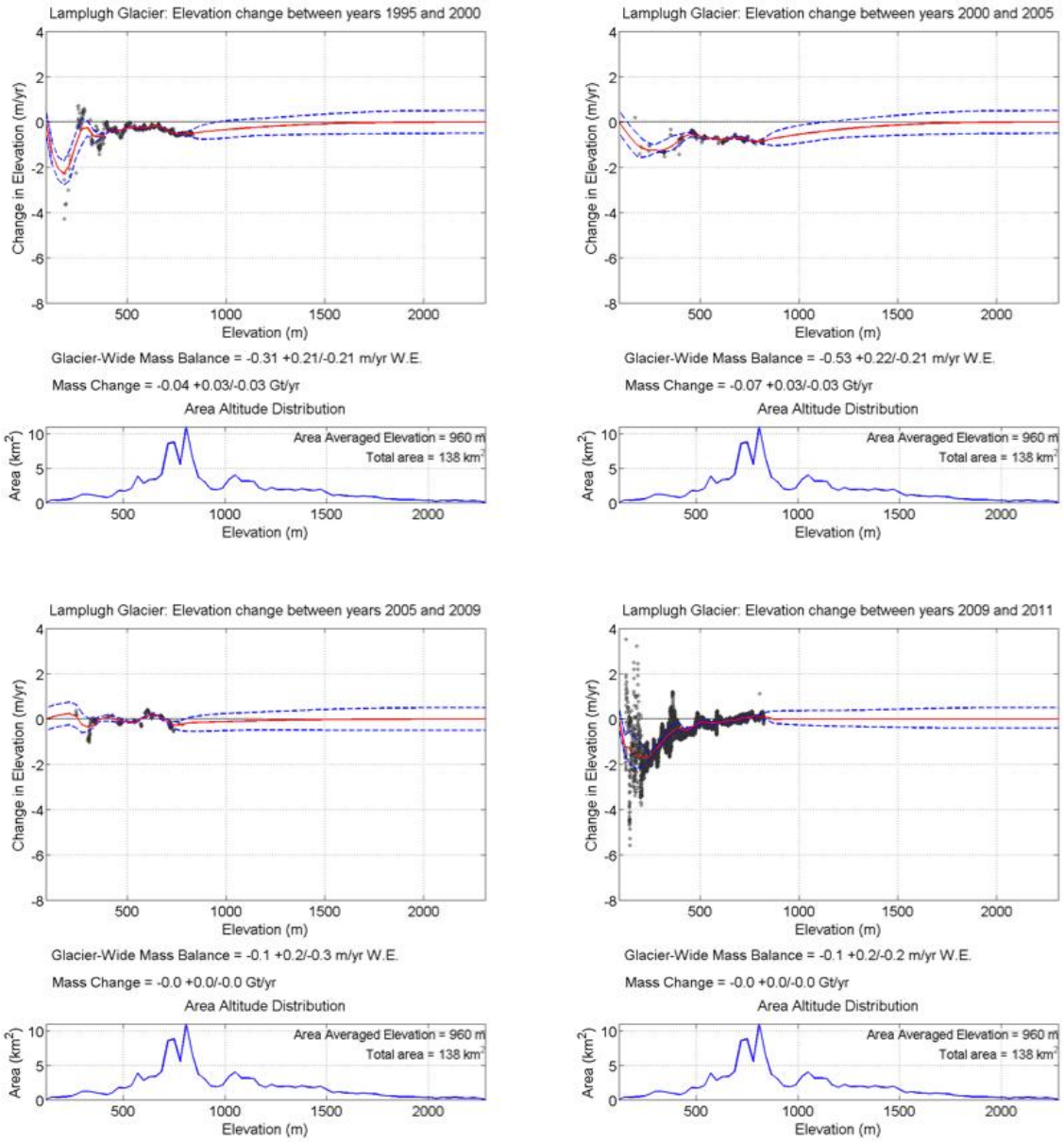

Fig. 30: Rate of thinning profiles for Lamplugh Glacier.

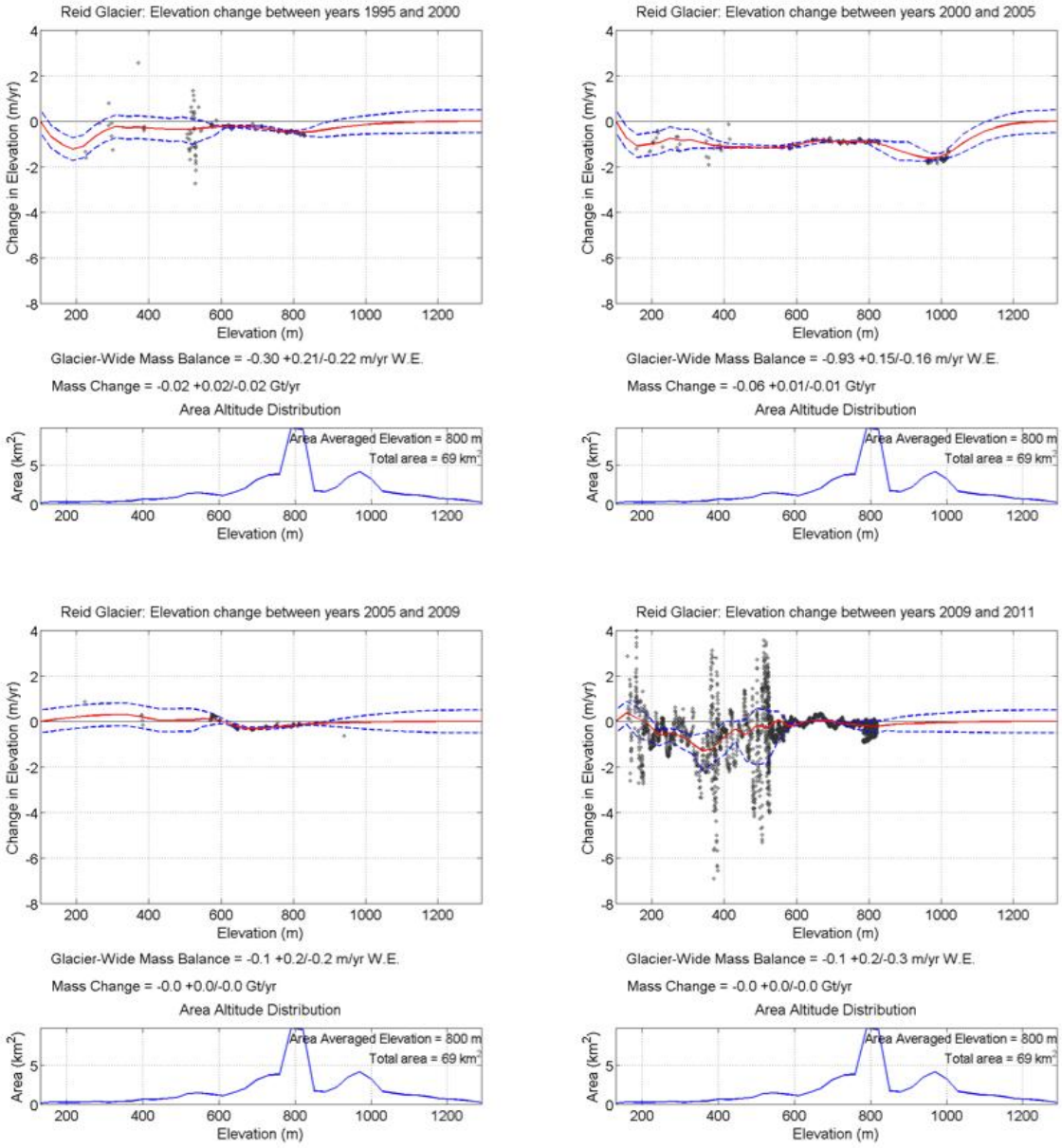

Fig. 31: Rate of thinning profiles for Reid Glacier.

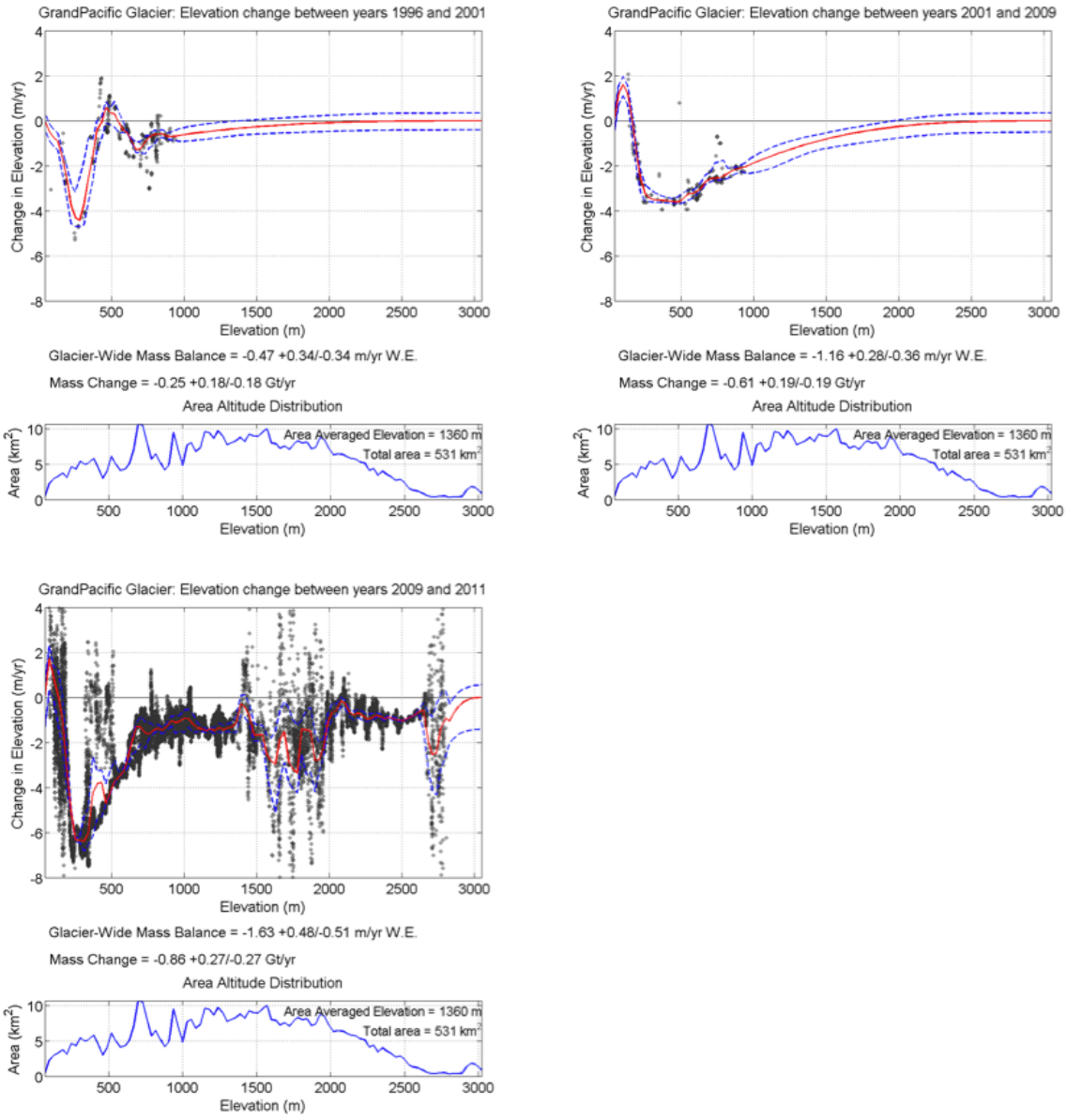

Fig. 32: Rate of thinning profiles for Grand Pacific Glacier.

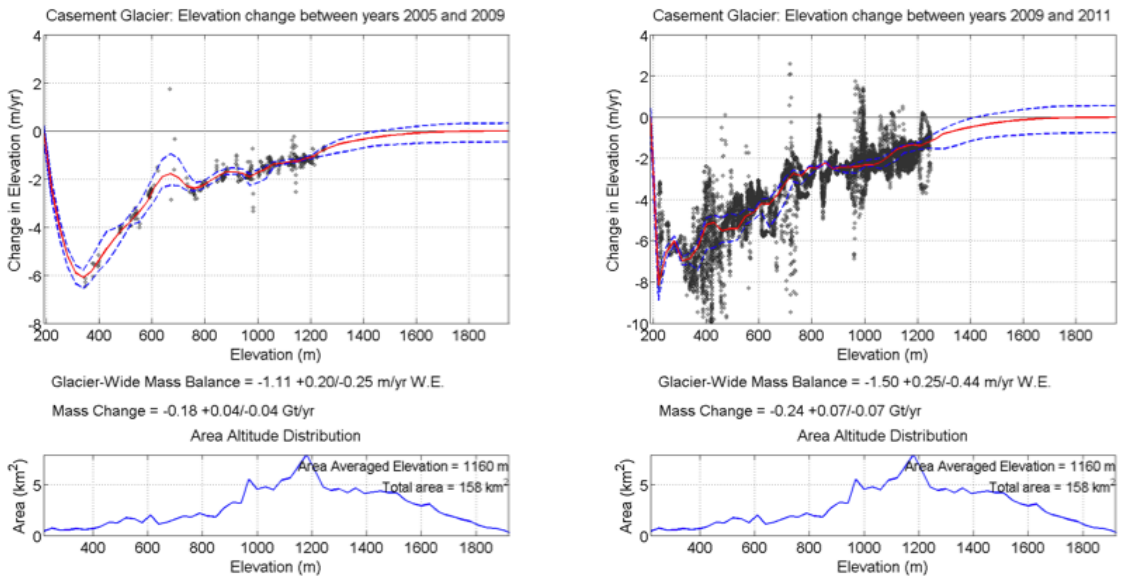

Fig. 33: Rate of thinning profiles for Casement Glacier.

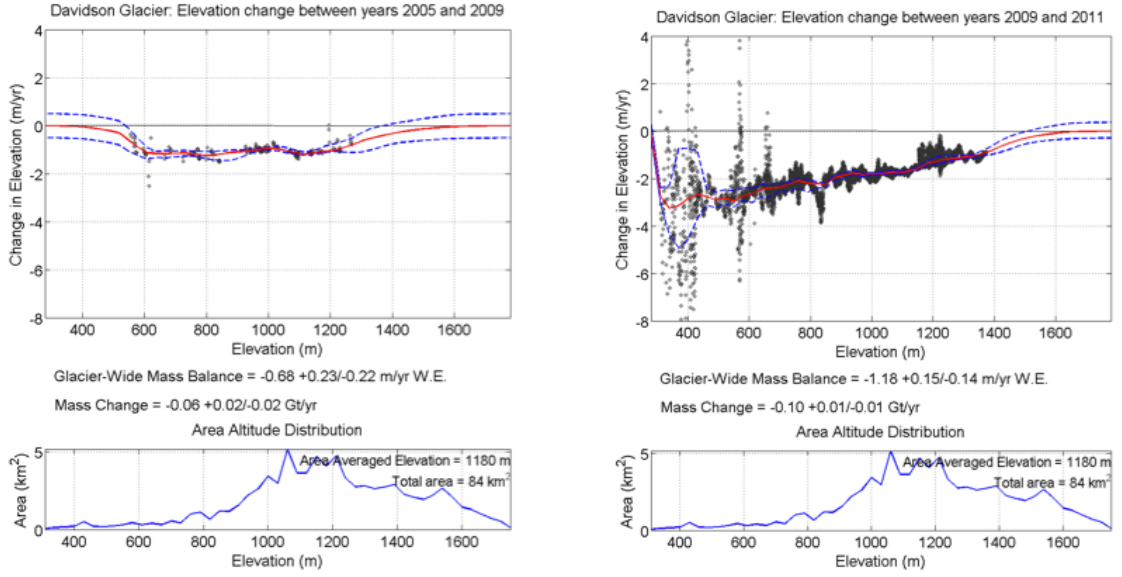

Fig. 34: Rate of thinning profiles for Davidson Glacier.

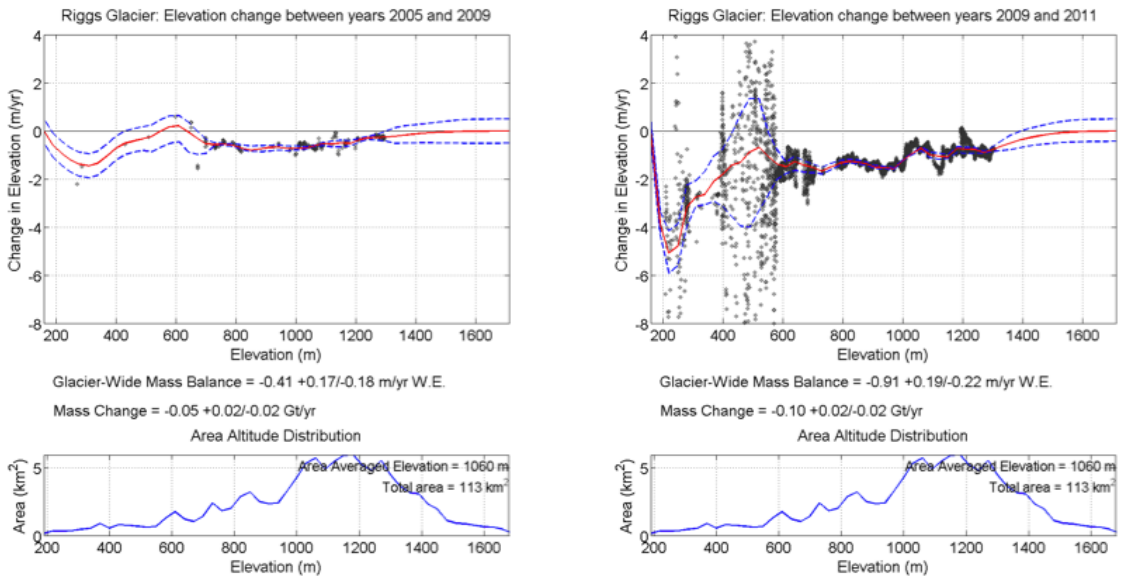

Fig. 35: Rate of thinning profiles for Riggs Glacier.

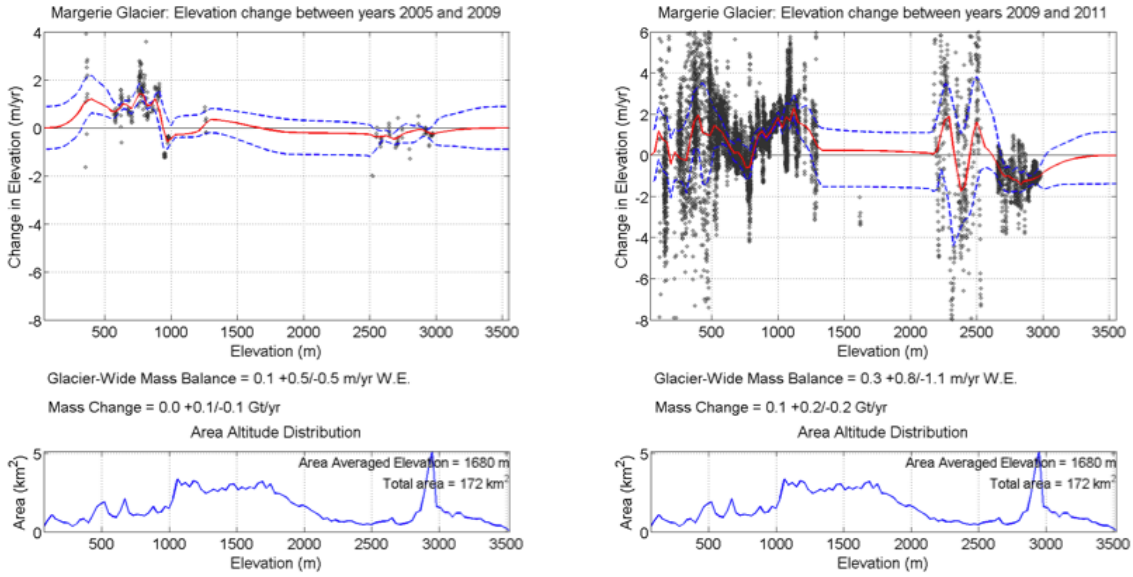

Fig. 36: Rate of thinning profiles for Margerie Glacier.

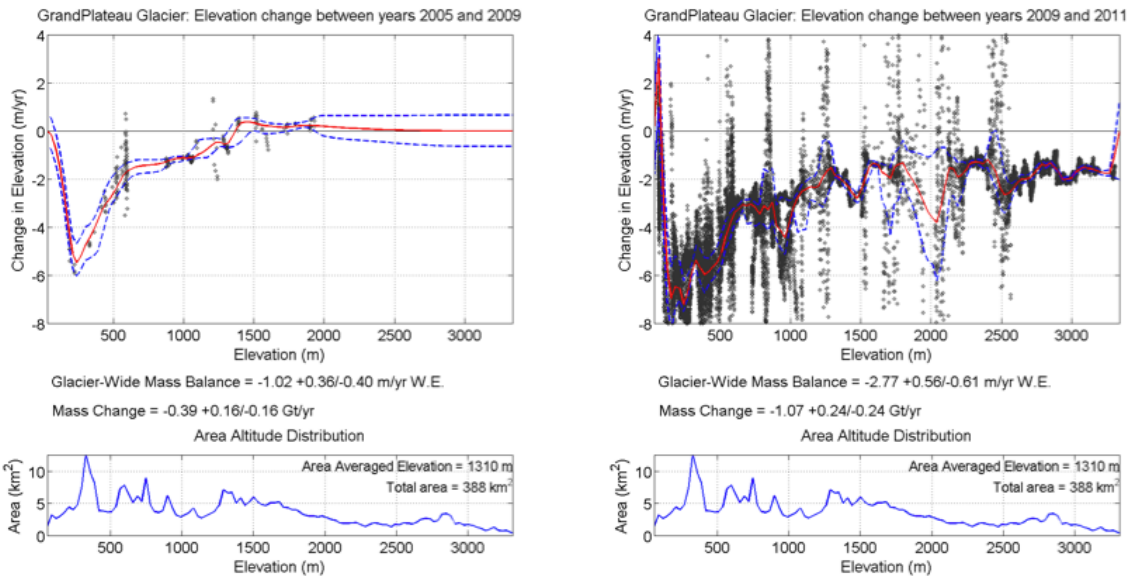

Fig. 37: Rate of thinning profiles for Grand Plateau Glacier.

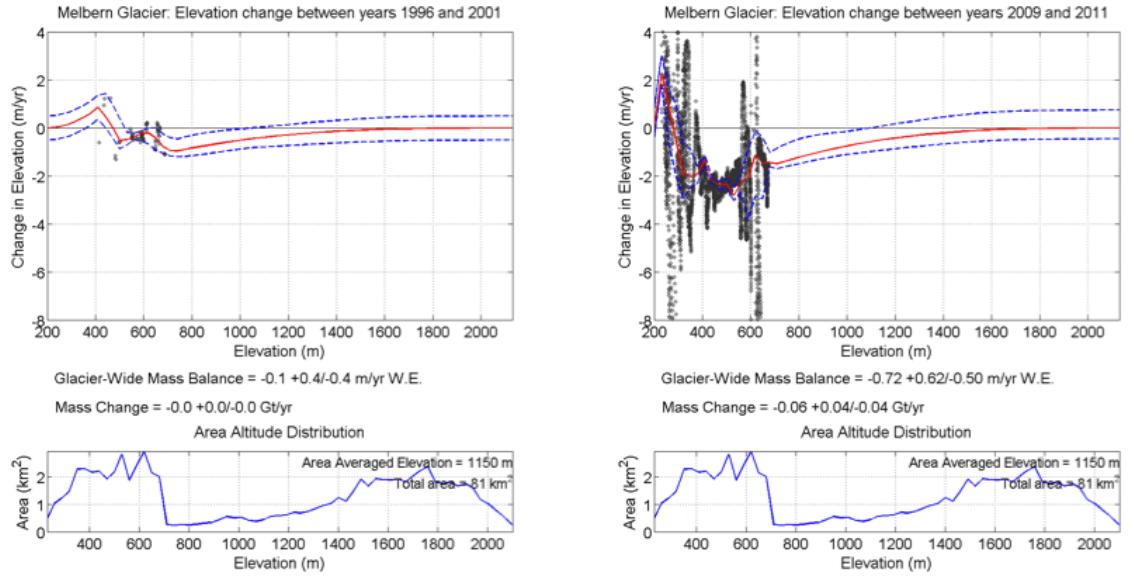

Fig. 38: Rate of thinning profiles for Melbern Glacier.

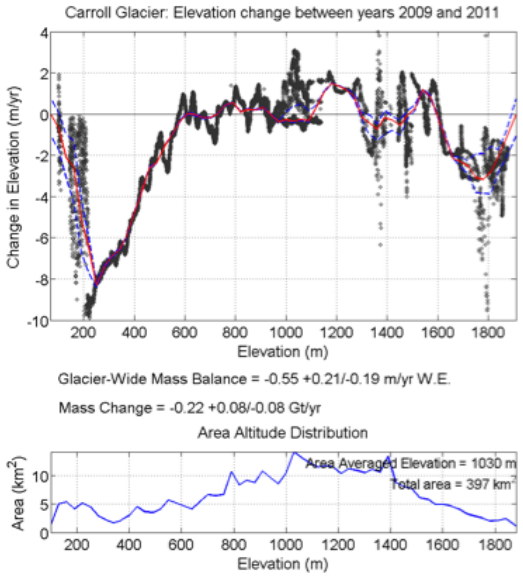

Fig. 39: Rate of thinning profile for Carroll Glacier.

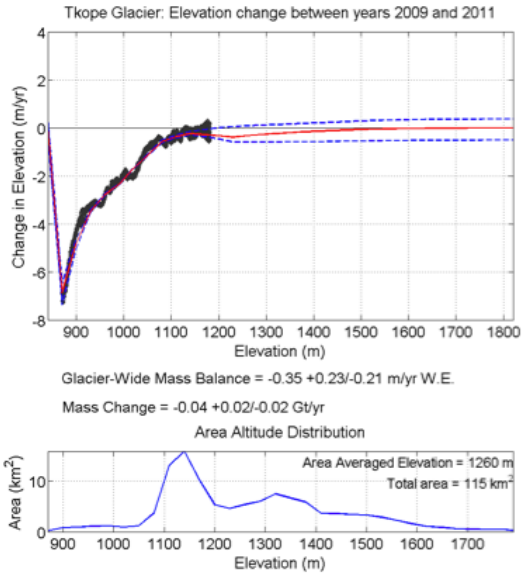

Fig. 40: Rate of thinning profile for Tkope Glacier.

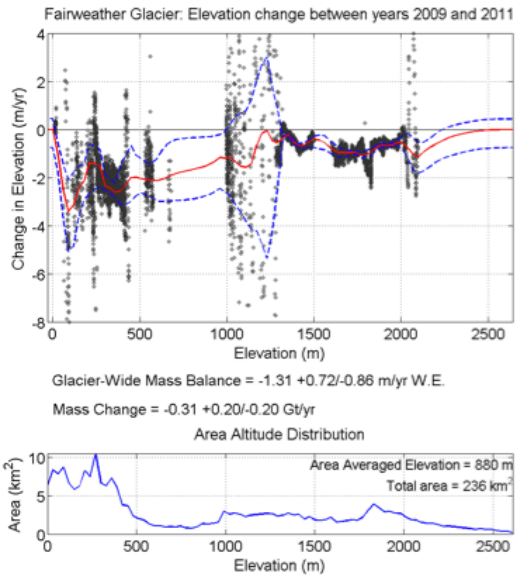

Fig. 41: Rate of thinning profile for Fairweather Glacier.

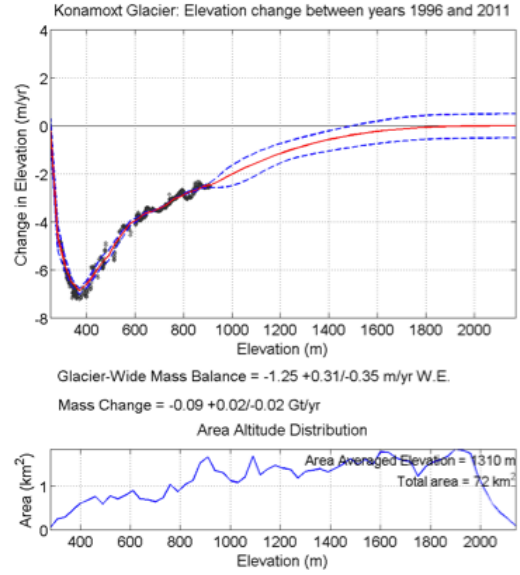

Fig. 42: Rate of thinning profile for Konamoxt Glacier.

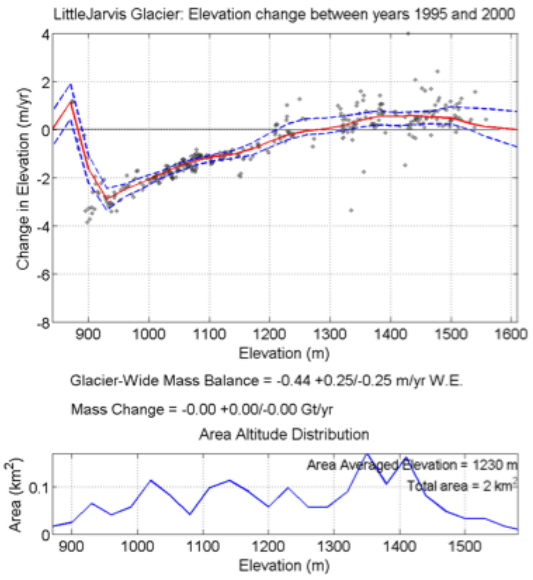

Fig. 43: Rate of thinning profile for Little Jarvis Glacier.

APPENDIX D

Other Figures

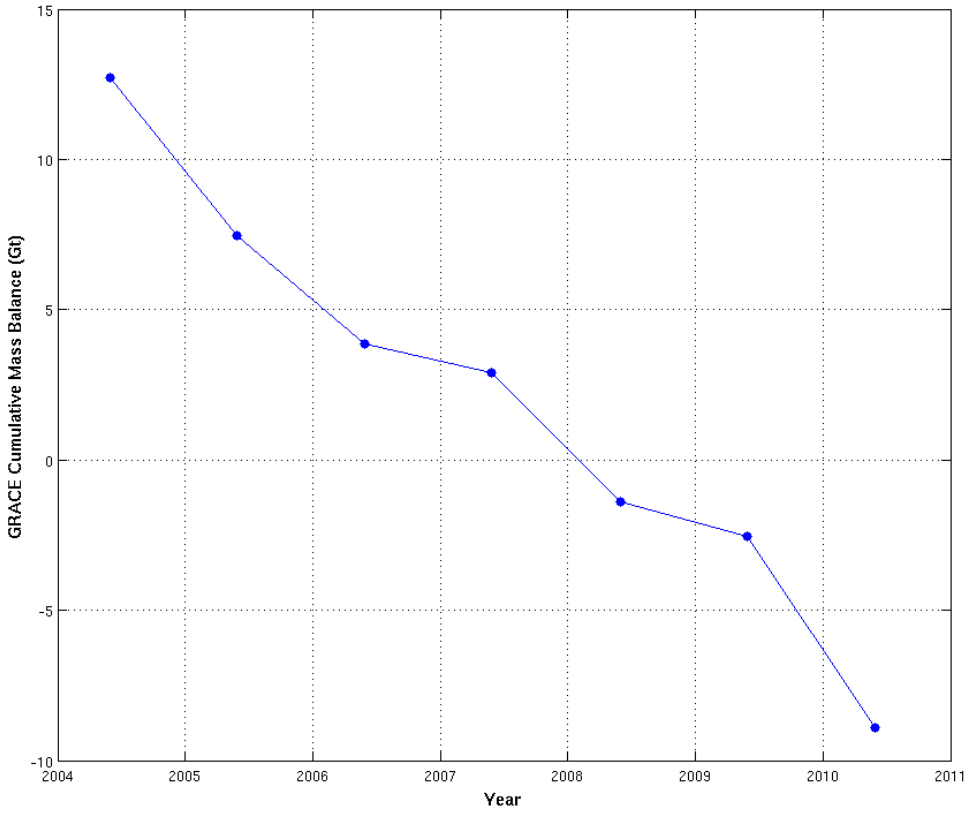

Fig. 44: GRACE cumulative mass balance in Glacier Bay from the end May of each year, 2004 through 2010.

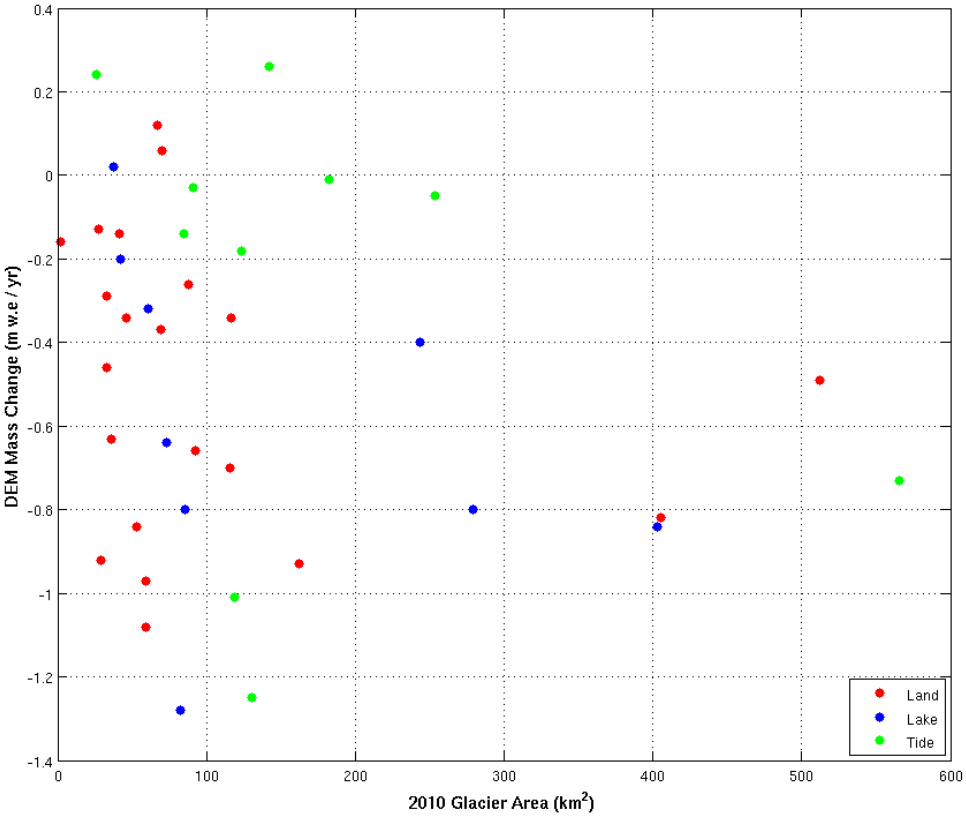

Fig. 45: DEM mass change vs. 2010 glacier area.

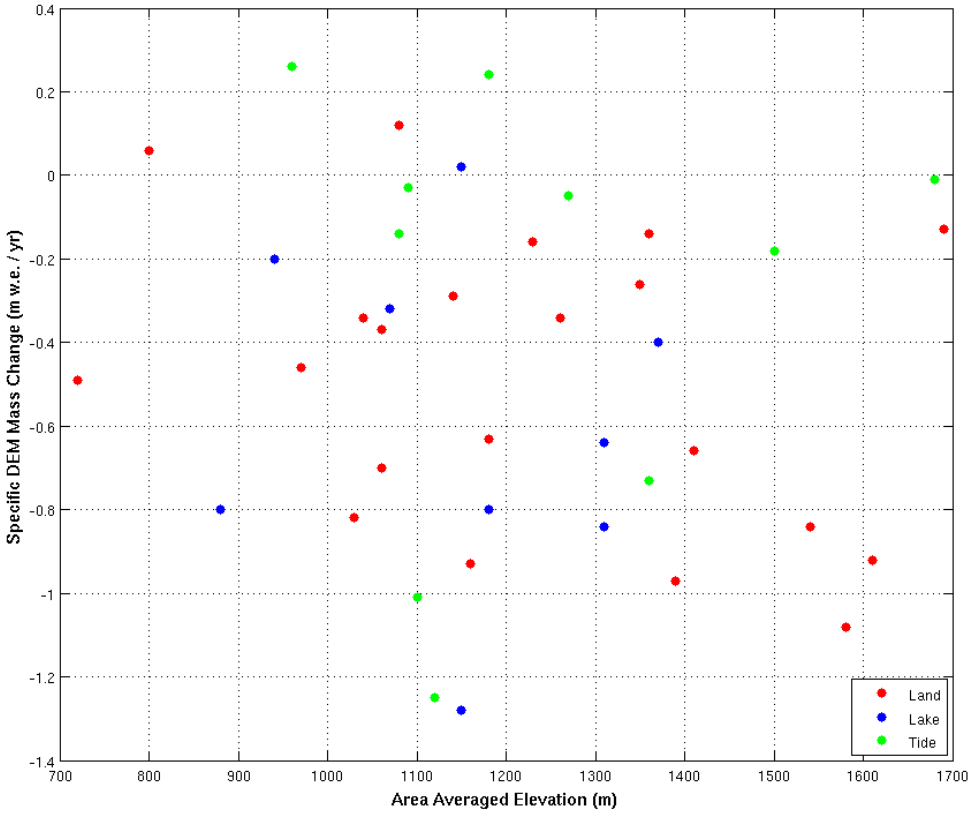

Fig. 46: DEM mass change vs. area averaged elevation.

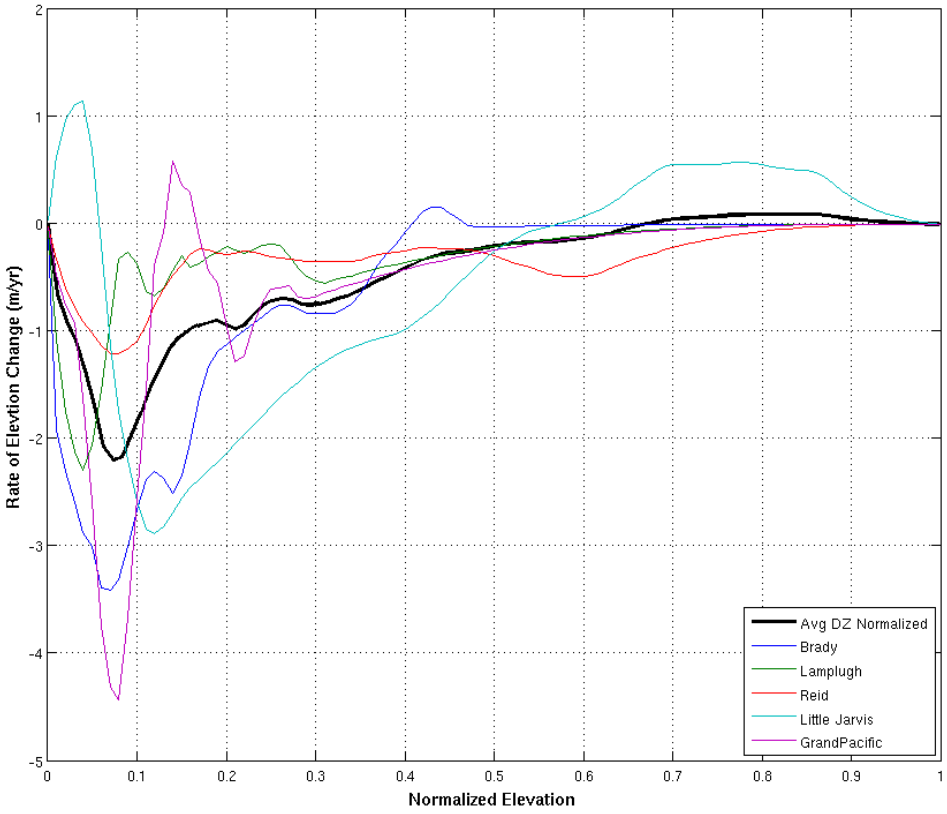

Fig. 47: Δh/Δt vs. normalized elevation for all glaciers profiled during period 1. The average curve that is integrated over the AAD is the solid black line.

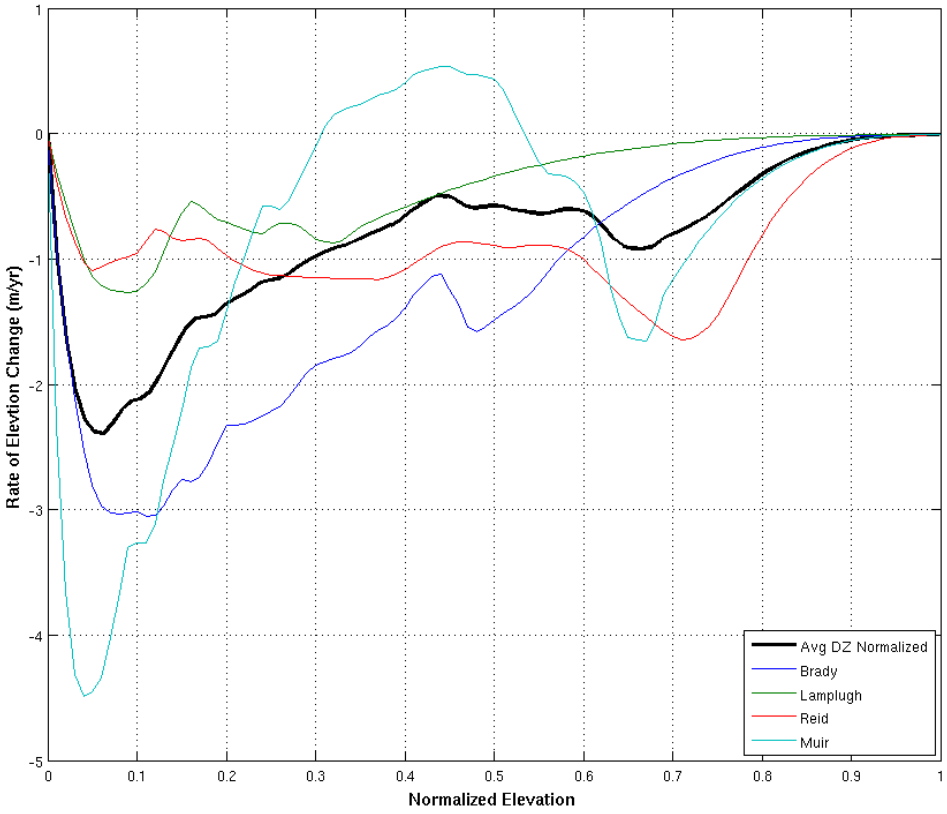

Fig. 48: Δh/Δt vs. normalized elevation for all glaciers profiled during period 2. The average curve that is integrated over the AAD is the solid black line.

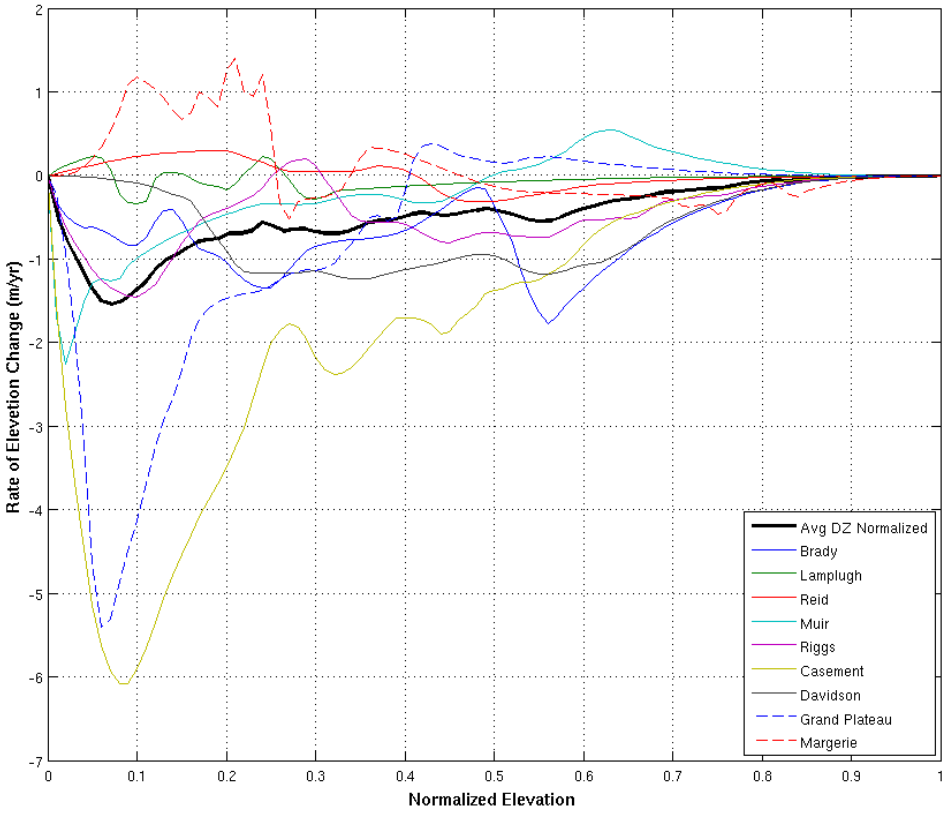

Fig. 49: Δh/Δt vs. normalized elevation for all glaciers profiled during period 3. The average curve that is integrated over the AAD is the solid black line.

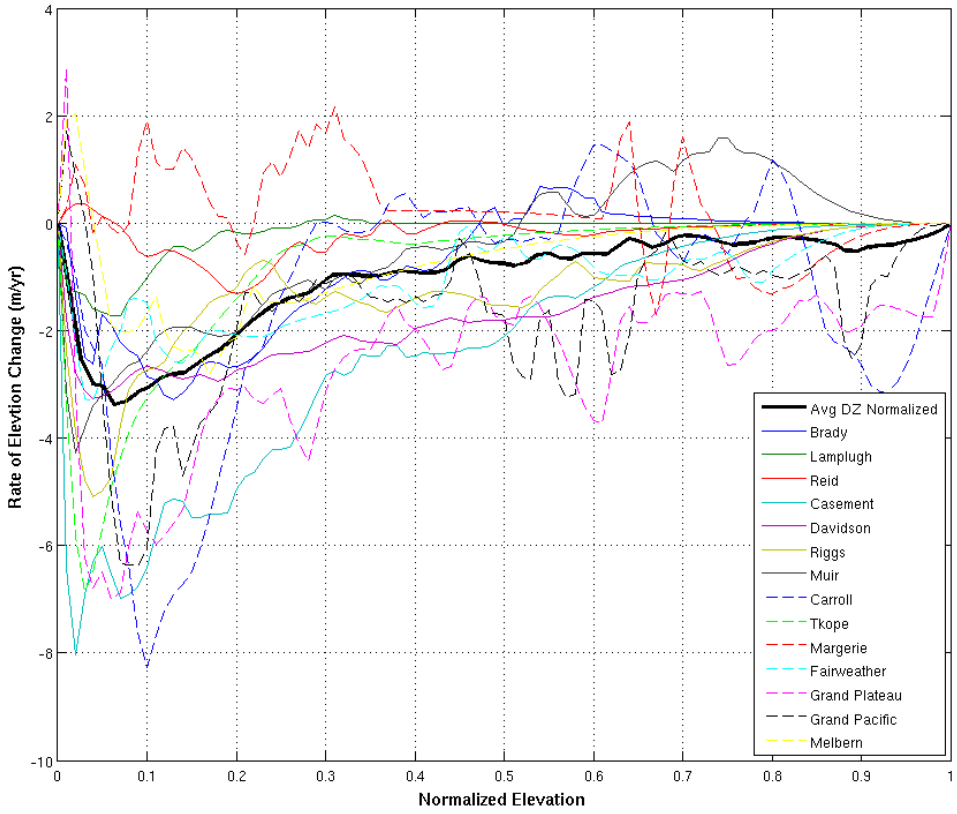

Fig. 50: Δh/Δt vs. normalized elevation for all glaciers profiled during period 4. The average curve that is integrated over the AAD is the solid black line.

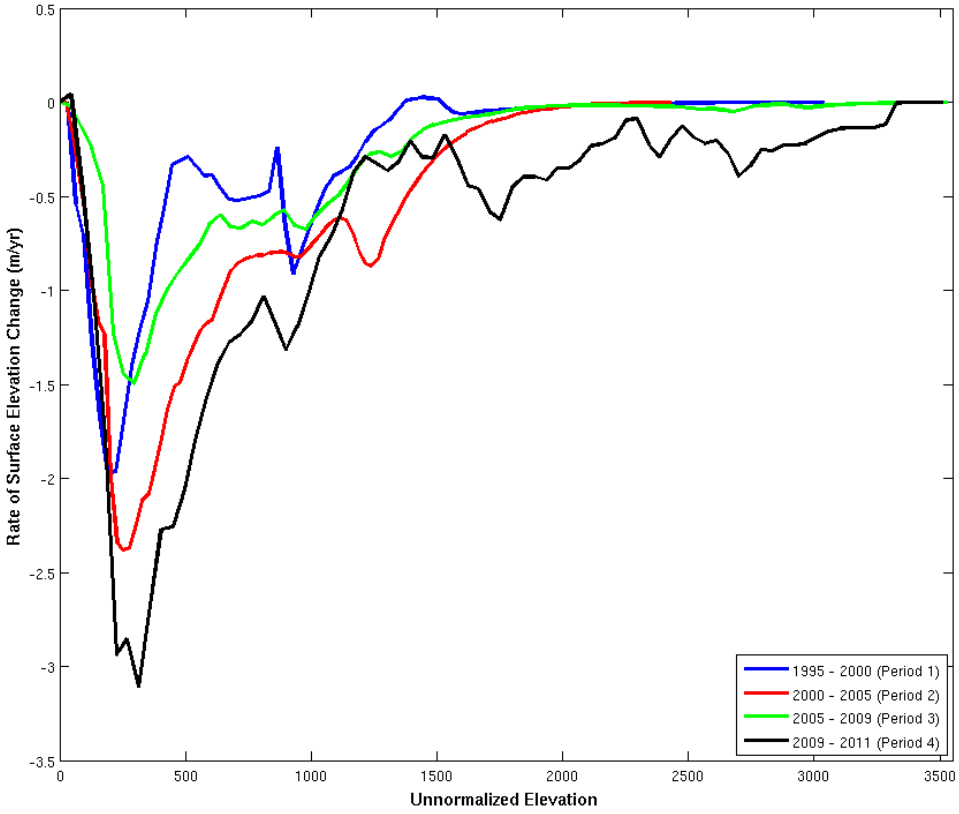

Fig. 51: Δh/Δt vs. average un-normalized elevation curves for periods 1 through 4.

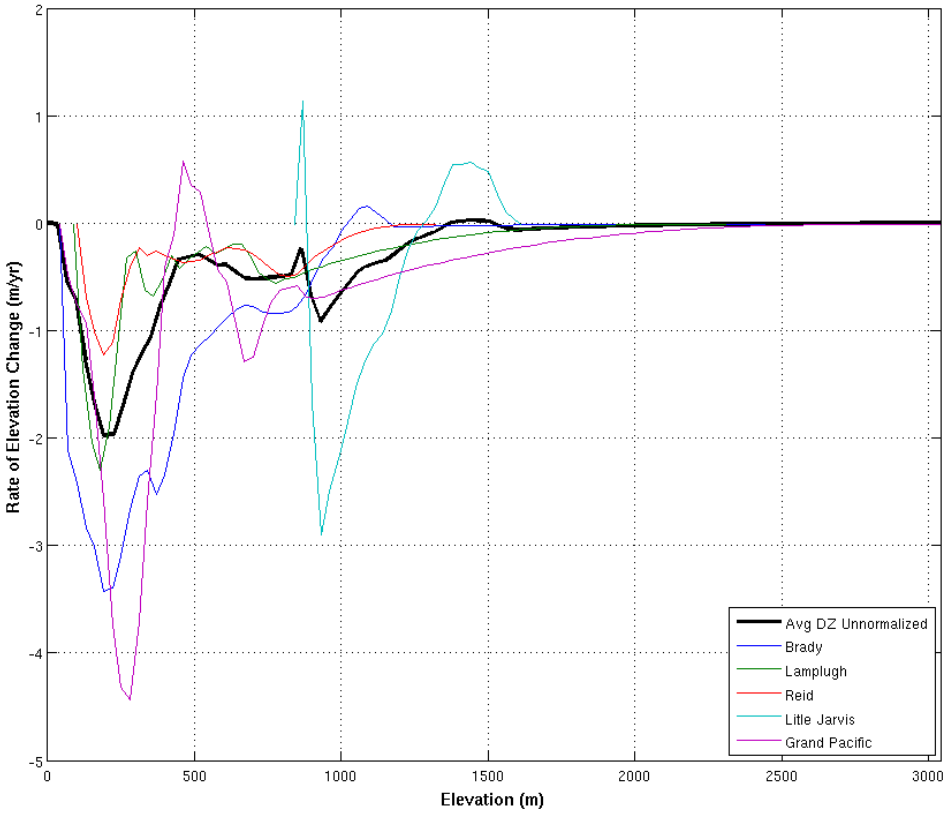

Fig. 52: Δh/Δt vs. un-normalized elevation for all glaciers profiled during period 1. The average curve that is integrated over the AAD is the solid black line.

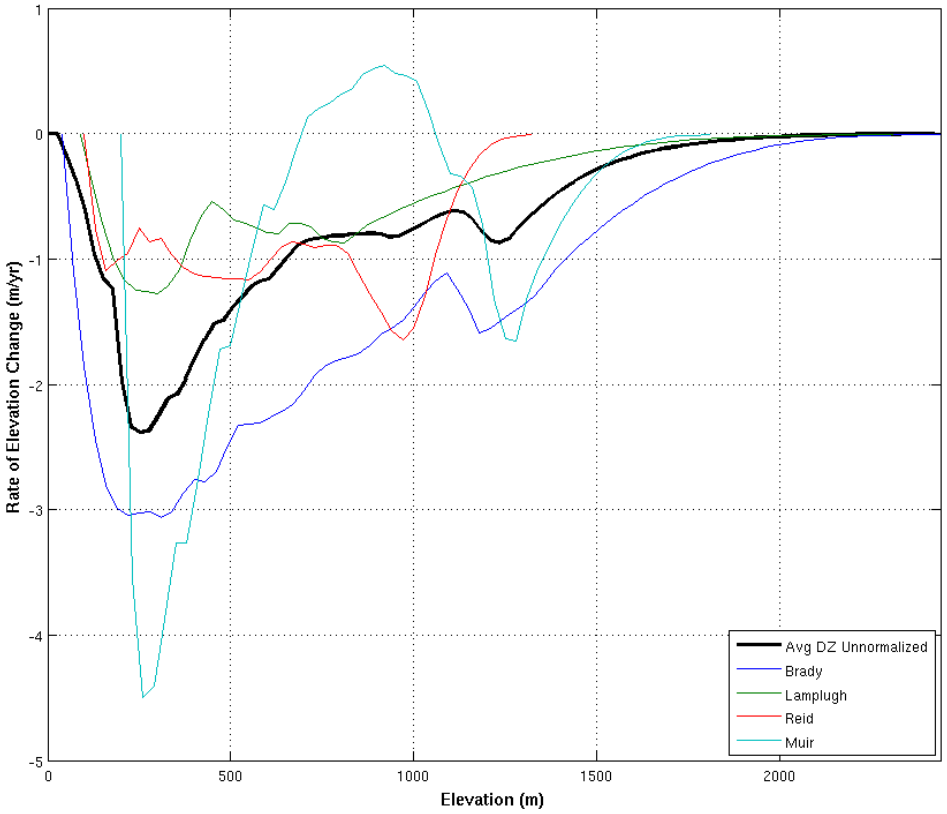

Fig. 53: Δh/Δt vs. un-normalized elevation for all glaciers profiled during period 2. The average curve that is integrated over the AAD is the solid black line. Notice the varying elevation of the glacier termini and heads.

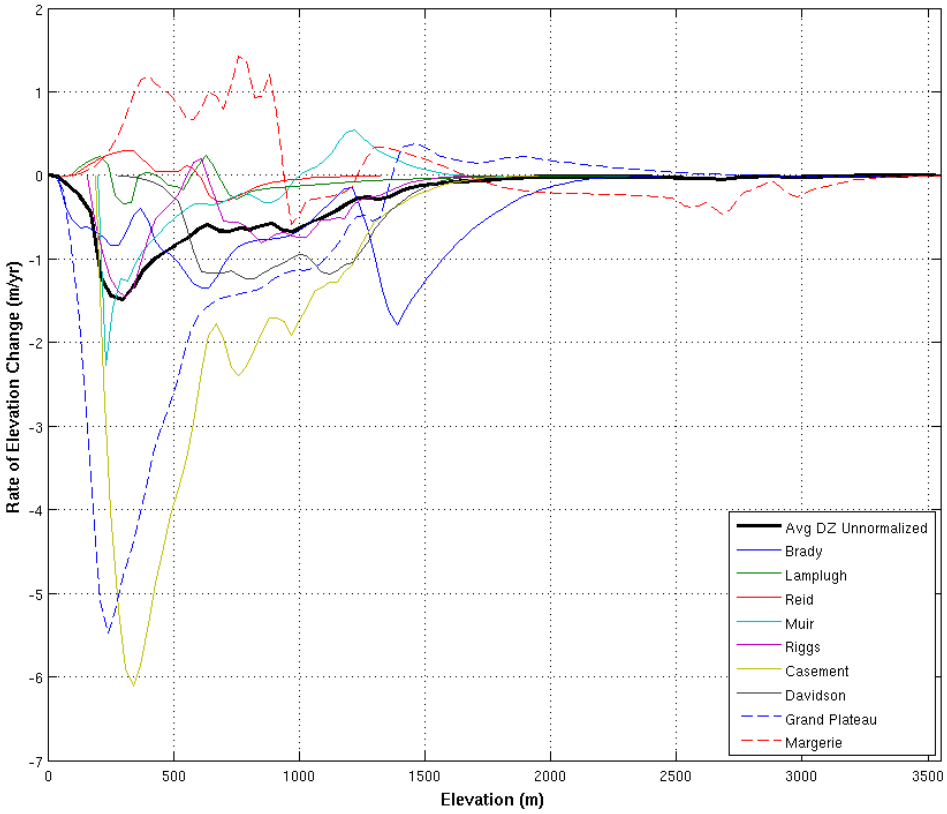

Fig. 54: Δh/Δt vs. un-normalized elevation for all glaciers profiled during period 3. The average curve that is integrated over the AAD is the solid black line.

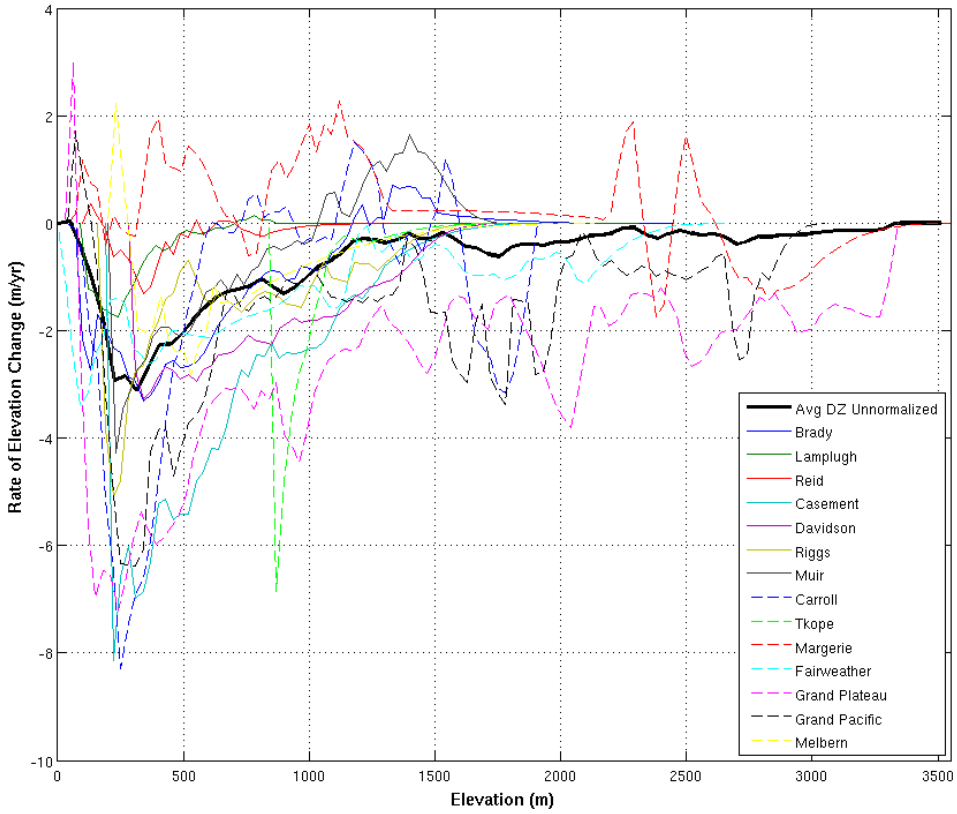

Fig. 55: Δh/Δt vs. un-normalized elevation for all glaciers profiled during period 4. The average curve that is integrated over the AAD is the solid black line.

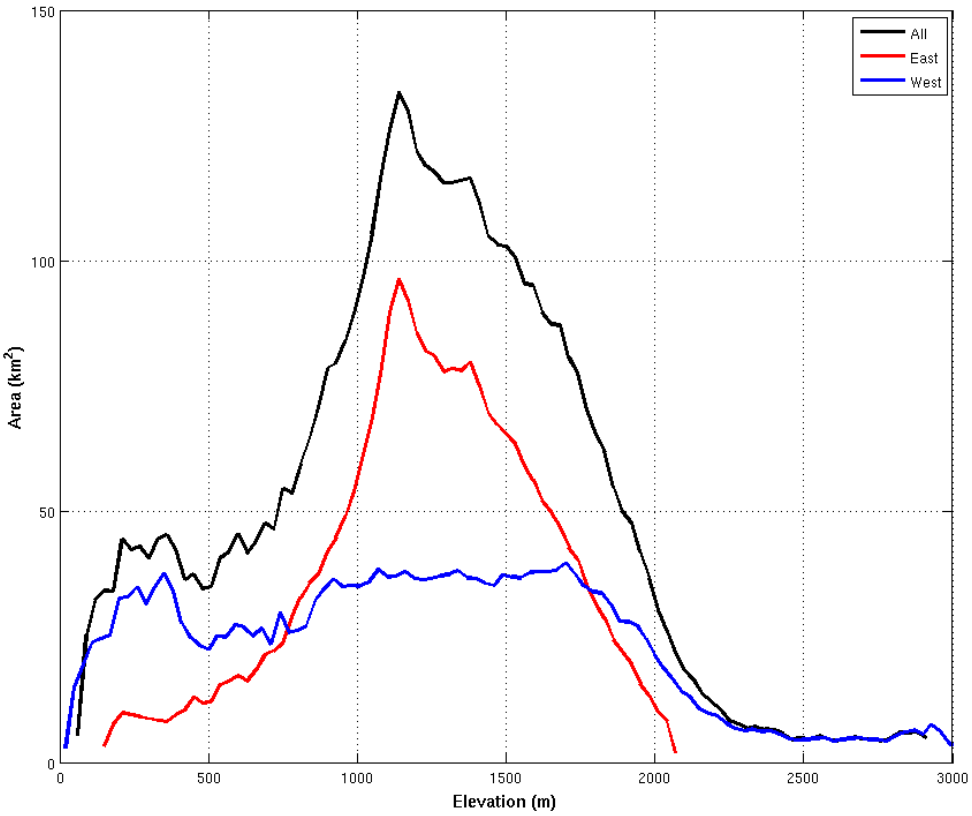

Fig. 56: The AAD of glaciers not profiled during period 1 within Glacier Bay.

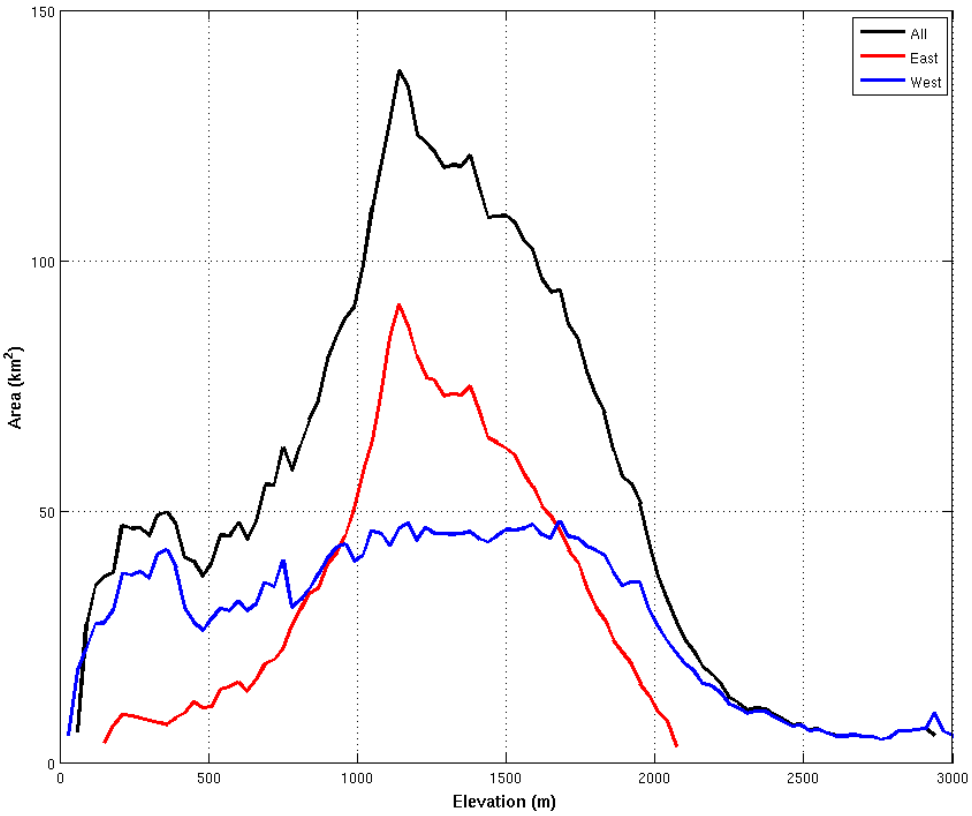

Fig. 57: The AAD of glaciers not profiled during period 2 within Glacier Bay.

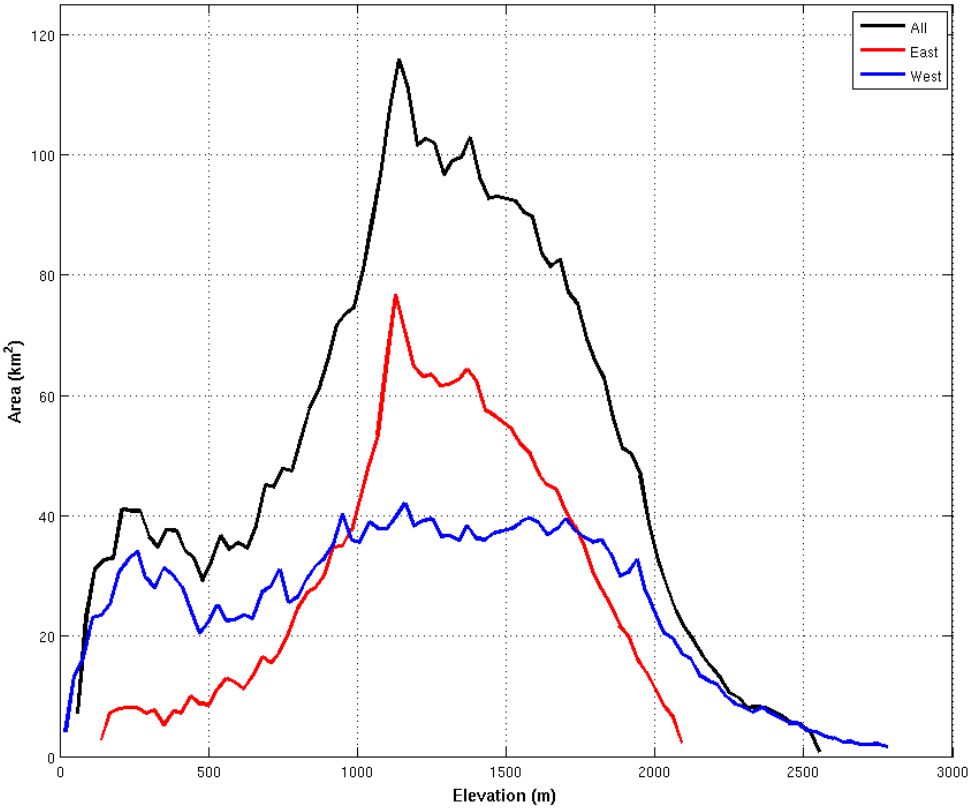

Fig. 58: The AAD of glaciers not profiled during period 3 within Glacier Bay.

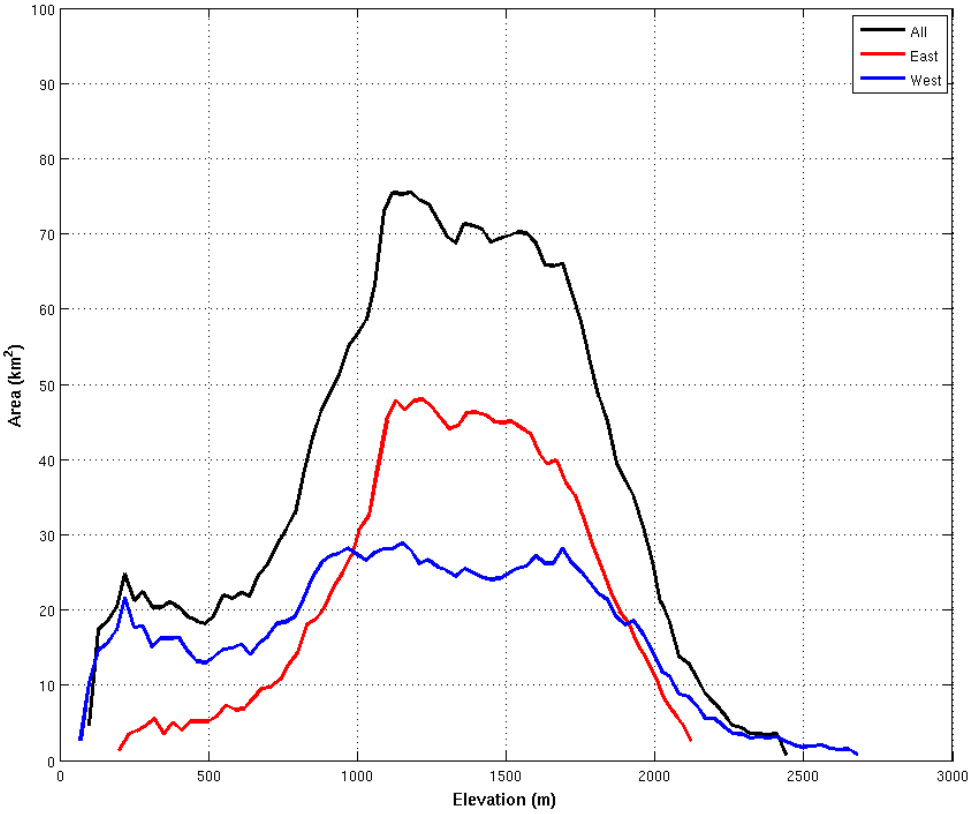

Fig. 59: The AAD of glaciers not profiled during period 4 within Glacier Bay.

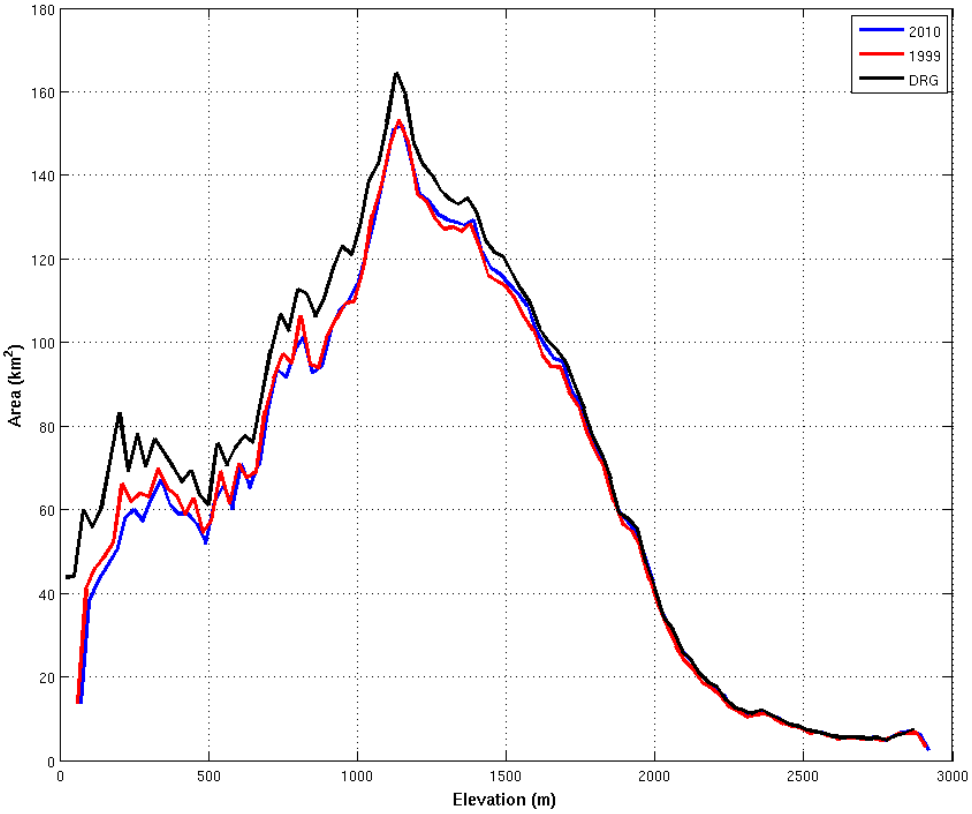

Fig. 60: The AAD of the entire glaciated area within Glacier Bay in 1948, 1999, and 2010. Black line is calculated using the AAD of the National Elevation Dataset DEM that is derived from air photos prior to the 1950s and glacier outlines based on the topographic maps made from the NED DEM. Red line is the 1999 AAD and the blue line is the 2010 AAD. Both the 1999 and 2010 AADs are calculated using the SRTM DEM as there is not a high quality DEM available from 2010. Glacier extents in 1999 and 2010 were mapped as part of the GLIMS project.

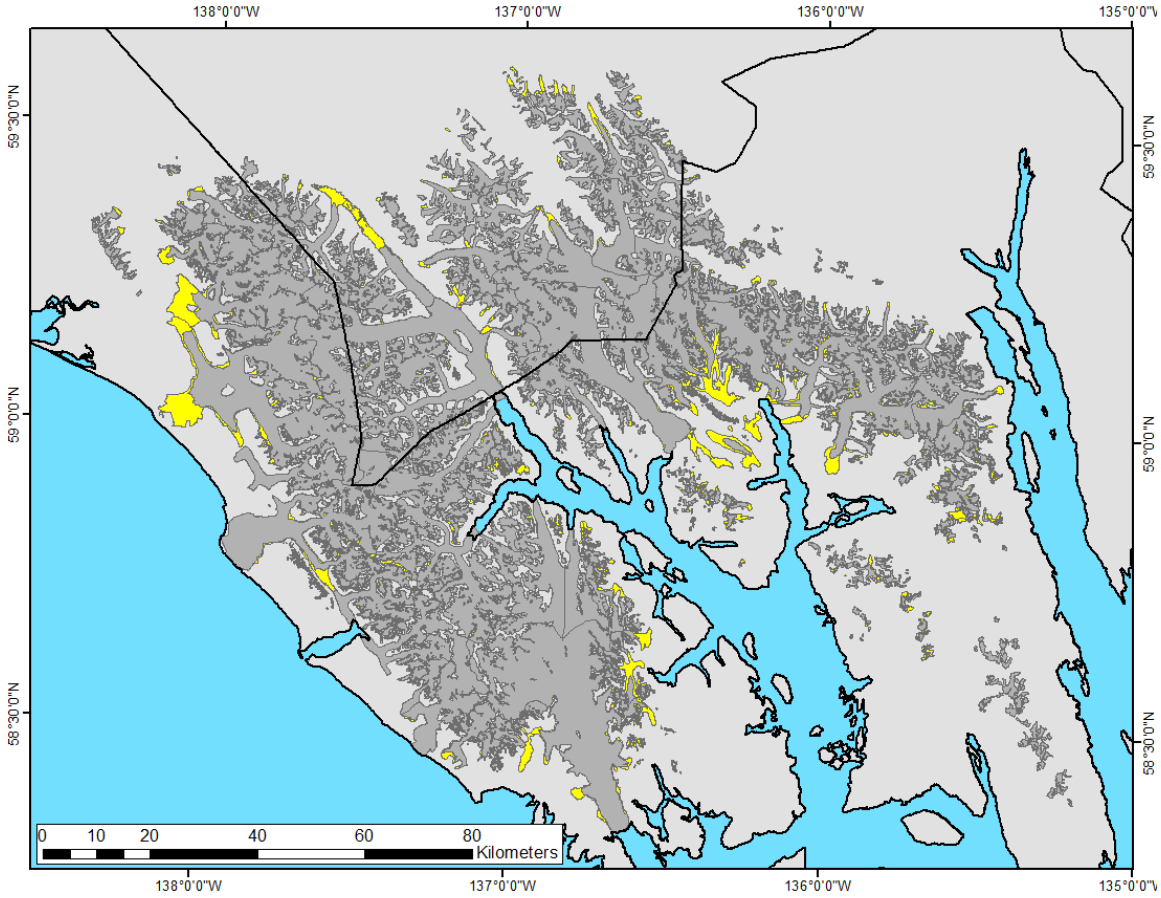

Fig. 61: The retreat of glaciers in Glacier Bay between 1948 and 2010. The base layer in yellow is glacier extents from 1948 and the gray layer is 2010 glacier extents. The largest areas of retreat are lake calving glaciers and those in the East Arm of Glacier Bay that experienced tidewater retreat up through the 1980s.